

University of Windsor

Scholarship at UWindor

Electronic Theses and Dissertations

Theses, Dissertations, and Major Papers

2002

In-cylinder pressure measurements with optical fiber and piezoelectric pressure transducers.

Kevin J. Roth
University of Windsor

Follow this and additional works at: <https://scholar.uwindsor.ca/etd>

Recommended Citation

Roth, Kevin J., "In-cylinder pressure measurements with optical fiber and piezoelectric pressure transducers." (2002). *Electronic Theses and Dissertations*. 2422.
<https://scholar.uwindsor.ca/etd/2422>

This online database contains the full-text of PhD dissertations and Masters' theses of University of Windsor students from 1954 forward. These documents are made available for personal study and research purposes only, in accordance with the Canadian Copyright Act and the Creative Commons license—CC BY-NC-ND (Attribution, Non-Commercial, No Derivative Works). Under this license, works must always be attributed to the copyright holder (original author), cannot be used for any commercial purposes, and may not be altered. Any other use would require the permission of the copyright holder. Students may inquire about withdrawing their dissertation and/or thesis from this database. For additional inquiries, please contact the repository administrator via email (scholarship@uwindsor.ca) or by telephone at 519-253-3000ext. 3208.

In-Cylinder Pressure Measurements with Optical Fiber and Piezoelectric Pressure Transducers

By

Kevin J. Roth

A Thesis

Submitted to the Faculty of Graduate Studies and Research
through Mechanical, Automotive, and Materials Engineering
in Partial Fulfillment of the Requirements for
the Degree of Masters of Applied Science at the
University of Windsor

Windsor, Ontario, Canada

2002

© 2002 Kevin J. Roth



Library and
Archives Canada

Bibliothèque et
Archives Canada

Published Heritage
Branch

Direction du
Patrimoine de l'édition

395 Wellington Street
Ottawa ON K1A 0N4
Canada

395, rue Wellington
Ottawa ON K1A 0N4
Canada

Your file *Votre référence*

ISBN: 0-494-04963-4

Our file *Notre référence*

ISBN: 0-494-04963-4

NOTICE:

The author has granted a non-exclusive license allowing Library and Archives Canada to reproduce, publish, archive, preserve, conserve, communicate to the public by telecommunication or on the Internet, loan, distribute and sell theses worldwide, for commercial or non-commercial purposes, in microform, paper, electronic and/or any other formats.

The author retains copyright ownership and moral rights in this thesis. Neither the thesis nor substantial extracts from it may be printed or otherwise reproduced without the author's permission.

AVIS:

L'auteur a accordé une licence non exclusive permettant à la Bibliothèque et Archives Canada de reproduire, publier, archiver, sauvegarder, conserver, transmettre au public par télécommunication ou par l'Internet, prêter, distribuer et vendre des thèses partout dans le monde, à des fins commerciales ou autres, sur support microforme, papier, électronique et/ou autres formats.

L'auteur conserve la propriété du droit d'auteur et des droits moraux qui protègent cette thèse. Ni la thèse ni des extraits substantiels de celle-ci ne doivent être imprimés ou autrement reproduits sans son autorisation.

In compliance with the Canadian Privacy Act some supporting forms may have been removed from this thesis.

Conformément à la loi canadienne sur la protection de la vie privée, quelques formulaires secondaires ont été enlevés de cette thèse.

While these forms may be included in the document page count, their removal does not represent any loss of content from the thesis.

Bien que ces formulaires aient inclus dans la pagination, il n'y aura aucun contenu manquant.


Canada

ABSTRACT

Highly accurate cylinder pressure data can be acquired using a wall-mounted and water-cooled quartz piezoelectric transducer. However, this type of transducer does not satisfy the cost and packaging constraints for use in a production engine application. A potential solution to these issues is the much smaller and less expensive optical fiber based pressure transducer.

This research compares Kistler piezoelectric transducers to Optrand optical fiber transducers. The influence of the transducer type and mounting arrangement on the quality of cylinder pressure data was examined. The transducers were evaluated on a DaimlerChrysler 4.7L V-8 Compressed Natural Gas fuelled test engine. The analysis method is comprised of examining measured individual cycle and ensemble-averaged cylinder pressure records to assess the quality of the data and its potential usefulness for engine management.

The variation in performance in terms of thermal shock error among the four Optrand transducers was much larger than those among the four Kistler transducers. The best performing Optrand transducer both over and underestimated cylinder pressure, leading to more accurate results of Indicated Mean Effective Pressure and overestimations in peak cylinder pressure compared to the Kistler transducer which always underestimated cylinder pressure.

The individual cycle analysis showed that the Optrand transducer indicated a larger amount of intracycle variability than the Kistler transducers, regardless of their mounting location.

Prolonged recovery of the Optrand transducer from thermal shock introduced drastic errors in Pumping Mean Effective Pressure. In all remaining calculated parameters investigated, the Optrand and Kistler transducers measured reliably and had comparable results up until the Optrand transducer failed. After only less than 100 hours of testing, the Optrand transducer started to produce erroneous pressure data and had to be replaced by another transducer from Optrand.

The individual cylinder analysis showed that there is a maximum deviation in Indicated Mean Effective Pressure of approximately $\pm 5\%$ between all eight cylinders, suggesting that all cylinders are not receiving a similar charge. Standard Deviations of Indicated Mean Effective Pressure for all cylinders are small, suggesting that each cylinder is receiving a similar charge from cycle to cycle.

ACKNOWLEDGEMENTS

It has been a rewarding experience to work under the supervision of Dr. Sobiesiak. His insight and encouragement are greatly appreciated.

The assistance of many people must be acknowledged, for without their support this project would not have been possible. These are: Jim Lanigan, Shawn Yates, Larry Robertson, Remko Brouerius, Bernd Windisch, Egidio Mosca, Gary Unis, and Dennis Soltis,

Many thanks for the resources supplied by DaimlerChrysler Technology Centre, MI, USA and the University of Windsor/DaimlerChrysler Canada Automotive Research and Development Centre, Windsor, Canada.

The financial support of the Natural Sciences and Engineering Research Council, DaimlerChrysler Canada, and the University of Windsor School of Graduate Studies is gratefully acknowledged.

TABLE OF CONTENTS

ABSTRACT	III
ACKNOWLEDGEMENTS	V
TABLE OF CONTENTS	VI
LIST OF FIGURES	VIII
LIST OF TABLES	XI
LIST OF SYMBOLS AND ABBREVIATIONS	XII
CHAPTER 1: INTRODUCTION	1
CHAPTER 2: LITERATURE REVIEW	4
CHAPTER 3: PIEZOELECTRIC PRESSURE TRANSDUCERS	7
3.1 Transducer Design.....	9
3.2 Charge Amplification.....	11
3.2.1 Filtering.....	12
3.2.2 Time Constant.....	12
CHAPTER 4: OPTICAL FIBER PRESSURE TRANSDUCERS	14
4.1 Diaphragm.....	15
4.2 Opto-Electronic Module.....	16
CHAPTER 5: PRESSURE TRANSDUCER MOUNTING AND TEMPERATURE EFFECTS	17
5.1 Flush Mount	17
5.2 Recessed Mount	18
CHAPTER 6: EXPERIMENTAL SETUP	20
6.1 Engine.....	20
6.2 Transducers	21
6.3 Data Acquisition and Processing.....	23
6.3.1 Auto-tracking	24
6.3.2 Pegging	27
6.4 Crankshaft Encoder	28
6.4.1 Top Dead Center Find.....	29
6.5 Measuring Chain	30
6.6 Uncertainty	30

CHAPTER 7: EXPERIMENTAL MATRIX	33
CHAPTER 8: PRESSURE TRACE ANALYSIS	35
CHAPTER 9: RESULTS AND DISCUSSION	40
9.1 Performance Variation	40
9.2 Global Comparison.....	43
9.3 Intracycle Variability Analysis.....	50
9.4 Combustion Performance Parameters	56
9.5 Cylinder-to-Cylinder Variations.....	66
9.6 Bank-to-Bank Variations.....	78
9.7 Durability.....	80
CHAPTER 10: SUMMARY, CONCLUSIONS, AND RECOMMENDATIONS	82
CHAPTER 11: REFERENCES.....	85
APPENDIX A: COMPLETE ENGINE DATA USING KISTLER SPARK TRANSDUCER.....	87
APPENDIX B: COMPLETE ENGINE DATA USING OPTRAND SPARK TRANSDUCER.....	95
APPENDIX C: CYLINDER-TO-CYLINDER VARIATIONS ARRANGED BANK- TO-BANK.....	103
APPENDIX D: MANUFACTURER SPECIFICATIONS.....	107
VITA AUCTORIS	113

LIST OF FIGURES

Figure 1: Relative Sensitivity Change vs. Temperature	7
Figure 2: Transverse Piezoelectric Effect.....	8
Figure 3: Kistler Piezoelectric Pressure Transducer Design	9
Figure 4: Typical Frequency Response of a Piezoelectric Transducer.....	11
Figure 5: Filtering Effects.....	12
Figure 6: Optical Fiber Transducer Layout	14
Figure 7: Transducer Head Construction.....	14
Figure 8: Light Intensity vs. Fiber to Diaphragm Distance	15
Figure 9: Engine Dynamometer Facility	20
Figure 10: Cylinder No. 1 Combustion Chamber.....	21
Figure 11: Reference and Test Transducers	22
Figure 12: MTS Adapt-CAS System.....	23
Figure 13: Analog to Digital Conversio	25
Figure 14: Signal Drift.....	26
Figure 15: Autotracking Effects	26
Figure 16: AVL Crankshaft Encoder.....	28
Figure 17: Crankshaft Encoder Output.....	29
Figure 18: Typical Kistler Spark Pressure Difference.....	36
Figure 19: Typical Optrand Spark Pressure Difference.....	37
Figure 20: Kistler Spark Transducer Comparison	40
Figure 21: Optrand Spark Transducer Comparison.....	41
Figure 22: Effect of Engine Speed on Kistler Spark Transducer	43
Figure 23: Effect of Engine Speed on Optrand Spark Transducer	45
Figure 24: Average ΔP (a) and Maximum Thermal Shock Error (b) at Varying Engine Speeds.....	47
Figure 25: Effect of Engine Load on Kistler Spark Transducer	48
Figure 26: Effect of Engine Load on Optrand Spark Transducer.....	48
Figure 27: Average ΔP (a) and Maximum Thermal Shock Error (b) at Varying Engine Loads	49
Figure 28: Description of Segments used for the Intracycle Variability Anaylsis	52
Figure 29: Intracycle Variability Anaylsis.....	53
Figure 30: Effect of Engine Load on IMEP Difference (bar).....	57
Figure 31: Effect of Engine Load on IMEP Difference (%).....	58
Figure 32: Effect of Engine Load on Peak Pressure Difference (bar)	59
Figure 33: Effect of Engine Load on Peak Pressure Difference (%).....	59
Figure 34: Effect of Engine Load on Location of PP Difference (CAD).....	60
Figure 35: Effect of Engine Load on CA50 Difference (CAD)	61
Figure 36: Effect of Engine Speed on IMEP Difference (bar)	63
Figure 37: Effect of Engine Speed on IMEP Difference (%).....	63
Figure 38: Effect of Engine Speed on Peak Pressure Difference (bar)	64
Figure 39: Effect of Engine Speed on Peak Pressure Difference (%)	64
Figure 40: Effect of Engine Speed on Location of PP Difference (CAD)	65
Figure 41: Effect of Engine Speed on CA50 Difference (CAD).....	65
Figure 42: IMEP and its SD at WOT and Varying Engine Speeds	67

Figure 43: Peak Pressure and its SD at WOT and Varying Engine Speeds	67
Figure 44: Location of PP and its SD at WOT and Varying Engine Speeds.....	68
Figure 45: CA50 and its SD at WOT and Varying Engine Speeds	68
Figure 46: IMEP and its SD at 3000 RPM and Varying Engine Loads	70
Figure 47: Peak Pressure and its SD at 3000 RPM and Varying Engine Loads.....	71
Figure 48: Location of PP and its SD at 3000 RPM and Varying Engine Loads	71
Figure 49: CA50 and its SD at 3000 RPM and Varying Engine Loads	72
Figure 50: Effect of Engine Speed on IMEP Cylinder-to-Cylinder Variations.....	74
Figure 51: Effect of Engine Speed on Peak Pressure Cylinder-to-Cylinder Variations	74
Figure 52: Effect of Engine Speed on Location of PP Cylinder-to-Cylinder Variations	75
Figure 53: Effect of Engine Speed on CA50 Cylinder-to-Cylinder Variations.....	75
Figure 54: Effect of Engine Load on IMEP Cylinder-to-Cylinder Variations	76
Figure 55: Effect of Engine Load on Peak Pressure Cylinder-to-Cylinder Variations	76
Figure 56: Effect of Engine Load on Location of PP Cylinder-to-Cylinder Variations.....	77
Figure 57: Effect of Engine Load on CA50 Cylinder-to-Cylinder Variations	77
Figure 58: Effect of Engine Speed on Cylinder #3.....	87
Figure 59: Effect of Engine Load on Cylinder #3	87
Figure 60: Effect of Engine Speed on Cylinder #5.....	88
Figure 61: Effect of Engine Load on Cylinder #5	88
Figure 62: Effect of Engine Speed on Cylinder #7.....	89
Figure 63: Effect of Engine Load on Cylinder #7	89
Figure 64: Effect of Engine Speed on Cylinder #1 (Repeated).....	90
Figure 65: Effect of Engine Load on Cylinder #1 (Repeated).....	90
Figure 66: Effect of Engine Speed on Cylinder #2.....	91
Figure 67: Effect of Engine Load on Cylinder #2	91
Figure 68: Effect of Engine Speed on Cylinder #4.....	92
Figure 69: Effect of Engine Load on Cylinder #4	92
Figure 70: Effect of Engine Speed on Cylinder #6.....	93
Figure 71: Effect of Engine Load on Cylinder #6	93
Figure 72: Effect of Engine Speed on Cylinder #8.....	94
Figure 73: Effect of Engine Load on Cylinder #8	94
Figure 74: Effect of Engine Speed on Cylinder #3.....	95
Figure 75: Effect of Engine Load on Cylinder #3	95
Figure 76: Effect of Engine Speed on Cylinder #5.....	96
Figure 77: Effect of Engine Speed on Cylinder #5.....	96
Figure 78: Effect of Engine Speed on Cylinder #7.....	97
Figure 79: Effect of Engine Speed on Cylinder #7.....	97
Figure 80: Effect of Engine Speed on Cylinder #1 (Repeated)	98
Figure 81: Effect of Engine Load on Cylinder #1 (Repeated).....	98
Figure 82: Effect of Engine Speed on Cylinder #2.....	99
Figure 83: Effect of Engine Load on Cylinder #2	99
Figure 84: Effect of Engine Speed on Cylinder #4.....	100
Figure 85: Effect of Engine Load on Cylinder #4	100
Figure 86: Effect of Engine Speed on Cylinder #6.....	101
Figure 87: Effect of Engine Load on Cylinder #6	101
Figure 88: Effect of Engine Speed on Cylinder #8.....	102

Figure 89: Effect of Engine Load on Cylinder #8	102
Figure 90: IMEP and its SD at WOT and Varying Engine Speeds	103
Figure 91: CA50 and its SD at WOT and Varying Engine Speeds	103
Figure 92: Peak Pressure and its SD at WOT and Varying Engine Speeds	104
Figure 93: Location of PP and its SD at WOT and Varying Engine Speeds.....	104
Figure 94: IMEP and its SD at 3000 RPM and Varying Engine Loads	105
Figure 95: CA50 and its SD at 3000 RPM and Varying Engine Loads	105
Figure 96: Peak Pressure and its SD at 3000 RPM and Varying Engine Loads.....	106
Figure 97: Location of PP and its SD at 3000 RPM and Varying Engine Loads	106
Figure 98: Technical Data for Kistler Reference Transducer 6052A1	107
Figure 99: Schematic of Kistler Reference Transducer 6052A1	107
Figure 100: 6052A1 Pressure Difference Curve compared to a Water-Cooled Kistler 7061B [22].....	108
Figure 101: Technical Data and Schematic for Kistler Test Transducer 6117.....	108
Figure 102: Schematic of Kistler Test Transducer 6117	109
Figure 103: Technical Data for Optrand Transducer.....	110
Figure 104: Calibration Certificate for Reference Transducer	111
Figure 105: Calibration Certificate for Kistler Test Transducer #13.....	112

LIST OF TABLES

Table 1: Test Transducer Configurations.....	23
Table 2: PMEP Errors averaged over 500 Cycles at 3000 RPM	50
Table 3: ANOVA on the Two Sets of Reference Transducer Data.....	55
Table 4: ANOVA on the Three Types of Pressure Transducer Tested	56
Table 5: Effect of Engine Speed on Combustion Performance Parameters arranged Bank-to-Bank	79
Table 6: Effect of Engine Load on Combustion Performance Parameters arranged Bank-to-Bank	80

LIST OF SYMBOLS AND ABBREVIATIONS

Adapt-CAS	Advanced Drivetrain and Powertrain Testing Combustion Analysis System
ADC	Analog-to-Digital Converter
ANOVA	Analysis of Variance
ASIC	Application Specific Integrated Circuit
ATDC	After Top Dead Center
BDC	Bottom Dead Center
BMEP	Brake Mean Effective Pressure
BTDC	Before Top Dead Center
CA50	Crank Angle of 50% Mass Fraction Burned
CAD	Crank Angle Degrees measured with respect to TDC of the firing stroke
CDM	Crankshaft Data Marker
CNG	Compressed Natural Gas
DOF	Degrees of Freedom
EDM	Electrical Discharge Machining
FSR	Full Scale Range
IMEP	Indicated Mean Effective Pressure
LED	Light Emitting Diode
MAP	Manifold Absolute Pressure
MBT	Minimum Spark Advance for Best Torque
PMEP	Pumping Mean Effective Pressure
PP	Peak Pressure
PPR	Pulse Per Revolution
RPM	Revolutions Per Minute
RTP	Real Time Processor
RTV	Silicone Sealant
SD	Standard Deviation
TDC	Top Dead Center
WOT	Wide Open Throttle
a_b	Mounting base or reference acceleration ($f/f_n = 1$)
a_o	Output acceleration
A_p	Area of the passage
c	Speed of sound
Δp	Pressure drop
ΔP	Pressure difference
$\overline{\Delta P}$	Average pressure difference
δP_{test}	Uncertainty in test transducer output
δP_{ref}	Uncertainty in reference transducer output
δZ	Total uncertainty

f	Frequency at any given point of the curve (Hz)
f_n	Undamped natural (resonant) frequency (Hz)
l_p	Length of the passage
μ	Viscosity
n	Number of engine cycles
P_{ref}	Cylinder pressure from the reference transducer
P_{test}	Cylinder pressure from the test transducer
Q	Factor of amplitude increase at resonance
ρ_c	Density in the cavity
R_H	Hydraulic Radius
V_c	Volume of the cavity
ω_n	Helmholz resonant frequency
ω_s	Standing wave resonant frequency

CHAPTER 1: INTRODUCTION

In present day automotive engineering, a substantial challenge faced by engineers is that of emission reduction. Vehicle emissions have been reduced approximately 95% since pre-controlled times, and reductions up to 98% are required in the near future. Specifically, this translates into emission reduction at cold start, since approximately 90% of the pollutants that come from the tailpipe of a vehicle occur within the first two minutes of engine operation. With current engine configurations and control strategies, these cold start emissions are mainly due to the warm-up period required for the oxygen sensor and catalytic converter.

Future engine control strategies have been proposed that rely on cylinder pressure as a fundamental operating principle. The main advantage of such a system is that feedback can be given immediately from the moment of engine firing for use in closed-loop control. There is no warm-up period required for the pressure transducer.

Internal combustion engine cylinder pressure is an almost instantaneous and direct measure of the engine operation and thus offers several engine monitoring and control capabilities. For instance the implementation might include:

- Air-fuel ratio balancing between cylinders by accurate estimates of inducted air and residual gas fraction
- Individual cylinder spark timing control
- Detection of misfire and knock
- Cylinder disabling
- Transition from homogenous to stratified charge (lean burn) operation in a directly fuelled engine

A number of sensors used at present such as the mass airflow sensor, boost pressure sensor, oxygen sensor, and knock sensor could become obsolete with the application of an individual cylinder pressure sensor.

There has been and continues to be a growing amount of research on cylinder pressure based engine control from automotive manufacturers [1, 2, 3], academia and government [4, 5, 6], and pressure transducer manufacturers [2, 7].

It is universally recognized that a successful cylinder pressure based engine management system requires a low-cost, durable transducer that: produces highly accurate data, has a high frequency response, is not too large to present installation challenges, has low power consumption, and is insensitive to varying thermal loads during engine operation.

The European Community partially funded a program named AENEAS [2], which was set up by Ricardo, Kistler, and DaimlerChrysler to study the application of a new cylinder pressure transducer and innovative algorithms for engine management systems. The prototype transducer evaluated in the AENEAS program was a piezo-resistive pressure transducer with a silicon-on-insulator sensor chip to reduce the cost and increase reliability.

Another innovative transducer that was developed to meet the stringent requirements of not only range and stability, but also price, size, and durability is the optical fiber based pressure-measuring device from Optrand Incorporated. Such a unit currently costs only about half as much as its piezoelectric equivalent, with the intent that it will one day be mass produced for only ten dollars per transducer.

The overall objective of the present study is to evaluate the performance of a spark plug mounted optical fiber pressure transducer and a spark plug mounted piezoelectric pressure transducer. The evaluation is focused on quantifying the effects of thermal shock on both ensemble-averaged and individual cycle cylinder pressure over a wide range of operating conditions. The specific objectives include:

1. To gain an understanding of how thermal shock impacts both types of transducers and how thermal shock errors vary with engine operating conditions in terms of absolute and percentage values.
2. To quantify the variability of thermal shock effects on a cycle-to-cycle basis for both types of transducers.
3. To quantify cylinder-to-cylinder variations within the engine utilizing the better performing transducer.

CHAPTER 2: LITERATURE REVIEW

For almost as long as the internal combustion engine has been in existence, so has the method of measuring in-cylinder pressure been used for engine analysis. Early mechanisms used for cylinder pressure measurements are described in books by Stone [8], Obert [9], and Heywood [10]. Modern systems described in [11] prove to be much better at accurately measuring in-cylinder pressure and can be used to quantify the amount of thermal shock experienced by different types of pressure transducers.

Such work has been completed in the past, as far back as 1967 by Brown [12]. In his experiments, a sector wheel was rotated by an electrical motor in front of both a transducer and a surface thermocouple mounted in a dummy transducer. A propane torch was held so that the flame either touched the diaphragm or was chopped by the sector wheel. By completely eliminating pressure as a variable, the sensitivity of each transducer to periodic heating was measured.

In 1975, work by Lancaster et al [13] compared the logarithmic P-V diagram of an engine cycle from a water-cooled transducer to one obtained with another transducer known to have significant thermal effects. With the latter transducer, the expansion line of the $\log P - \log V$ diagram curved drastically near bottom dead center and the gas exchange process showed a crossover in pressures, forming what they called the “bowtie” effect.

In 1990, Randolph [14] fitted three types of passage adapters aimed at reducing the amount of thermal shock to Kistler 6121 transducers and compared them to a flush mounted transducer of the same type. The three types of passages were (1) single slot, 1 mm diameter, 2 mm deep, (2) multiple slot, 13 parallel slots, 0.15 mm wide, 0.45 mm centers, 2 mm deep,

and (3) sintered porous metal disk. The third type of passage was quickly eliminated from the comparison due to excessive pressure drop. The first type of passage was found to degrade data quality under some operating conditions due to Helmholtz resonances occurring around 21 kHz. However, when comparing the flush mounted transducer to the transducer with the multiple slot it was found that the thermal shock effects on the flush mounted transducer were greater, leading to an increase in intracycle variability as demonstrated by his unique method of analysis.

In 1992, Kuratle and Marki [15] investigated the possible shortcomings of the individual components of a pressure indicating measuring chain. They found a relationship between short term drift (thermal shock) and Indicated Mean Effective Pressure (IMEP) error for the transducers used. They also concluded that the low pressure signal can be considerably wrong due to long recovery times of the transducer, and that an accurate gas exchange analysis may be impossible. Further, in 1993, Kuratle [16] suggested that the Kistler spark-plug mounted transducer is a powerful and easy to use development tool for internal combustion engines. This was substantiated with performance data of 0.65 bar maximum thermal shock error, IMEP error of 0.2%, and a similar coefficient of variation of IMEP compared to the 7061 Kistler water-cooled transducer

In 1999, Rai et al [3] compared many types of non-cooled Kistler transducers (6125A, 6123, 6052A) against a water-cooled Kistler transducer (6061B) in a Ford 1.8L 4 cylinder gasoline engine. From their research, they concluded that the type 6052A was the best performing non-cooled Kistler transducer, producing a maximum thermal shock error of -0.2 bar and a difference in IMEP of only -0.7% at 2000 Revolutions Per Minute (RPM) and 7 bar brake mean effective pressure. They also found that coating the diaphragm of the

transducer with a silicone sealant reduced thermal shock errors of IMEP by 75% and had no adverse effects on pressure data quality.

In 2001, Ulrich et al [7] tested their Optrand 1.7 mm optical fiber based pressure transducer against a coated and un-cooled Kistler 6051 transducer in a single cylinder Genset engine. They quoted the high pressure data from the optical fiber transducer as being within 0.5% of the Kistler transducer and its low pressure data as superior to that of the Kistler transducer. The superior performance was attributed to the miniature diaphragm size.

The application of the in-cylinder pressure transducer for the purpose of engine control has been studied extensively by Powell [4]. He states that no one application of cylinder pressure measurements alone justifies the cost of the transducers, but that if more than one capability is utilized the additional cost is acceptable, the most promising of which appear to be misfire detection, individual cylinder spark control, and air-fuel ratio balancing between cylinders. This approach has been adopted by General Motors where they have developed a low-cost cylinder pressure based engine control system for optimizing spark timing, exhaust gas recirculation, air-fuel ratio balancing, misfire and partial burn detection, knock detection, and cold start emissions [17]. The method called Pressure Ratio Measurement relies on pressure data from their non-intrusive Spark-Plug-Boss transducer which is divided by the motored pressure to form the pressure ratio. Both papers demonstrated improvements in engine efficiency and power and concluded that both the cost and time of engine calibration could be reduced.

CHAPTER 3: PIEZOELECTRIC PRESSURE TRANSDUCERS

In order to generate a conveniently measurable electrical output from a pressure input, that pressure must first be converted into a proportional strain. This strain is then transmitted to an electrical transduction element that generates the required signal. Thus, piezoelectric pressure transducers are comprised of two main components, one mechanical and one electrical. The mechanical element is the diaphragm, and the electrical element is the quartz crystal.

Quartz (silicon dioxide, SiO_2) occurs in nature in the form of crystals. For a long time natural quartz was used to make transducers, but its inevitable impurities gave rise to widely scattered sensitivities from one transducer to another. Consequently, there is now a trend toward artificially grown quartz with much higher purity, giving transducers of uniform sensitivity. Although the charge yield (coulombs/Newton) of these quartz crystals is relatively low compared with other piezoelectric materials, quartz exhibits some particularly valuable properties. These include:

- High stiffness around $350 - 400 \text{ kN/cm}^2$ and resulting high natural frequency
- Temperature resistance up to some 500°C
- Almost constant sensitivity over a wide temperature range (Figure 1)
- High insulation resistance around 10^{14} ohms
- High linearity and negligible hysteresis

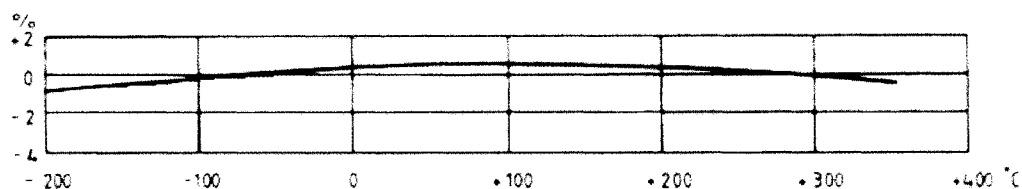


Figure 1: Relative Sensitivity Change vs. Temperature [17]

Of the large number of piezoelectric materials available today, quartz is preferred in transducer designs on account of these good measuring properties and ease of use. Unlike piezoelectric ceramics which are a result of extensive manufacturing, quartz is able to generate electrical charges on certain crystal faces under mechanical stressing already in its raw state. This physical effect, discovered by the brothers Pierre and Jacques Curie in 1880 is called the direct piezoelectric effect. The following direct piezoelectric effects are distinguished according to the position of the quartz crystal axes in relation to the force sustained:

- Longitudinal effect
- Transverse effect
- Shear effect

Assemblies utilizing the transverse effect in quartz are employed almost exclusively in current pressure transducers. With the transverse effect, under the action of a force F_y in the direction of one of the neutral crystal y-axes, an electrical charge is set up on the surfaces of the x-axis polar to it (Figure 2). It is therefore possible to obtain a greater charge by suitable geometry and arrangement of the quartz elements.

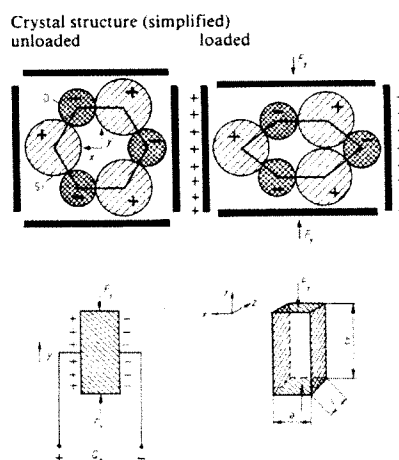


Figure 2: Transverse Piezoelectric Effect [17]

3.1 Transducer Design

A transducer utilizing the transverse piezoelectric effect is shown in Figure 3 and consists of three quartz columns Q joined rigidly to the support G through the temperature compensator T by the preload sleeve H. Due to this preloading, good linearity is attained and measurement of under pressures is made possible.

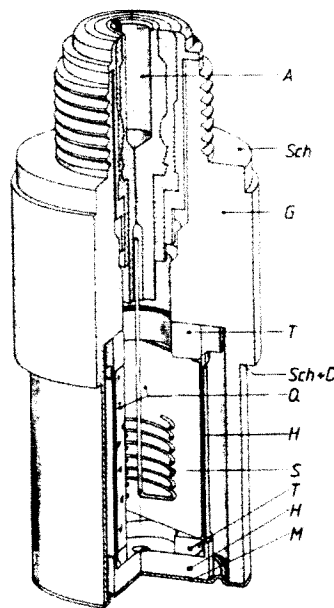


Figure 3: Kistler Piezoelectric Pressure Transducer Design [19]

The pressure P_y acts on the diaphragm M and is converted according to the active surface A_y into a force F_y , which loads the three quartz columns. This gives:

$$F_y = A_y * P_y$$

The quartz columns give a high impedance electrical charge signal (measured in picocoulombs) that is directly proportional to the force applied. The contact surfaces of the quartz are coated with silver and are arranged so that under compressive stressing the inner

conductors acquire a negative charge. A centrally arranged noble metal spiral S conducts the charge from the inner quartz surfaces to the insulated plug connection A. The outer surfaces are connected conductively with the housing (ground). The transducers are fitted by restraining them between the two shoulders Sch. The seal D on the bottom shoulder assures sealing against the measuring space.

Piezoelectric transducers may be regarded as under-damped, spring mass systems with a single degree of freedom. They are modeled by the second order differential equation whose solution is:

$$\frac{a_0}{a_b} \equiv \frac{1}{\sqrt{\left[1 - \left(\frac{f}{f_n}\right)^2\right]^2 + \left(\frac{1}{Q^2}\right)\left(\frac{f}{f_n}\right)^2}}$$

f_n = undamped natural (resonant) frequency (Hz)
 f = frequency at any given point of the curve (Hz)
 a_o = output acceleration
 a_b = mounting base or reference acceleration ($f/f_n = 1$)
 Q = factor of amplitude increase at resonance

A typical frequency response curve is shown in Figure 4. The natural frequency of the piezoelectric transducers used in this study occurs at approximately 120 kHz. The usable frequency range is found by multiplying the natural frequency by 9/40, giving a value of 27 kHz. This is a very important transducer characteristic when investigating knock in internal combustion engines. The usable frequency range should extend far beyond the knock frequencies in order to avoid resonance and thus incorrect measured results. The first harmonic of engine knock occurs at between 6-8 kHz. In order to capture up to the third harmonic from the pressure signal, the usable frequency range must be at least 24 kHz, which in this case it is.

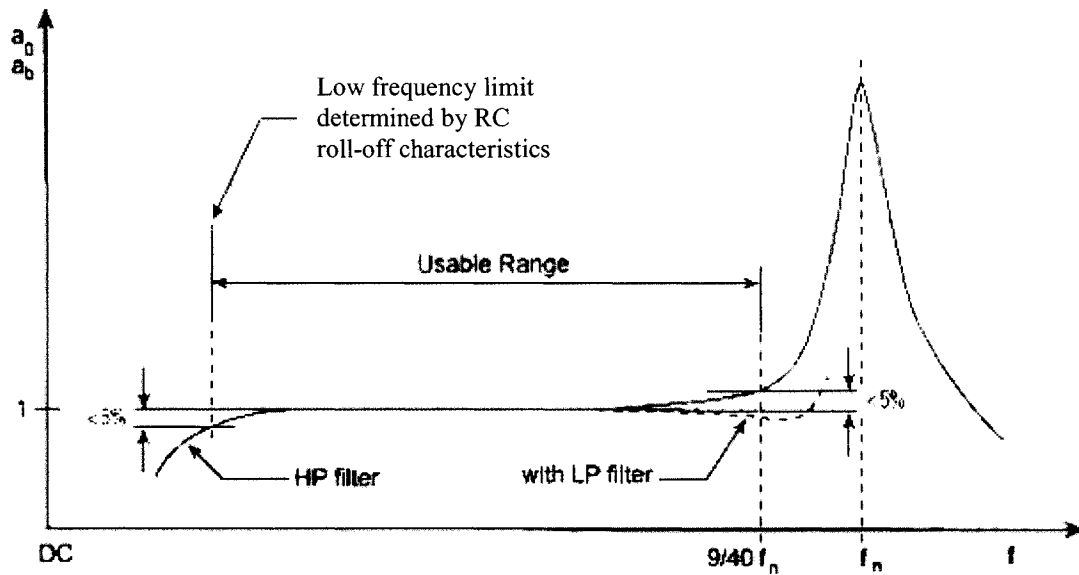


Figure 4: Typical Frequency Response of a Piezoelectric Transducer [20]

3.2 Charge Amplification

The charge amplifier converts the high impedance electrical charge from the quartz crystal to a low impedance voltage that is usable by the Analog-to-Digital Converter (ADC). As the charge is passed from the transducer to the charge amplifier, it is extremely sensitive to corruption from electromagnetic interference, radio frequency interference and triboelectric (motion induced) effects. For this reason a short, low-noise cable is required between the transducer and amplifier. High insulation resistance is also required within the transducer, connector, and amplifier, otherwise the electrical charge would leak away. As there is never infinitely high impedance, no long-term static measurements can be performed with piezoelectric transducers. Environmental contaminants on the connector such as moisture, dirt, oil, or grease, contribute to reduced insulation resulting in signal drift and inconsistent results.

Two important considerations in the practical use of charge amplifiers are the level of filtering applied and time constant used.

3.2.1 Filtering

Both valve closure noise and engine vibration at high engine speeds can disturb the pressure transducer signal. A low pass filter in the amplifier can reduce this noise, however a phase shift occurs which has a negative effect on the pressure trace. In Figure 5, the same pressure data is plotted with a 180 kHz filter and a 1 kHz filter.

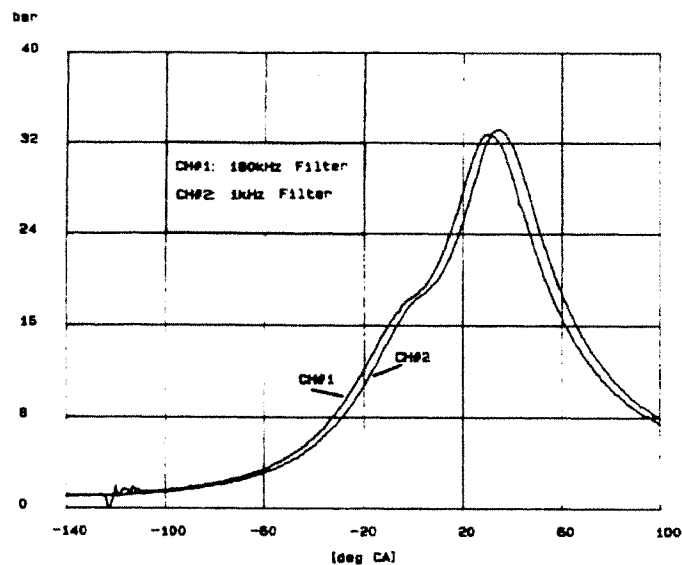


Figure 5: Filtering Effects [14]

By applying the 1 kHz filter, a phase shift of approximately 4.5 Crank Angle Degrees (CAD) leading to an error in IMEP of +12%. Thus it is noted that neither a filter nor any analytical smoothing functions are good solutions for high precision measurements.

3.2.2 Time Constant

The rate at which charge leakage occurs in the resistive-capacitive circuit of the charge amplifier follows an exponential decay. Time constant is defined as the time required

for a transducer or measuring system to discharge its signal to 37% of the original value from a step change of measure. With most charge amplifiers, either a Short, Medium, or Long time constant is selectable. With a long time constant, very low frequencies are transmitted and no signal distortion occurs. With a Medium or Short time constant, the measuring signal always returns exponentially to zero and low frequencies are cut off (acting as a high pass filter). The only situation where a time constant shorter than Long would be used is if the measuring system had significant charge leakage due to insulation problems. In this case a short time constant would prevent the amplifier from saturating.

CHAPTER 4: OPTICAL FIBER PRESSURE TRANSDUCERS

An Optrand optical fiber pressure transducer consists of the following three basic components which are arranged as shown in Figure 6:

- Sensing head directly exposed to the combustion pressure
- Fiber optic cable
- Module containing all optical and electronic components

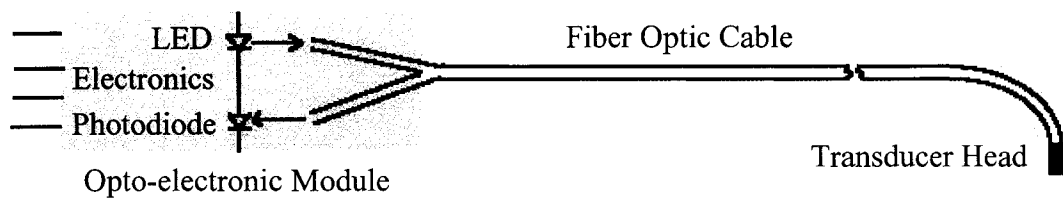


Figure 6: Optical Fiber Transducer Layout [21]

The transducer head (Figure 7) consists of an Inconel diaphragm that is laser welded to a metal housing containing a fiber holding ferrule and two fibers bonded inside the ferrule.

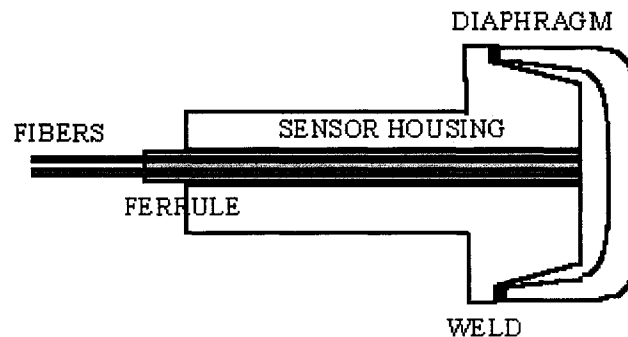


Figure 7: Transducer Head Construction [21]

The transducer's response results from the pressure-induced diaphragm displacement that changes the optical signal transmitted from the sending fiber to the receiving fiber upon reflection from the diaphragm. Over a large displacement range, the light intensity collected by the receiving fiber may either decrease or increase with increasing diaphragm to fiber

distance as shown in Figure 8. The linearity is affected by the diaphragm's mechanical stiffness as well as the linearity of the light intensity change due to diaphragm movement.

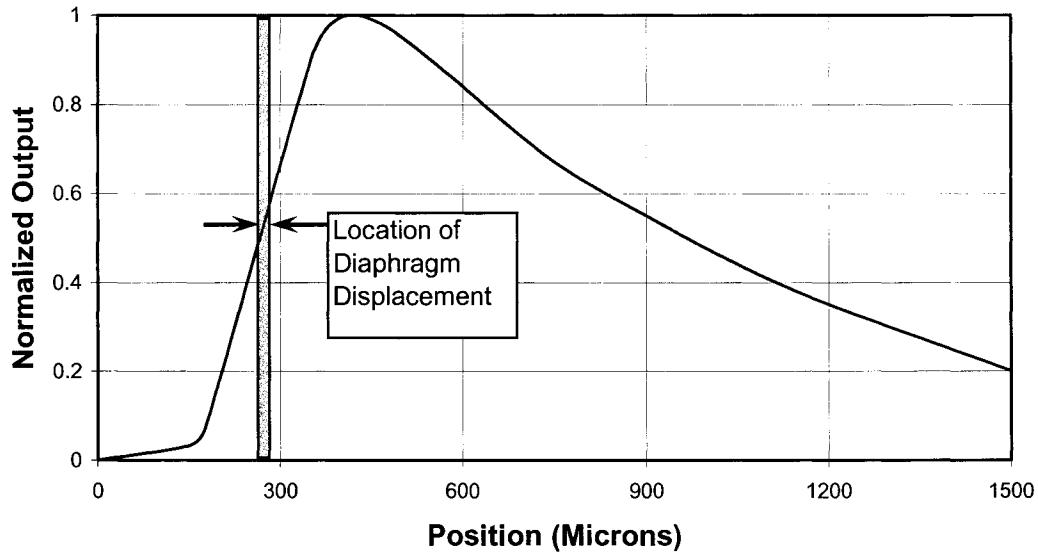


Figure 8: Light Intensity vs. Fiber to Diaphragm Distance [21]

4.1 Diaphragm

In an optical fiber pressure transducer, the diaphragm displacement is quite small, typically around 20 microns. The hat-shaped Inconel diaphragm with varying thickness across its diameter is used to meet the requirement of high strength at combustion temperatures, low creep, and a fatigue life of hundreds of millions of pressure cycles. Preferably, the diaphragm has to be as small as possible so that the transducer requires the least amount of space for mounting. At present, the smallest transducer has a diaphragm diameter of 1.7 mm, making it suitable for integration into production spark plugs. However, a very small diameter creates a significant design challenge due to the simultaneous requirement of large diaphragm deflection (for high signal to noise ratio) and low stresses required for a long lifetime.

4.2 Opto-Electronic Module

The opto-electronic module contains a photodiode, a Light Emitting Diode (LED), and a dedicated Application Specific Integrated Circuit (ASIC). Two input electrical pins are for power supply and ground while the output pin is for sensor output and fault diagnostics. Unlike high impedance piezoelectric devices, optical fiber transducers require an external power source and provide an output signal in the range of 0-5 volts, thus not requiring a charge amplifier in the measuring chain.

The ASIC controls light intensity, amplifies and filters the photodiode signal (filtering characteristics not available), and provides the Auto-Referencing function. This technique corrects for signal drift by regulating LED light intensity in response to any undesirable environmental conditions that may alter minimum detected light intensity. Baseline light intensity in fiber optic sensors may vary due to optical link transmission fluctuations resulting from connectors' mechanical and thermal instabilities, fiber bending, light source or detector temperature dependence, or their aging over time. A side benefit of the technique is the availability of sensor health monitoring output. By continuously monitoring the LED current level or its rate of change, one can identify potential sensor failure before it occurs. This ability is particularly important in control applications where transducer failure may cause malfunction of the controlled device.

CHAPTER 5: PRESSURE TRANSDUCER MOUNTING AND TEMPERATURE EFFECTS

When used in combustion environments, there are generally two ways of mounting a pressure transducer. In either case, it is essential to minimize the effects of thermal shock.

5.1 Flush Mount

The first mounting strategy is the flush mount, in which the sensing face is flush with the wall of the combustion chamber. This method makes the transducer exceedingly susceptible to thermal shock. Thermal shock is described as high temperature transients within one engine cycle resulting in transducer thermal shock error. The transducer is heated up by the propagating flame and the burned gas that the temperature of which can reach more than 2000°C. The exposed parts of the transducer may reach up to 300°C [16] causing distortions of the diaphragm and mount and also a variation in the Young's Modulus of the quartz crystal in piezoelectric devices. Therefore, thermal shock causes the transducer to produce an output that is also temperature and not just pressure dependant.

There are a number of ways to reduce this temperature dependency in pressure transducers. One method is to water-cool the transducer. Water-cooling ensures that the transducer operates in an environment with a constant temperature, thus negating the effects of thermal shock. However, a water-cooled transducer is significantly larger than a non-cooled transducer, and presents installation challenges in engines where combustion chamber space is limited. Another method is to coat the transducer diaphragm with a thin layer of RTV (silicone sealant), effectively damping out rapid changes in heat flux at the diaphragm. However, this method is limited in operation because the combustion process will eventually burn the RTV away over time.

5.2 Recessed Mount

The second mounting strategy involves recessing the transducer face from the combustion chamber and thus removing it from the high temperature environment. The passage leading to the transducer face can quench the flame before it contacts the diaphragm, and if designed properly will not cause any channel resonances. If is not designed properly, the implementation of the passage will result in signal degradation and erroneous pressure signals.

The following equations describe the frequencies at which standing wave and Helmholtz resonances occur when a pressure disturbance is introduced at one end of the passage [14]:

$$\omega_s = \frac{c}{2l_p} \quad \omega_h = \frac{c}{2\pi} \sqrt{\frac{A_p}{l_p V_c}}$$

Both resonances are dependant on the length of the passage, and the Helmholtz resonance is also affected by the cross-sectional area of the passage and the volume of the cavity directly in front of the transducer face. It is desirable to keep both ω_s and ω_h large enough so that they cannot be confused with in-cylinder oscillations induced by knock. A resonance frequency of greater than 20 kHz is generally large enough to isolate the first few harmonics driven by knock. The pressure drop in the passage as a function of time is expressed as [14]:

$$\frac{d\Delta p}{dt} = \left[\frac{2l_p V_c}{R_H^2 A_p} \right] \mu(t) \frac{d \ln(\rho_c)}{dt}$$

The above equations show that in order to obtain cylinder pressure data without pipe oscillations and with minimal pressure drop, the length of the passage must be small and the cross-sectional area of the passage must be large. Also, short passages avoid a significant phase lag in the transducer output and result in only a very small increase (essentially negligible) in combustion chamber volume.

CHAPTER 6: EXPERIMENTAL SETUP

6.1 Engine

A DaimlerChrysler 4.7L V-8 Compressed Natural Gas (CNG) fuelled test engine is used for the experimental measurements (Figure 9).

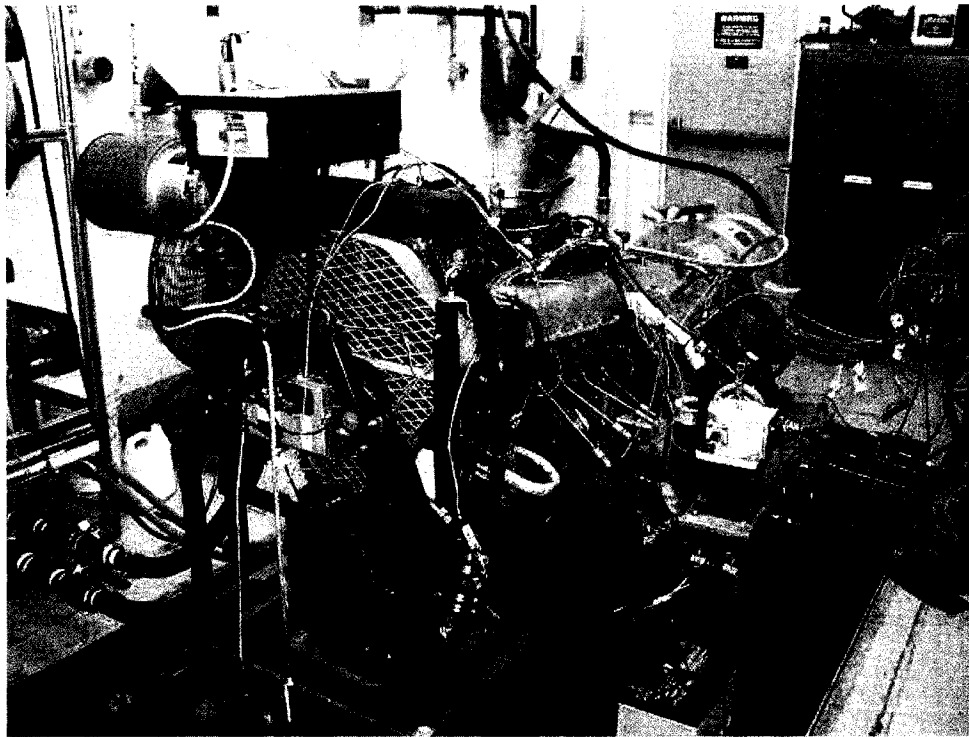


Figure 9: Engine Dynamometer Facility

The bore and stroke are 93 mm and 86.5 mm respectively with a compression ratio of 9.3:1. Figure 10 shows the configuration of cylinder No. 1's combustion chamber and the location of the wall mounted (red oval) and spark plug mounted (red circle) pressure transducers. The wall mounted transducer is shown removed from its mounting location in the cylinder head and is positioned directly above it for clarity (mounting hole not visible in this picture).

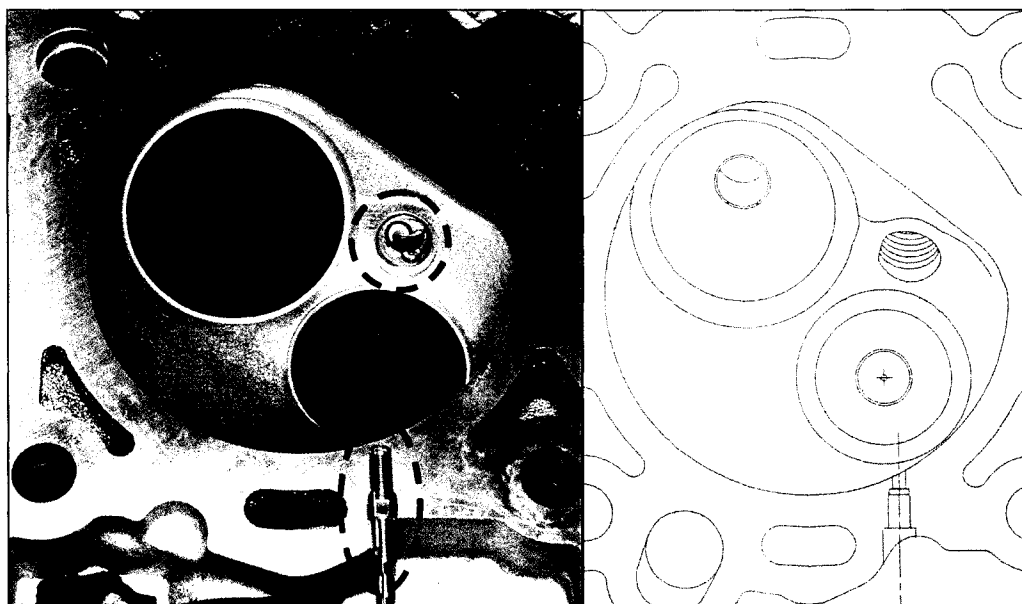


Figure 10: Cylinder No. 1 Combustion Chamber

6.2 Transducers

The wall mounted transducer is a Kistler 6052A1 (Figure 11) and was used as the reference transducer throughout this study since it is the most accurate non-cooled Kistler transducer for cylinder pressure measurement [3] (referred to as the “Kistler Wall” transducer hereafter). It exhibits a 0.5 bar maximum thermal shock error compared to the Kistler 7061B water-cooled transducer as shown in Figure 100 and was horizontally mounted into a specially machined cylinder head so that the transducer face is 4 mm from the combustion chamber wall. It sits in a heavily cooled area of the cylinder head surrounded by cooling jackets and a thin layer of silicone coating was placed on the diaphragm to reduce the effects of thermal shock. After collecting data from each cylinder, the reference transducer was removed and the layer of silicone coating was inspected to ensure that it had not burned away.

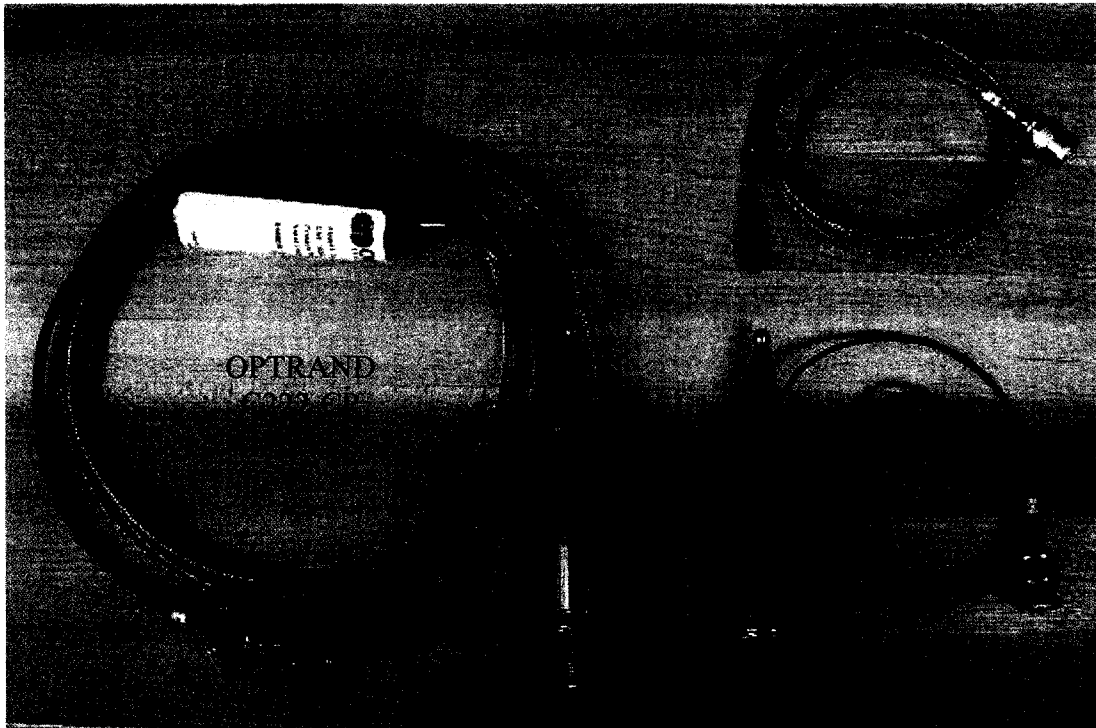


Figure 11: Reference and Test Transducers

The test transducers were the spark plug mounted transducers supplied by Kistler Instrument Corp. and Optrand Inc. (referred to as the “Kistler Spark” and “Optrand Spark” transducers in this paper). The Kistler Spark assemblies are type 6117 (Figure 11) and feature a 5 mm diameter piezoelectric transducer fitted into a custom spark plug with an off-center electrode (manufactured by BERU Corp.). The Optrand Spark assemblies are type C222-CP (Figure 11) and feature a 1.7 mm diameter optical fiber transducer fitted into the same type of BERU spark plug. By fabricating these assemblies, an unbiased comparison was ensured. A description of each spark plug mounted transducer assembly can be found in Table 1. The manufacturers specifications for all types of transducers used can be found in Appendix D as well as the calibration certification for the Kistler transducers. There is no calibration certificate for the optical fiber transducer as Optrand does not guarantee its

calibration. All transducer assemblies were tested in cylinder No. 1 against the Kistler 6052A1 wall mounted reference transducer.

	Type	Dia. (mm)	Electrode Orientation	Electrode Gap (mm)	Mounting	Recess (mm)	Heat Range
Optrand 7	C222-CP	1.7	Vertical	1	EDM	2	7
Optrand 8	C222-CP	1.7	Vertical	1	EDM	2	7
Optrand 9	C222-CP	1.7	Horizontal	1	Nut	2	7
Optrand 10	C222-CP	1.7	Horizontal	1	Nut	1	7
Kistler 11	6117BFD17	5	Vertical	1	Nut	3.5	7
Kistler 12	6117BFD17	5	Vertical	1	Nut	3.5	7
Kistler 13	6117BF17	5	Horizontal	1	Nut	3.5	7
Kistler 14	6117BF17	5	Horizontal	0.4	Nut	3.5	7

Table 1: Test Transducer Configurations

6.3 Data Acquisition and Processing

To collect and analyze the transducer data, an MTS Advanced Drivetrain and Powertrain Testing, Combustion Analysis System (Adapt-CAS) was used (Figure 12).

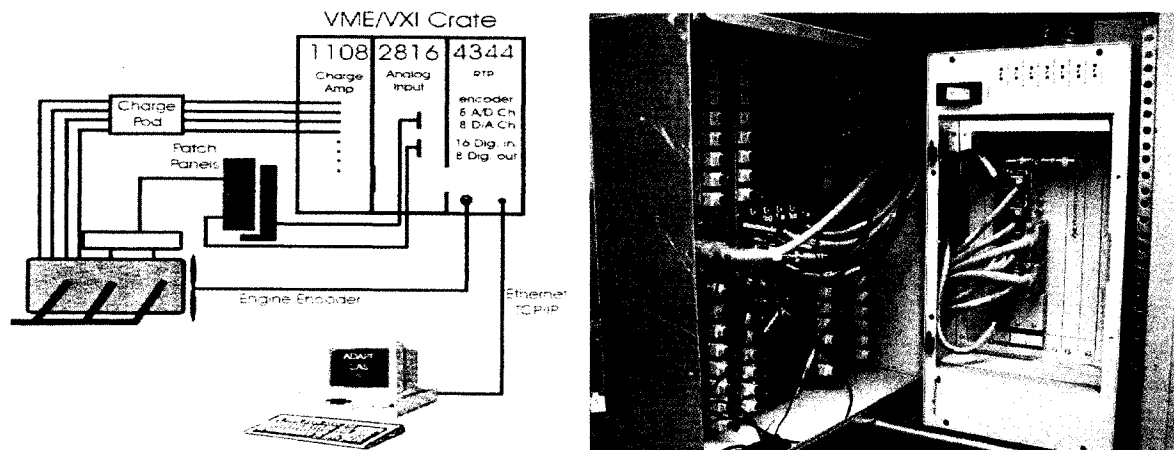


Figure 12: MTS Adapt-CAS System

The heart of this system is the V4344 Real-Time Processor (RTP) and controller module. This module stores digitized data and performs real-time, floating-point combustion

calculations. It also processes the engine encoder input, controls the flow of data, and communicates over an Ethernet connection to transfer data and results to the PC.

The V2816 analog input module is an Analog to Digital Converter (ADC) complete with sixteen input channels that sample at up to 1 MHz per channel with 12 bit resolution ($2^{12} = 4096$ discrete values). The input ranges are software selectable between ± 10 , 5, 2, and 1 volt Direct Current (DC). Up to four V2816 modules can be added to the CAS system for a total of 64 analog input channels.

The V1108 charge amplifier includes a charge pod mounted in the test cell to avoid the occurrence of noise and signal degradation common with long, low-level signal runs. This module uses a proprietary circuit to self-calibrate each signal channel. A valuable feature of the V1108 is its ability to “Auto-Track” cylinder pressure signals.

6.3.1 Auto-tracking

Whereas analog data is represented by continuously variable, measurable, physical quantities such as length, pressure or voltage, digital technology employs the binary system to represent discrete values that a computer (V4344) can read. The V1108 charge amplifier produces an analog signal that must be converted to a digital signal by the V2816 ADC. As shown in Figure 13, for any voltage value in the ± 5 volt Full Scale Range (FSR), there is a corresponding discrete bit value. How closely the bit value represents the voltage signal depends on the resolution. Resolution is used to describe how finely and precisely an analog signal can be converted into a digital signal. The greater the bits of resolution, the finer and more clearly an analog signal can be represented (resolved).

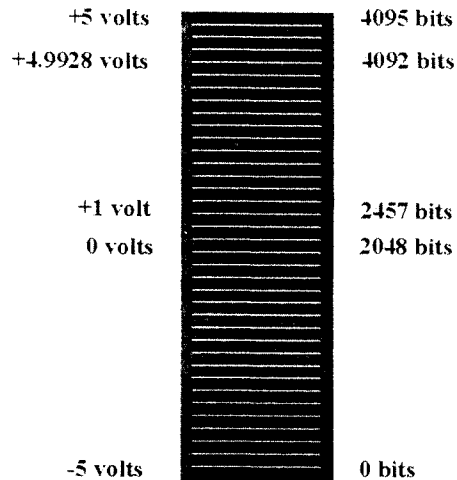


Figure 13: Analog to Digital Conversion [11]

Auto-tracking provides a non-zero offset voltage to extend the dynamic range of the recorded signal. It effectively doubles the resolution at which the pressure data is digitized, by forcing the range of the charge amplifier's output to increase from 0 to +5 volts to -5 to +5 volts. In addition to optimizing use of the full digitizer range (10 volts instead of 5 volts), auto-tracking also attempts to remove drift from the pressure signal.

During transient engine testing (speed and load change) thermal loads on the pressure transducer fluctuate. The ensuing thermal stresses cause the transducer to slightly deform and its output may not return at the end of an engine cycle to the exact same spot at which it started the engine cycle. This is known as signal drift and may cause the charge amplifier to saturate and clip the cylinder pressure trace if it is not compensated for. Figure 14 shows an example of the signal drift produced by a transducer when operating conditions change from high to low load.

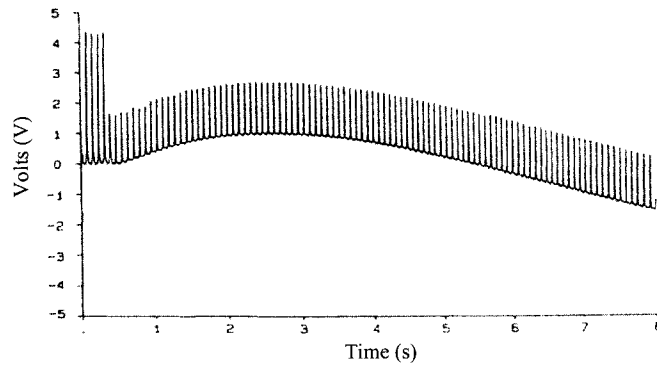


Figure 14: Signal Drift [23]

Auto-tracking keeps a cylinder pressure signal that is drifting due to thermal loads within the ADC range. It removes signal drift by forcing the analog voltage of the cylinder pressure signal to -4V at -180 CAD After Top Dead Center (ATDC) for every engine cycle. The benefits of autotracking on a drifting cylinder pressure signal are shown in Figure 15. As you can see, the signal encompasses the full +5V to -5V ADC range without exceeding it.

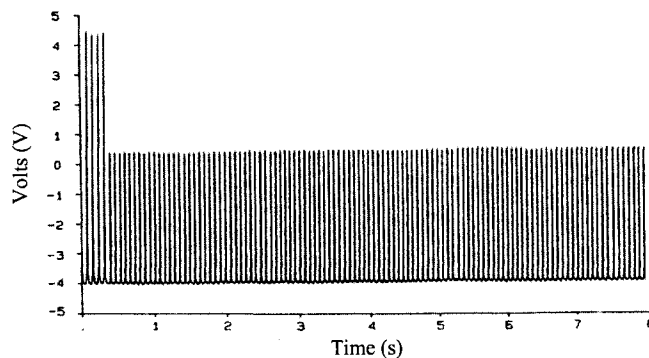


Figure 15: Autotracking Effects [23]

Since auto-tracking is applied within the V1108 charge amplifier, optical fiber pressure transducers do not take advantage of this feature. To compensate for signal drift, Optrand transducers use their own patented technique called auto-referencing, which is applied within the opto-electronic module.

6.3.2 Pegging

Piezoelectric pressure transducers are not absolute devices and thus only provide a relative measurement. They are dynamic devices that will provide an output only if the applied force is constantly changing. If a sudden force is exerted and held on a piezoelectric transducer, it will generate an equivalent charge signal that will eventually return to zero. Therefore, the transducer relies on the constantly changing pressure within the engine in order to output a signal. It is due to this non-absolute signal that an external reference is required to “peg” the cylinder pressure.

The reference value used is taken from the Manifold Absolute Pressure (MAP) transducer in the intake manifold. In order to complete the pegging process, this reference needs to be applied at some known point in the engine cycle where it most closely represents cylinder pressure. At -180 CAD when the crankshaft has reached Bottom Dead Center (BDC) and the intake valve is fully open, the pressure in the cylinder and that in the intake manifold are approximately equal. Therefore it is possible to use the MAP signal to peg or reference the cylinder pressure signal at this point. The MAP signal is sampled at -180 CAD and the cylinder pressure signal at -180 CAD is assigned the MAP value. Because pegging compensates for both relative pressures and signal drift, optical fiber transducers must also be pegged even if they are absolute devices.

It is worth noting the difference between auto-tracking and pegging. Auto-tracking is performed by the charge amplifier on the analog voltage signal to keep a drifting signal within the ADC range. Pegging is performed by the RTP on digitized data to produce absolute pressure values by referencing the MAP signal, which in turn compensates for temperature induced signal drift.

6.4 Crankshaft Encoder

An engine crankshaft encoder is used to “clock” the CAS system in the event-based mode. Unlike the time-based mode which lets a desired sampling rate be selected (ie. 100 kHz), the event-based mode captures data whenever it receives the appropriate signal from the encoder attached to the end of the crankshaft (Figure 16).

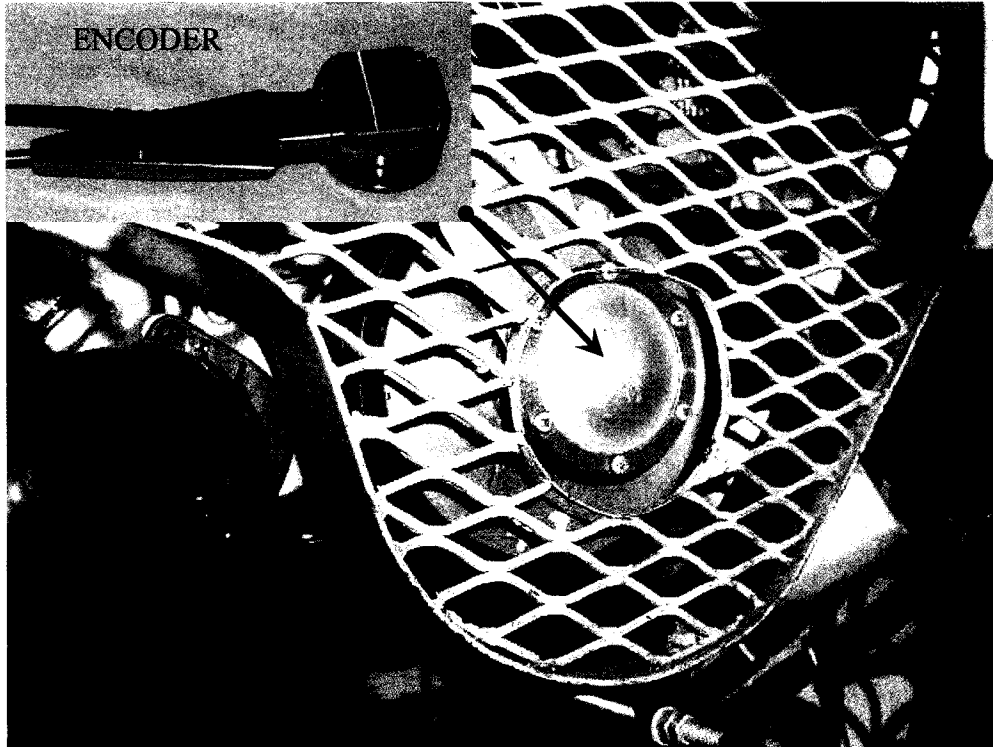


Figure 16: AVL Crankshaft Encoder

All crankshaft encoders output the following two signals:

- CDM (Crankshaft Data Marker, sometimes referred to as “clock”)
- PPR (Pulse Per Revolution, sometimes referred to as “reset”)

The PPR signal provides one pulse per engine revolution, indicating the crankshaft’s angular location relative to Top Dead Center (TDC) of cylinder No. 1. The CDM signal output is dependant on the encoder resolution. If the encoder resolution is 1° , the CDM signal provides one pulse for every crankshaft degree totalling 360 pulses per engine revolution. If

the encoder resolution is 0.5° , the CDM signal provides two pulses for every crankshaft degree totalling 720 pulses per engine revolution. It is at the rising edges of the CDM signal that CAS records all signal channels such as cylinder pressure and manifold absolute pressure. An example of the output from an encoder with 1° resolution is shown in Figure 17.

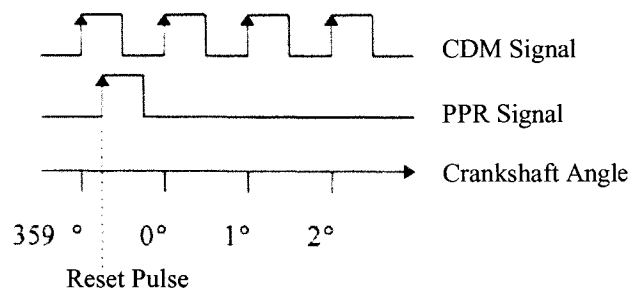


Figure 17: Crankshaft Encoder Output

In this example, CAS would record data at every CAD from 0° to 360° , and would then start to count over when it receives the reset pulse from the PPR signal. However, an engine cycle has 720° , requiring a reset pulse every engine cycle (1 per 720°) and not every engine revolution (1 per 360°). Therefore CAS calculates peak cylinder pressure at both reset pulse locations within an engine cycle and automatically ignores the reset pulse with the lower peak pressure. The final result is 720 crank-angle-based cylinder pressure measurements per engine cycle, all in relation to TDC firing of cylinder No. 1.

6.4.1 Top Dead Center Find

This utility within the CAS software will calculate the difference in CAD between the location of the reset pulse of the PPR signal and TDC of cylinder No. 1. Based on this calculation and the firing order and intervals, the exact location of the crankshaft relative to

TDC can be found for every cylinder. The calculation is done by computing the average motored cylinder pressure waveform of cylinder No. 1 and then using linear interpolation to find the crankshaft angles at which amplitudes on the right side of the curve equal amplitudes on the left side of the curve. The average value of these crankshaft angles is the resultant location of TDC cylinder No.1 relative to the reset pulse. This method assumes that peak cylinder pressure in a non-firing cylinder occurs at TDC.

6.5 Measuring Chain

The Kistler transducer signals were first passed through the 1108 charge amplifier with a long time constant and no filtering to convert the charge into a usable voltage. This step was not necessary with the Optrand transducer since its packaging performs the signal conditioning itself and outputs an appropriate voltage. The signals were then transferred to the V2816 ADC, which subsequently sent data to the V4344 module for calculations and logging. The transducers' outputs were pegged by referencing to manifold absolute pressure at inlet bottom dead center. CDM and PPR signals were generated by an AVL encoder at 1-degree crank angle resolution throughout the cycle.

6.6 Uncertainty

The method of pressure difference is used extensively when determining how closely the estimates of cylinder pressure from the test transducer are to the reference transducer and essentially to actual cylinder pressure. The equation describing the pressure difference is as follows:

$$\Delta P_{\text{test, ref}} = P_{\text{test}} - P_{\text{ref}}$$

The amount of uncertainty must be found in such measurements as part of an error analysis.

The total uncertainty is described by the following equation:

$$\delta Z = \sqrt{\left(\frac{\partial \Delta P}{\partial P_{test}} \delta P_{test}\right)^2 + \left(\frac{\partial \Delta P}{\partial P_{ref}} \delta P_{ref}\right)^2}$$

Since the partial derivative of the pressure difference with respect to each term is equal to one, this equation now becomes:

$$\delta Z = \sqrt{\delta P_{test}^2 + \delta P_{ref}^2}$$

In this equation, each term under the square root sign is the linear combination of the error present in the transducer and the error present in the CAS system. For both types of Kistler transducers the uncertainty as supplied by the manufacturer was equal to 0.1% FSR and amounts to 0.05 bar. For the Optrand transducer, the uncertainty in the measurements was not available from the manufacturer and therefore an error analysis cannot be completed. The uncertainty in the CAS system was supplied by the manufacturer and was given to be 1.0% FSR and amounts to 0.50 bar. By summing the squares of each type of error for each transducer and then taking the square root, an uncertainty of 0.50 bar was found for each transducer. Inserting these values into the above equation gives a total uncertainty in the pressure difference of 0.71 bar. This value is the uncertainty in the pressure difference if only one measurement was to take place. In the experiments completed for this research, data was averaged over 500 engine cycles and will therefore decrease the level of uncertainty as shown by the following equation:

$$\delta Z_{average} = \frac{\delta Z_{oncycle}}{\sqrt{n-1}}$$

Applying this equation to our data, the final uncertainty in the pressure difference averaged over 500 engine cycles is 0.03 bar.

For the individual cylinder analysis, the Kistler reference transducer was used for all measurements, and the uncertainty in the average estimated cylinder pressure provided by this transducer can be calculated as follows:

$$\delta Z_{average} = \frac{0.50}{\sqrt{500-1}}$$

Entering the uncertainty in the estimated pressure of one cycle for this transducer (0.50) and the number of engine cycles used in the analysis (500), a final uncertainty of 0.02 bar is calculated.

CHAPTER 7: EXPERIMENTAL MATRIX

The results presented in Chapter 9 were obtained at different operating conditions and with different data logging options for each analysis completed. This chapter summarizes the set-up used in each instance.

The operating conditions used for the Performance Variation was 1500 RPM and Wide Open Throttle (WOT). The purpose of this was to subject each transducer to the maximum amount of thermal shock possible and rank the performance of each transducer based upon their calculated percent difference in IMEP. The same operating conditions were used for the Intracycle Variability Analysis in order to minimize fluctuations in the transducers output due to vibration.

The remaining analyses (Global Comparison, Combustion Performance Parameters, and Cylinder-to-Cylinder Variations) involved investigating the effects of engine speed and engine load on cylinder pressure data quality from both types of transducers. Engine speed effects were examined at WOT and 1500, 2500, 3500, and 5000 RPM. Engine load effects were examined at 3000 RPM and Brake Mean Effective Pressures (BMEP) of 1.1 bar, 2.2 bar, 4.4 bar, and 8.8 bar (WOT).

Data quality was evaluated by calculating the following parameters:

- Pressure Difference
- Indicated Mean Effective Pressure (IMEP)
- Pumping Mean Effective Pressure (PMEP)
- Intracycle Variability
- Combustion Performance Parameters

In terms of data logging, 500 consecutive cycles of data were collected and averaged for each analysis except for the Intracycle Variability Analysis in which case only 91 cycles of raw cylinder pressure data were logged. This constraint was due to Microsoft Excel's 16-bit spreadsheet where only $2^{16} = 65536$ rows of data could be imported. 91 cycles of pressure data taken at 1° resolution amounts to 65520 data entries.

Throughout the testing, a stoichiometric air-to-fuel ratio was used as verified by the Horiba emissions bench. Also, a calibrated engine controller ensured that the spark timing was set at the Minimum spark advance for Best Torque (MBT) .

CHAPTER 8: PRESSURE TRACE ANALYSIS

The pressure data were acquired simultaneously from two different transducers installed on cylinder number one. The pair of transducers always included the Kistler Wall transducer and either the Optrand Spark or the Kistler Spark transducer. A test was comprised of acquiring and processing 500 consecutive cycles of cylinder pressure data from each pair of transducers in order to obtain a good statistical sample size. The individual pressure records were ensemble-averaged and the output from the Kistler Wall transducer was then subtracted from either the Kistler Spark or Optrand Spark output (depending on which spark plug was used for that test) to produce the difference between the two signals. Typical examples of such processed data using test transducers Kistler No. 13 and Optrand No. 9 are shown in Figure 18 and Figure 19 respectively, at an arbitrary operating condition.

Differences between the signals are due to gain and thermal shock errors of the transducers. Gain errors arise when the transducers operate at a temperature other than what they are calibrated for, as is the case here since the exact operating temperature of the transducers is unknown. Also, as engine operating conditions change so does the average temperature of the entire transducer resulting in somewhat inaccurate results due to the temperature sensitivity of the transducers (Appendix D). Therefore, the initially measured gain errors were compensated by gradual sensitivity changes of the test transducer until the pressure difference curve was relatively flat up to event 2 when the flame arrives at the transducer face. The sensitivity of the reference transducer was left constant throughout all of the testing at a value calibrated for 200°C. Based on Kistler Instrument Corp. published data on the Kistler Wall transducer used in this study [22], one can expect a minimal and constant pressure difference between transducers up to event 2.

Examples of pressure difference curves calculated with a -2% and +2% gain error of the test transducer are shown in orange and green respectively. In the case of the -2% gain error, the point at which the flame arrives at the test transducer becomes unclear. This is not the case with the +2% gain error, however this curve increases at a rate proportional to actual cylinder pressure up to event 2. This behavior verifies over-calibration of the test transducer compared to the reference transducer. The black pressure difference curve was calculated so that there was no gain error of the test transducer relative to the reference transducer and therefore only exhibits thermal shock error. This type of curve is used to quantify the amount of thermal shock demonstrated by the test transducer throughout the analysis.

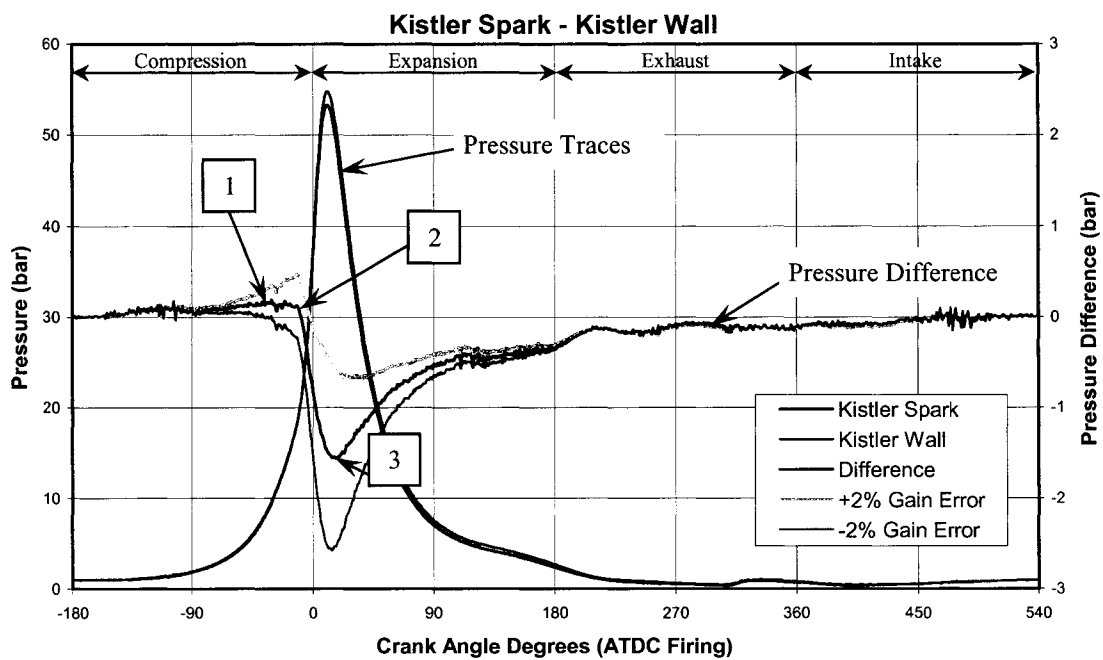


Figure 18: Typical Kistler Spark Pressure Difference

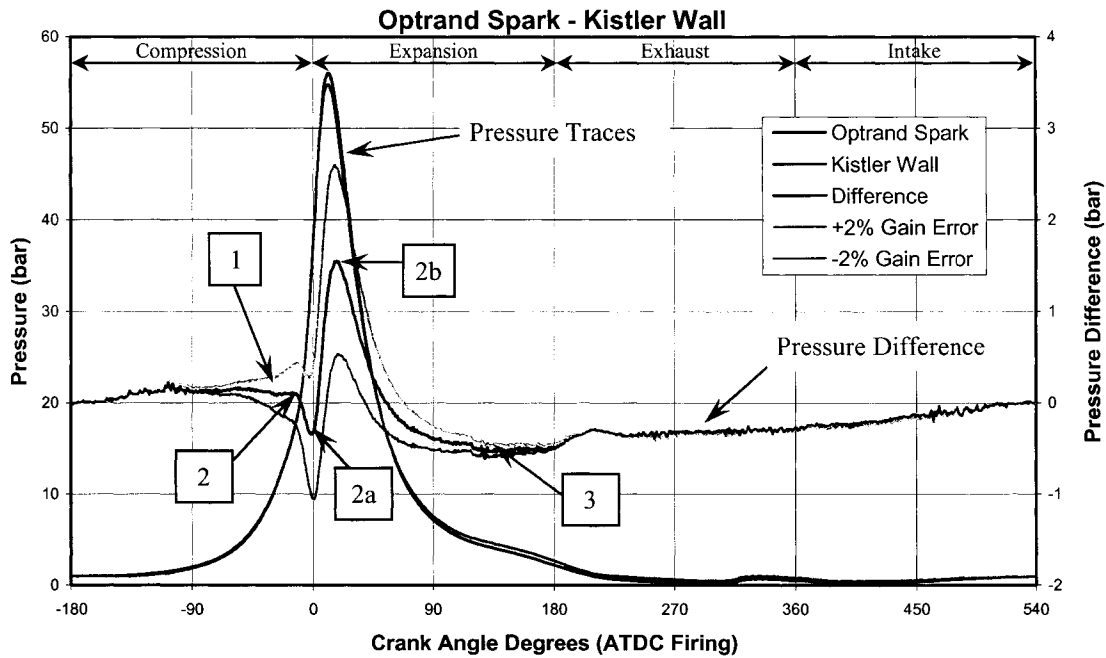


Figure 19: Typical Optrand Spark Pressure Difference

A number of characteristic events are identified on the pressure difference curves of Figure 18 and Figure 19. Event 1 marks the firing of the spark plug and onset of the combustion process.

Event 2 marks the instant at which the flame has arrived at the spark plug mounted transducer. The ensuing negative value of pressure difference indicates that while the Spark (test) transducer and the Wall (reference) transducer continue to measure increasing cylinder pressure, the rate of increase of the test transducer output is decreased due to the effects of thermal shock. The abruptness of these negative values indicates that both the Kistler Spark and Optrand Spark transducers respond rapidly to thermal shock.

Shortly after event 2 and throughout the region of peak pressure, the pressure difference curves show that the Kistler Spark and Optrand Spark transducers behave differently. In Figure 18, the Kistler Spark transducer's output continues to deteriorate with

respect to the Kistler Wall transducer until event 3. In Figure 19, the Optrand Spark transducer's output reverses relative to the Kistler Wall transducer at 0 CAD (event 2a). The pressure difference becomes positive and reaches a local maximum at 17 CAD (event 2b), and then starts to decline again until event 3.

Event 3 is where the test transducer starts to recover from the thermal shock impact. In Figure 18, event 3 occurs at 17 CAD. The pressure difference curve then increases to zero at approximately 270 CAD, showing that the Kistler Spark transducer takes about 255 CAD to fully recover from thermal shock. In Figure 19, event 3 occurs much later at 135 CAD. Then the Optrand Spark transducer does not fully recover from thermal shock until well into the compression stroke of the next engine cycle. This is shown by an increase in the pressure difference curve from 135 CAD to -90 CAD and results in a total recovery duration of 495 CAD. The recovery process of both transducers is slower than their rapid reaction to thermal shock due to the continued presence of high chamber temperatures past the peak pressure region.

When analyzing pressure difference curves such as those in Figure 18 and Figure 19, one has to be aware that these curves are shaped by the output from two transducers, and reflect their individual responses to thermal shock. Although the Kistler Wall transducer is mounted in a heavily cooled location of the cylinder head, it is unavoidable that at some (small) crank angle after event 2, the flame arrives at the Kistler Wall transducer face and its output also becomes affected by thermal shock. According to Kistler Instrument Corp. data [22], the maximum magnitude of this error is small (-0.45 bar at 50 CAD, for 1500 RPM and 9.0 bar operating conditions). For this reason, the pressure difference curves reflect for the most part only the test transducers' thermal shock errors.

To summarize, the Kistler Spark transducer responds to thermal shock by underestimating cylinder pressure from the moment that the flame arrives at the diaphragm to about 270 CAD. This negative temperature sensitivity is due to the expansion and contraction of the diaphragm and housing. The Oprand Spark transducer overestimates cylinder pressure in the region surrounding peak pressure and the first half of the compression stroke, and underestimates cylinder pressure during early combustion and from halfway into the expansion stroke to the end of the intake stroke. Therefore it is not possible to state that this transducer has either a negative or a positive temperature sensitivity. This may be due to the additional effects of changes in diaphragm shape and emissivity of the reflective surface with temperature as well as expansion and contraction of the transducer head.

This behavior of the Oprand Spark transducer demonstrates the need for an unambiguous definition of maximum thermal shock error. For the Kistler Spark transducer there is no doubt that the magnitude of the maximum negative pressure difference is a measure of its maximum thermal shock error. In the case of the Oprand Spark transducer, the sum of the magnitudes of local extreme points in the pressure difference curve was used as a measure of maximum thermal shock error.

CHAPTER 9: RESULTS AND DISCUSSION

9.1 Performance Variation

The pressure difference curves of Figure 20 and Figure 21 show performance variations between the four Kistler Spark transducers and the four Optrand Spark transducers listed in Table 1. Based upon this evaluation, the best performing Optrand Spark transducer and an appropriate Kistler Spark transducer were selected for further testing and comparison. The curves illustrate how small differences in transducer mounting and spark plug arrangement affect transducer output.

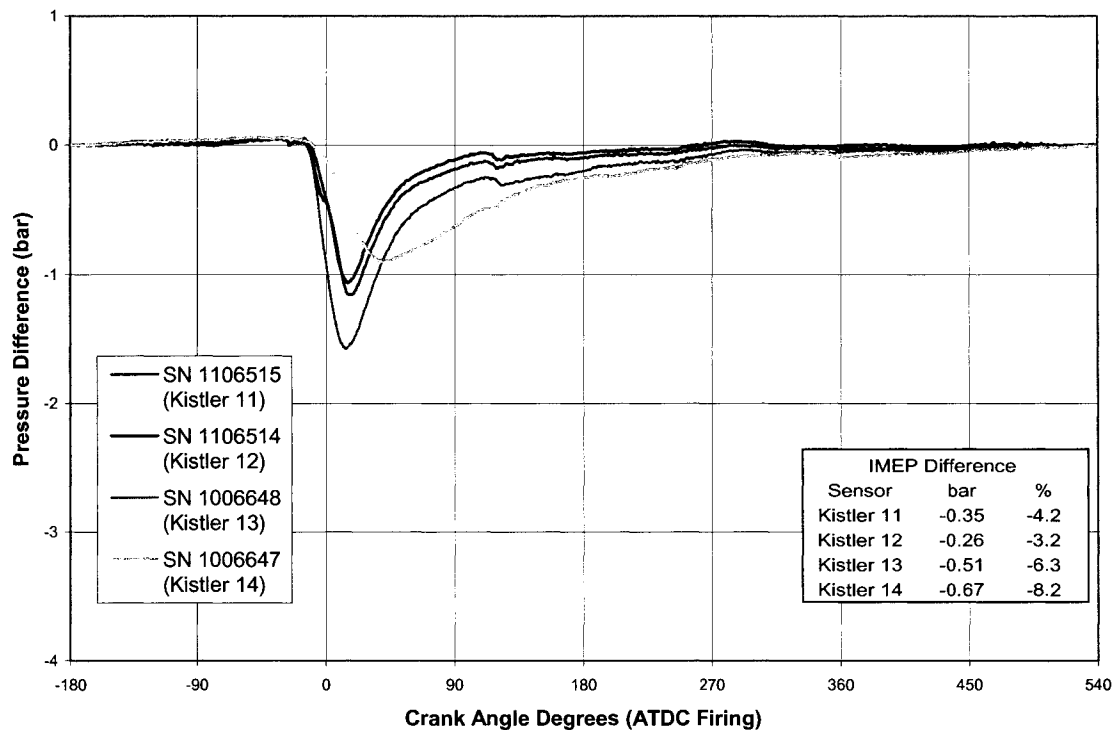


Figure 20: Kistler Spark Transducer Comparison

In Figure 20, all four Kistler transducers show the same trend, producing a negative pressure difference following the point of thermal shock impact. The Kistler No. 14 transducer shows the least amount of thermal shock error in terms of its maximum

magnitude, however its location is later in the cycle and thus the recovery duration is extended. For this reason, this transducer was deemed unacceptable for further testing. The No. 14 transducer was mounted into a spark plug with a small 0.4 mm gap between the electrodes, whereas all other spark plug assemblies had a 1 mm gap. With a smaller gap, less energy is needed for the spark plug to discharge and therefore combustion proceeds at a much slower rate. This explains why the result from the No. 14 transducer is different from the others. Maximum thermal shock errors range from 0.9 bar to 1.6 bar for all four Kistler transducers.

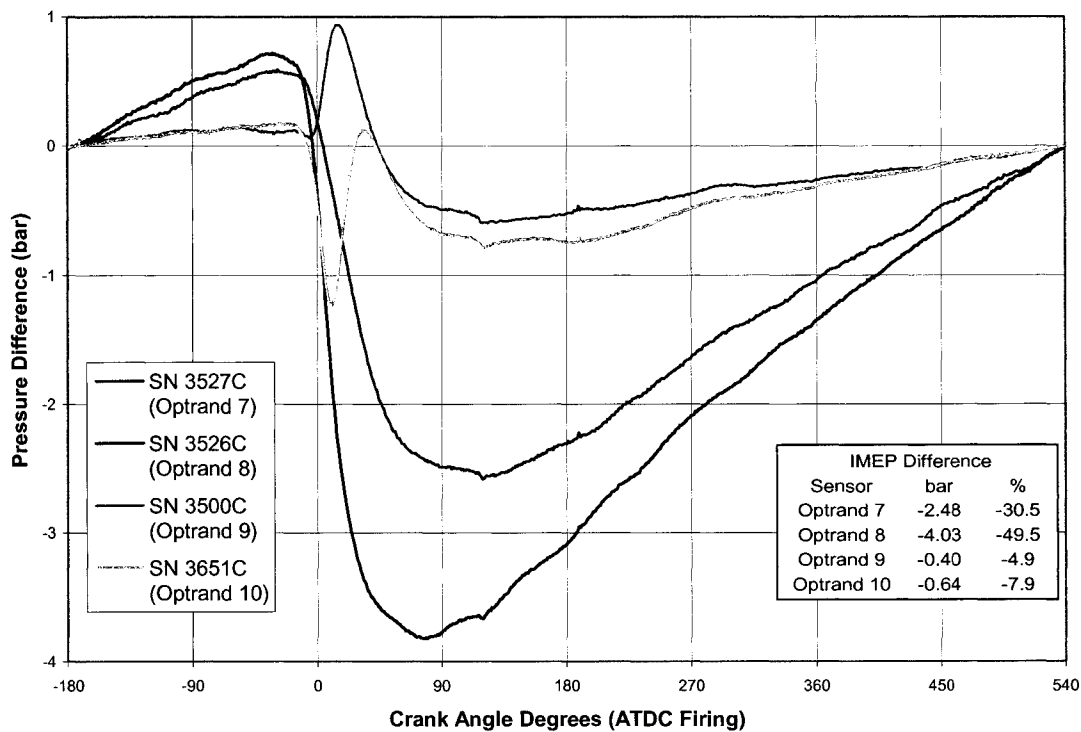


Figure 21: Optrand Spark Transducer Comparison

In Figure 21, there are much larger variations in performance among the four Optrand transducers. Maximum thermal shock error varies between 1.5 bar and 4.5 bar. This is due to the different mounting schemes of the transducers into the spark plug bodies. Transducers

No. 7 and No. 8 were inserted directly into a blank spark plug body with a Morris taper Electrically Discharge Machined (EDM) into it. These transducers' diaphragms were recessed 2 mm from the face of the spark plugs, which had a vertical electrode gap (inline with the axis of the plug). Because of these transducers' poor performance, they were not considered for further testing.

Transducers No. 9 and No. 10 were first mounted onto the same M5 retaining nut used by the Kistler transducers and then inserted into an already machined spark plug body. Transducer No. 9 was recessed 2 mm from the spark plug surface, whereas transducer No. 10 was recessed only 1 mm. Both were mounted into spark plugs with horizontal electrode gaps (perpendicular to the axis of the plug). A large dip in the curve for the Optrand No. 10 transducer between -10 and 20 CAD indicates that this transducer is strongly affected by thermal shock due to its shallow mounting in the spark plug body. Therefore, this transducer was also not considered for further testing. The Optrand No. 9 transducer shows the best performance of the four and was selected to be investigated further.

The analogous Kistler Spark transducer to the Optrand No. 9 transducer in terms of mounting and spark plug arrangement is the No. 13 transducer. Both feature a retaining nut, are similarly recessed, and are mounted into spark plugs with a horizontal electrode gap of the same dimension. All further testing will be completed with the Kistler No. 13 transducer as the Kistler Spark and the Optrand No. 9 transducer as the Optrand Spark. This is despite the fact that the Kistler Spark No. 13 transducer shows the largest thermal shock error among all Kistler Spark transducers and the Optrand No. 9 transducer shows the smallest thermal shock error among all Optrand Spark transducers.

9.2 Global Comparison

Figure 22, Figure 23, Figure 25, and Figure 26 show the effects of both engine speed and load on thermal shock error in terms of the difference between the Kistler Wall transducer output and the test transducer output. The figures also include tables displaying the calculated errors in IMEP in both absolute and percentage values between the Kistler Wall transducer and each test transducer. It is important to realize that it is not only the maximum thermal shock error of a transducer that produces errors in IMEP, but also the time it takes to recover from thermal shock. This is because IMEP is the integral of cylinder pressure between +/- 180 CAD with respect to cylinder volume change.

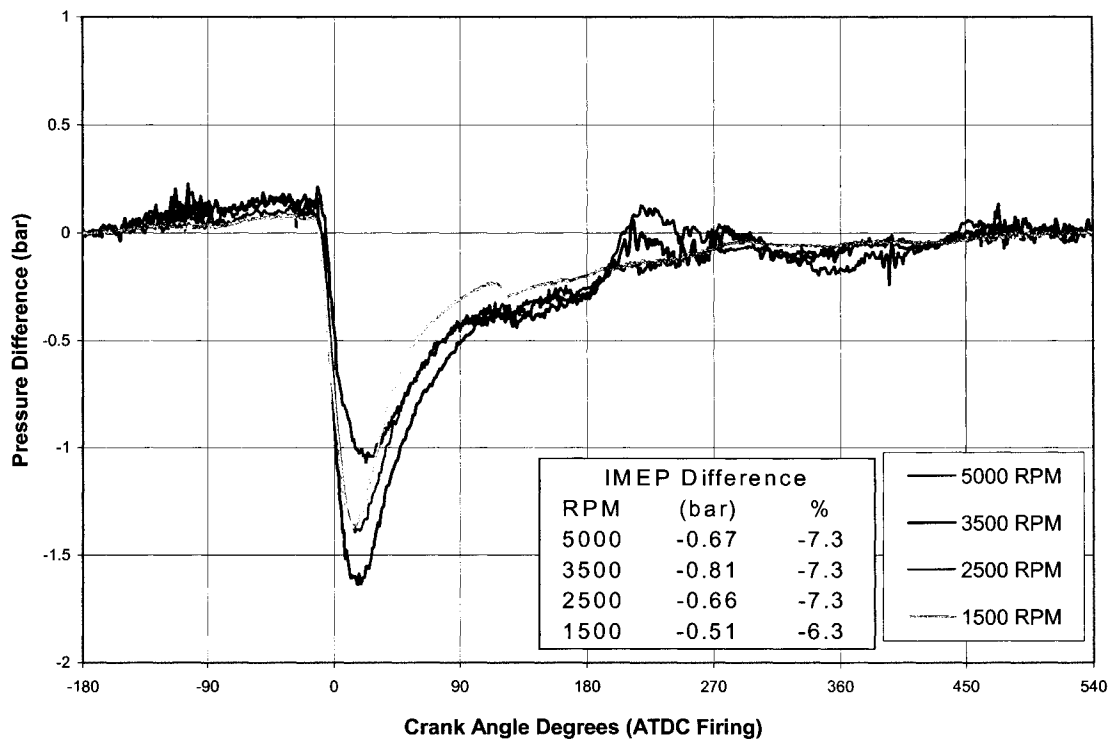


Figure 22: Effect of Engine Speed on Kistler Spark Transducer

Figure 22 shows the effect of engine speed on thermal shock errors demonstrated by the Kistler Spark transducer. It can be seen that thermal shock impact is most severe at

moderate to low engine speeds producing a maximum thermal shock error of 1.6 bar and an overall error in IMEP of -7.3% at 3500 RPM. The magnitude of thermal shock error is affected by two factors: 1) the time it takes the flame to pass over the diaphragm of the transducer and 2) peak cylinder pressure. An increase in engine speed results in higher turbulent flame velocities and shorter times that the flame impinges on the diaphragm of the transducer. An increase in engine speed up to 3500 RPM (for the engine tested) also results in higher peak pressures when operating at WOT, therefore applying larger thermal stresses to the diaphragm of the transducer.

Trends in thermal shock errors observed in this work follow in general those presented in the study by Rai et al [3], in which Kistler wall mounted transducers were evaluated against a Kistler water-cooled transducer. However, in the present work, thermal shock maximum error occurs at 3500 RPM rather than at 1500 RPM as reported in [3]. This shift of the maximum thermal shock error into a higher RPM range can be attributed to the shielding effect of the retaining nut, which is not used with wall mounted transducers. From 1500 RPM to 5000 RPM, maximum thermal shock errors range from 1.0 bar to 1.6 bar and maximum IMEP errors range from -6.3% to -7.3%.

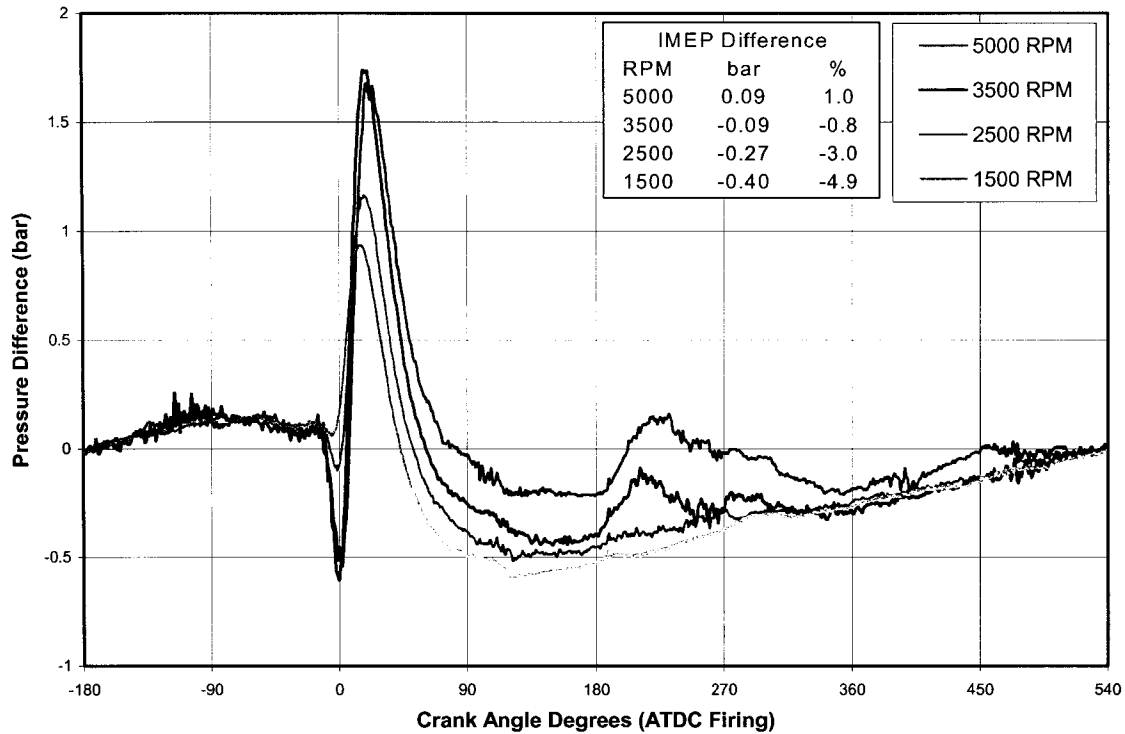


Figure 23: Effect of Engine Speed on Optrand Spark Transducer

Figure 23 shows the effect of engine speed on thermal shock errors demonstrated by the Optrand Spark transducer. An explanation of why this figure is so drastically different from Figure 22 was given with Figure 18 and Figure 19. To reiterate, this particular Optrand Spark transducer overestimates cylinder pressure during half of the compression stroke and in the peak pressure region, while underestimating cylinder pressure during early combustion and in the post combustion period.

By summing the magnitudes of the local extreme points for each of these curves, it is found that the thermal shock impact on the Optrand Spark transducer is also most severe at moderate engine speeds, producing a maximum thermal shock error of 2.7 bar and an overall IMEP error of -0.8% at 3500 RPM. From 1500 to 5000 RPM, maximum thermal shock errors range from 1.5 bar to 2.7 bar and maximum IMEP errors range from 1.0% to -4.9%.

In comparison to the Kistler Spark transducer, the maximum thermal shock errors of this transducer are much larger, however its IMEP errors are much smaller. This is due to the Optrand Spark transducer's overestimation of cylinder pressure in the peak pressure range and its subsequent smaller underestimation in the post combustion period. The Optrand Spark transducer reacts to thermal shock in opposite ways at different instants, causing these errors to cancel each other out in IMEP calculations. The Kistler Spark transducer always shows a negative pressure difference in the range where IMEP is calculated resulting in its underestimation of IMEP.

Perhaps another more unbiased method of determining how closely the output from the test transducers follows that of the reference transducer is to calculate the average ΔP over the entire engine cycle. Although this method is purely scientific, it does show that the thermal shock experienced by each transducer is similar in magnitude. This is defined as:

$$\overline{\Delta P} = \sqrt{\sum_{-180}^{540} \frac{(P_{test} - P_{ref})^2}{720}}$$

Therefore as this parameter increases the signal from the test transducer is worsening. Figure 24 shows the average ΔP and the maximum thermal shock error for the two previous graphs. The average pressure deviation of the Optrand transducer is similar to that of the Kistler transducer, if not better, whereas its maximum thermal shock error is generally worse. Both graphs show that the thermal shock effect is a maximum at 3500 RPM with the average ΔP value for the Optrand Spark transducer 0.08 bar smaller than that given by the Kistler Spark transducer under the same operating conditions. This suggests that the Optrand Spark transducer estimates actual cylinder pressure more closely than the Kistler Spark transducer

when evaluating over the entire engine cycle. It is also interesting to note that the average ΔP is almost constant over the RPM range for the Optrand transducer, whereas the Kistler transducer exhibits the same type of behaviour in terms of maximum thermal shock error.

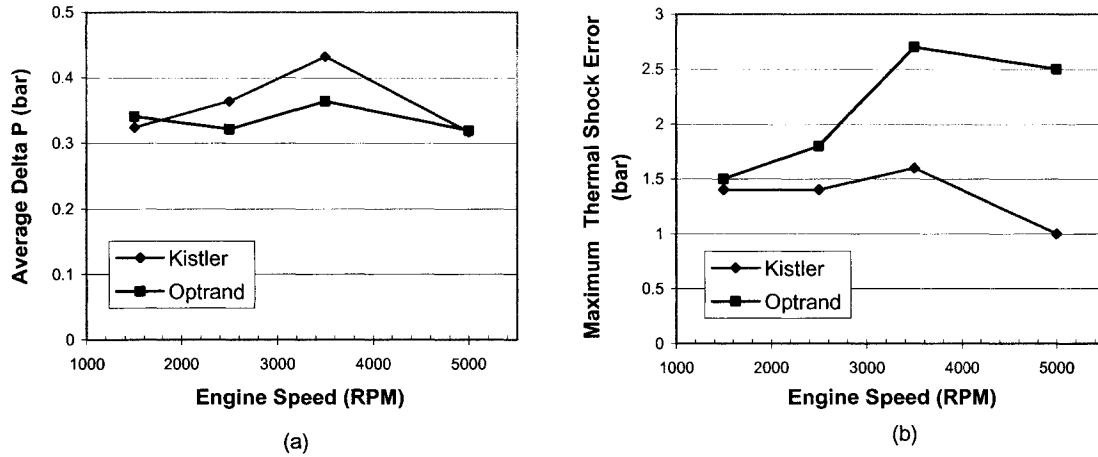


Figure 24: Average ΔP (a) and Maximum Thermal Shock Error (b) at Varying Engine Speeds

Figure 25 and Figure 26 show the effect of engine load on thermal shock errors demonstrated by the Kistler Spark and Optrand Spark transducers respectively. Errors increase as engine load increases from 1.1 bar BMEP to WOT. Maximum thermal shock errors for the Kistler Spark transducer range from 0.4 bar to 1.5 bar and maximum IMEP errors range from -6.4% to -8.0%. The percentage IMEP error does not change significantly with load because of the similar rates of increase in IMEP and IMEP absolute error with load.

Maximum thermal shock errors for the Optrand Spark transducer range from 0.5 bar to 2.4 bar and maximum IMEP errors range from -0.6% to -2.3%. Once again the Optrand Spark transducer produces larger maximum thermal shock error, but provides more accurate

values of IMEP than the Kistler Spark transducer due to its combined over/underestimation of cylinder pressure.

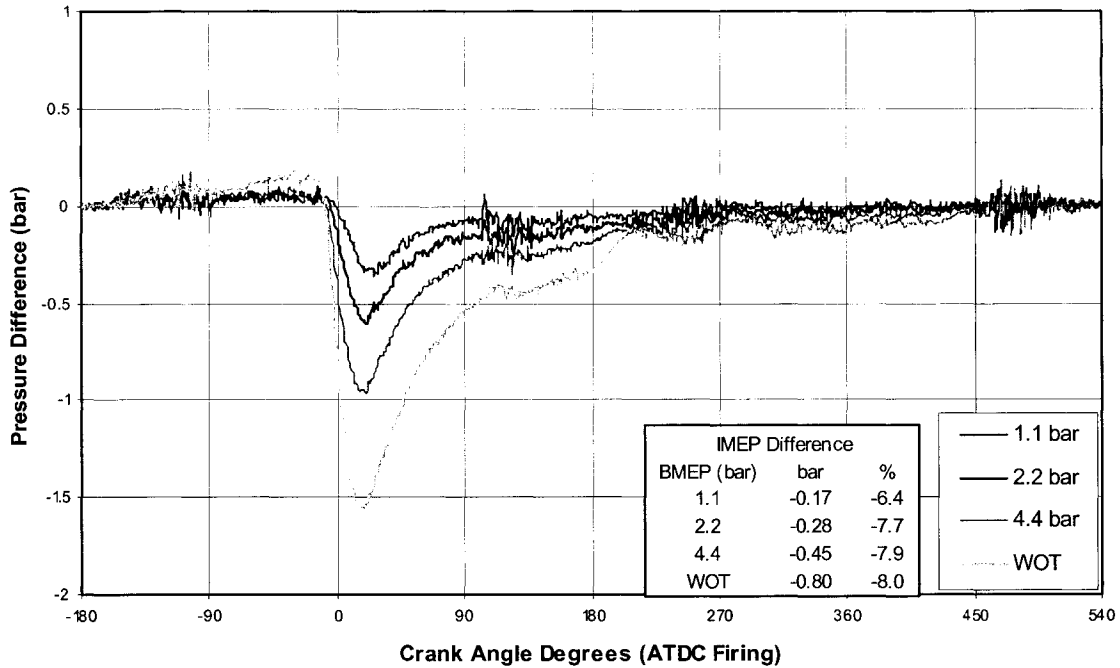


Figure 25: Effect of Engine Load on Kistler Spark Transducer

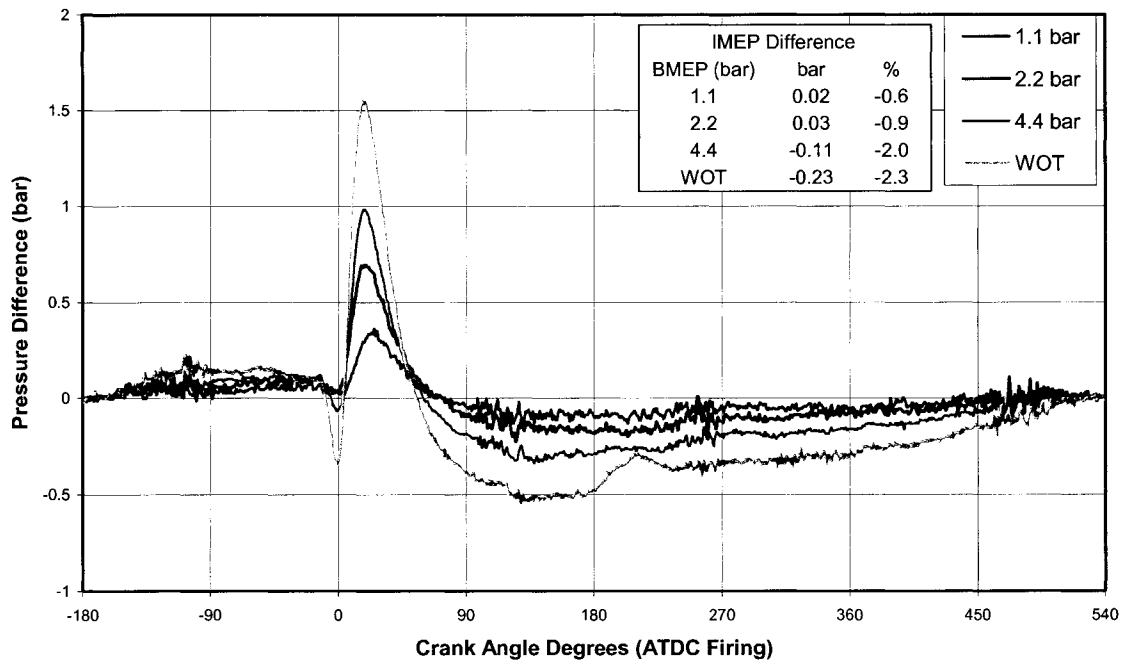


Figure 26: Effect of Engine Load on Optrand Spark Transducer

In terms of the average ΔP of these pressure difference curves, the same trends apply as with the constant load case. The Optrand Spark transducer exhibits similar performance compared to the Kistler Spark transducer in terms of average ΔP , but worse performance in terms of maximum thermal shock error. As the signals start to degrade with increasing load, the average ΔP increases to a maximum at WOT, with the Optrand Spark transducer providing better results. It shows a difference of only 0.37 bar compared to the Kistler Spark's 0.42 bar. When comparing Figure 27 to Figure 24, one can see that both thermal shock parameters are strongly sensitive to engine load but are only weakly sensitive to engine speed.

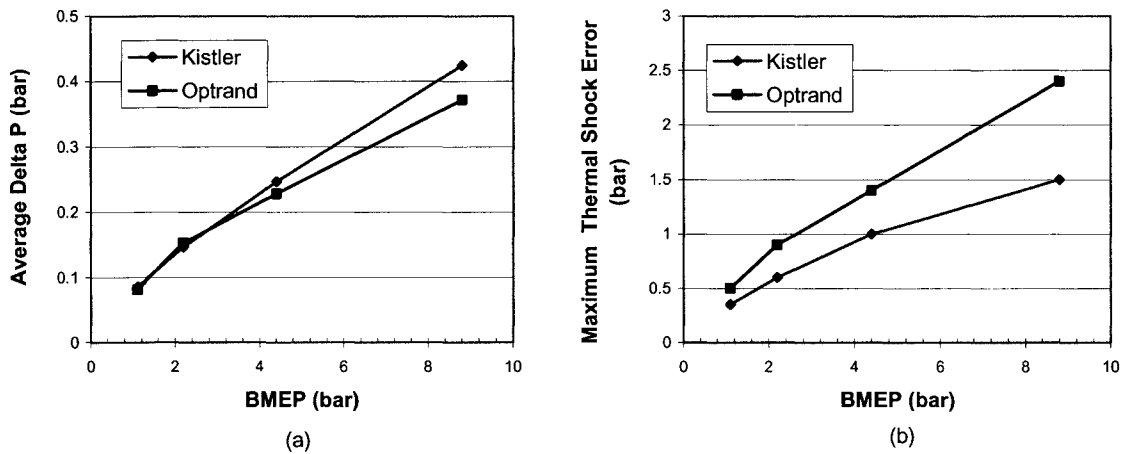


Figure 27: Average ΔP (a) and Maximum Thermal Shock Error (b) at Varying Engine Loads

In Figure 25 and Figure 26, as well as in Figure 22 and Figure 23, the location at which the test transducers start to recover from thermal shock and the rate at which they recover is much different. The Kistler Spark transducer produces its largest error at 20 CAD and recovers at 270 CAD. The Optrand Spark transducer does not start to recover until 130 CAD and does not fully recover until -90 CAD of the next engine cycle. This behavior gives

poorer performance of the Optrand Spark transducer in terms of Pumping Mean Effective Pressure (PMEP) errors as shown in Table 2. At each engine load, the error of the Optrand Spark transducer is approximately twice that of the Kistler Spark transducer in both absolute and percentage values. This is because PMEP is calculated between 360 CAD and 720 CAD, during which the Optrand Spark transducer is recovering from thermal shock.

BMEP	Kistler Spark Difference		Optrand Spark Difference	
	(bar)	(%)	(bar)	(%)
1.1	0.02	2.4	0.04	4.7
2.2	0.03	5.3	0.07	11.5
4.4	0.06	12.5	0.12	28.4
WOT	0.08	40.7	0.16	90.8

Table 2: PMEP Errors averaged over 500 Cycles at 3000 RPM

9.3 Intracycle Variability Analysis

The individual cycle data analysis method for quantifying thermal shock bias follows closely that proposed by Randolph [14] and only a brief description is given here. The approach makes a distinction between two types of variability in cylinder pressure data, an intracycle and an intercycle variability.

Intracycle variability originates from within a cycle and drifts through each measured cylinder pressure trace. This short-term variability is due to thermal shock experienced by the pressure transducer during the combustion process and it degrades transducer output. A high accuracy transducer should be insensitive to thermal shock or quickly and fully recover from the shock effects shortly after peak cylinder temperatures have been reached. The intracycle variability is evaluated from the raw pressure data during intake, compression and

exhaust by examining the deviations of each individual pressure trace from ensemble-averaged pressure along the crank angle axis.

Intercycle variability (better known as cyclic variability) is due to the non-repeatable character of the combustion process from cycle to cycle. This is a long-term variability and can still affect pressure transducer output. An accurate referencing process of the cylinder transducer can remove the intercycle variability effects. In this study the transducers' outputs were pegged by referencing to manifold pressure at inlet bottom dead center. The subsequent data reduction and analysis was conducted using individual cycle heat-release calculations.

Figure 28 is an example of the pressure difference between 91 individual cycles of cylinder pressure and the ensemble-averaged cylinder pressure over the same 91 engine cycles. This specific figure shows 91 pressure differences plotted for only the Kistler Wall transducer at 1500 RPM and WOT. With the exception of the expansion stroke, the thickness of the pressure difference band and its variation along the crank angle axis is a measure of intracycle variability during the engine cycle. Points A1 & A2 on the intake stroke, B1 & B2 on the compression stroke, and C1 & C2 on the exhaust stroke are used for the intracycle variability analysis.

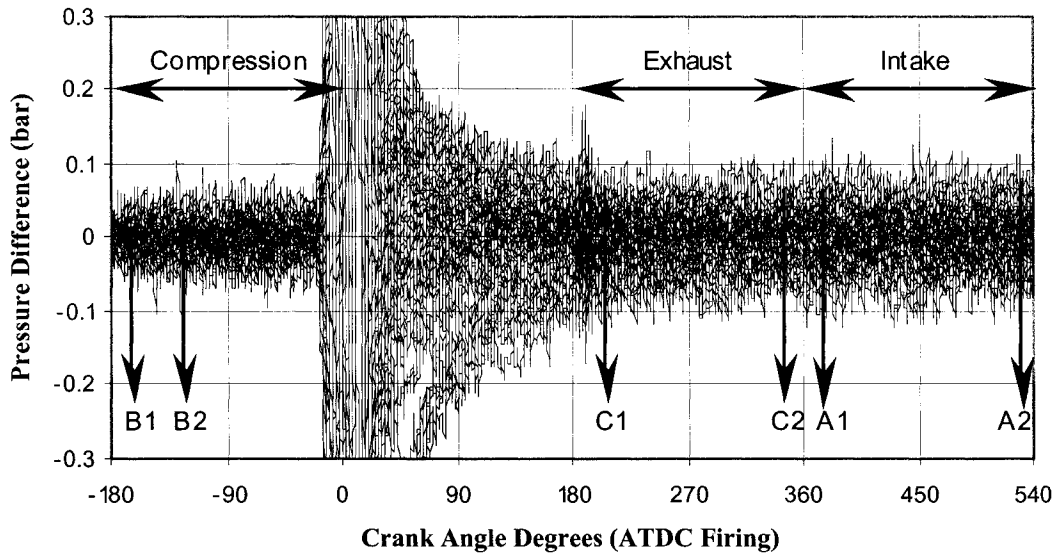


Figure 28: Description of Segments used for the Intracycle Variability Analysis

Individual graphs in Figure 29 are the cross-sections of the pressure difference band (such as in Figure 28) for the Kistler Wall, Kistler Spark, and Optrand Spark pressure transducers at points A1 and A2 (intake stroke), B1 and B2 (compression stroke), and C1 and C2 (exhaust stroke). The pressure differences are arranged as a correlation between points 1 and 2 at those locations for an individual trace (ie. each graph consists of 91 points). These graphs are useful for the intracycle variability analysis. Intracycle variability originates during the combustion event and drifts into the exhaust, intake and compression segments of the pressure trace while the transducer simultaneously recovers from thermal shock. With zero intracycle variability all pressure differences would lie at the graph center. Constant variability during any segment would cause all the pressure differences to lie along the graph diagonal, while a gradual change of variability during the segment would rotate the line around the graph origin away from the diagonal. The spread of the points along the graph diagonal is a measure of the intracycle variability range during the segment while the spread of the points away from the diagonal quantifies measurement repeatability.

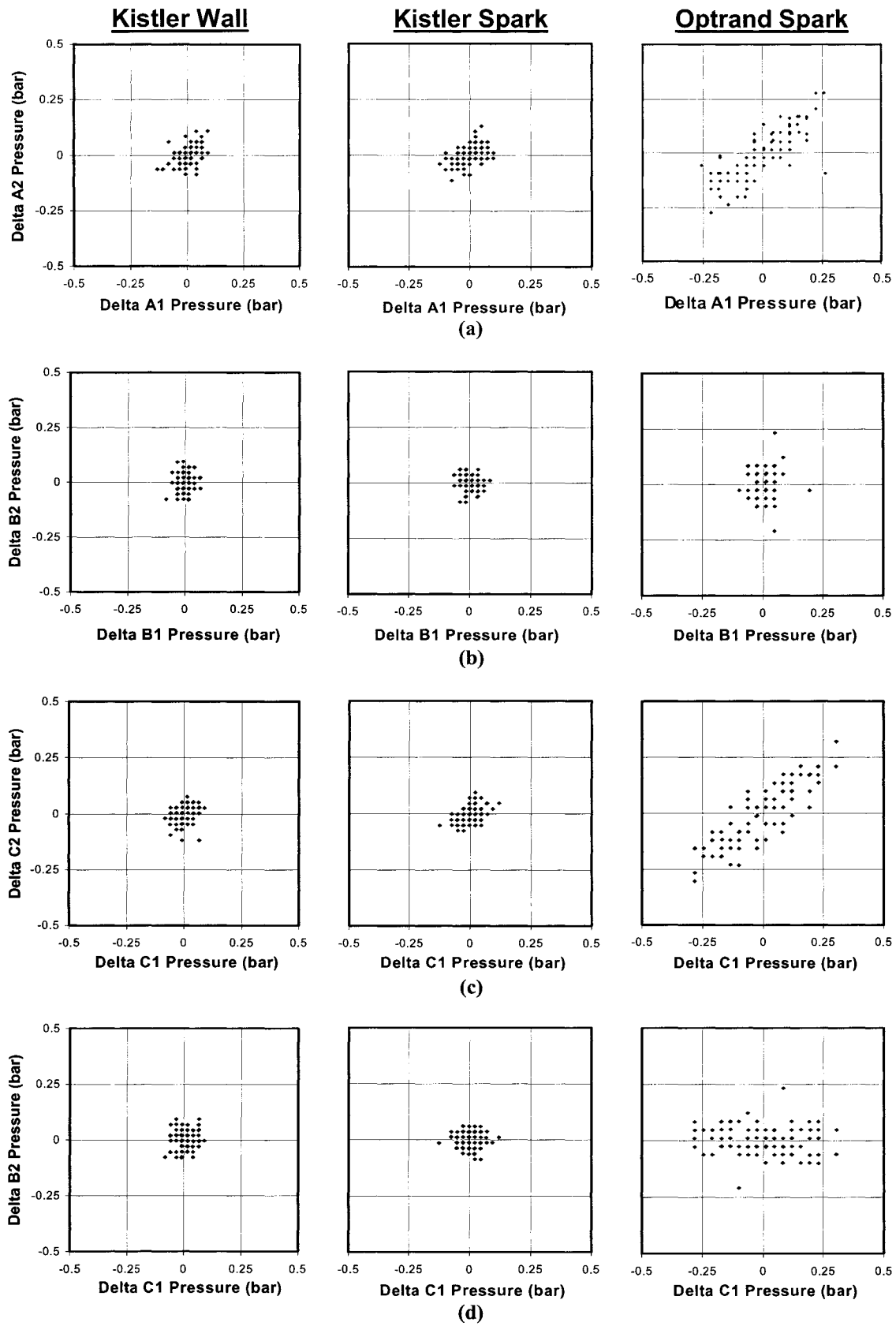


Figure 29: Intracycle Variability Analysis

Figure 29 compares intracycle variability during the intake, compression and exhaust strokes for each transducer. During the intake stroke (Figure 29a) the variability range is largest for the Optrand Spark transducer indicating that this transducer still recovers from thermal shock impact as intake proceeds. The two Kistler transducers show a similar range of intracycle variability.

The recovery process of the Optrand transducer continues into the compression stroke as evident in the graphs showing the pressure differences between points B1 and B2 (Figure 29b). However, the variability of this transducer decreases significantly in this segment indicating its potential for relaxation at lower temperatures during the engine cycle. The variability is small for the Kistler transducers in this segment.

The maximum amount of intracycle variability occurs during the exhaust stroke for all transducers (Figure 29c). This is expected because this segment of the pressure trace immediately follows the combustion event where the variability is originated. Variability is significantly larger for the Optrand transducer than for the Kistler transducers.

An estimate of the effects of thermal shock occurring during the combustion event can be made by comparing the intracycle variability at 210 CAD (C1) to the intracycle variability still present at -120 CAD of the next engine cycle (B2). As illustrated in Figure 29d, the difference between the intracycle variability at point C1 and at point B1 in the next engine cycle is smaller for the Kistler transducers. Data points are spread along the horizontal axis rather than along the diagonal (as seen in Figure 29c) indicating a large change in variability between C1 and B2 crank angles.

An Analysis of Variance (ANOVA) was also completed on the raw cylinder pressure data at -90 CAD to statistically prove whether the data from the three transducers have the same mean. The first step was to perform an ANOVA on the two sets of data collected with the reference transducer. One set of data was collected with the reference transducer when the Kistler Spark transducer was fitted into the combustion chamber and the other set was with the Oprand Spark transducer fitted into the combustion chamber. This procedure will prove whether the reference transducer produced statistically similar data at two different intervals.

For this test the number of Degrees of Freedom (DOF) between groups was 1 (two data sets) and the number of DOF within groups was 180 (91 data points for each data set) for a total of 181 DOF. This translates into a critical F-value of 3.9. If the ANOVA calculates an F-value that is larger than the critical F-value, then the conclusion is made that the two sets of data do not have the same mean.

Groups	Count	Sum	Average	Variance	
Kistler Wall w/ KS	91	150.8846	1.658072	0.001332	
Kistler Wall w/ OS	91	151.6093	1.666036	0.001959	
ANOVA					
Source of Variation	SS	df	MS	F	F crit
Between Groups	0.002886	1	0.002886	1.753753	3.893632
Within Groups	0.296168	180	0.001645		
Total	0.299054	181			

Table 3: ANOVA on the Two Sets of Reference Transducer Data

Table 3 shows that the calculated value of F is 1.75 and that the critical F-value is 3.9. The conclusion is made that the two sets of reference transducer data have the same mean, therefore it does not matter which set was used in Figure 29. Table 4 shows another

ANOVA done on the three types of pressure transducers again at -90 CAD. This table statistically proves that the data from the three transducers do not have the same mean since the calculated F-value is much larger than the critical F-value. The same analysis was completed at multiple CAD throughout the engine cycle with similar results. For all ANOVA's, a 0.05 level of significance was used.

Groups	Count	Sum	Average	Variance	
Kistler Wall	91	151.6093	1.666036	0.001959	
Kistler Spark	91	153.3903	1.685608	0.001402	
Optrand Spark	91	162.7542	1.788508	0.002629	
ANOVA					
Source of Variation	SS	df	MS	F	F crit
Between Groups	0.78779	2	0.393895	197.269	3.029214
Within Groups	0.53912	270	0.001997		
Total	1.326909	272			

Table 4: ANOVA on the Three Types of Pressure Transducer Tested

9.4 Combustion Performance Parameters

The individual cycle data analysis has shown that thermal shock can significantly increase intracycle variability of the indicated cylinder pressure. Furthermore, this intracycle variability is reflected in the variability of such engine performance and operation measures as IMEP, Crank Angle of 50% mass fraction burned (CA50), and peak cylinder pressure (PP) and its location as shown in Figure 30 to Figure 41. The difference between test and reference transducers is given for each performance parameter in both average and standard deviation values. The difference in Standard Deviation (SD) is affixed to the difference in the average values and is given as a +/- range. The percent difference between test and reference transducers is also given for IMEP and Peak Pressure but is not given for Location of Peak Pressure and CA50 since this reference to CAD would be meaningless.

Figure 30 to Figure 35 show the effect that engine load has on the difference in combustion performance parameters between the test and reference transducer. In Figure 30 both transducers follow the same trend by underestimating IMEP by larger amount as engine load increases from 1.1 bar BMEP to WOT. This is to be expected since thermal shock increases with engine load. The Optrand Spark transducer shows less error in IMEP than the Kistler Spark transducer, but it does show a significantly larger variability at each operating condition. In Figure 31 the percent difference in IMEP is much less for the Optrand Spark transducer producing a maximum error of only about -3% whereas the maximum error of the Kistler Spark transducer can reach as much as -8%.

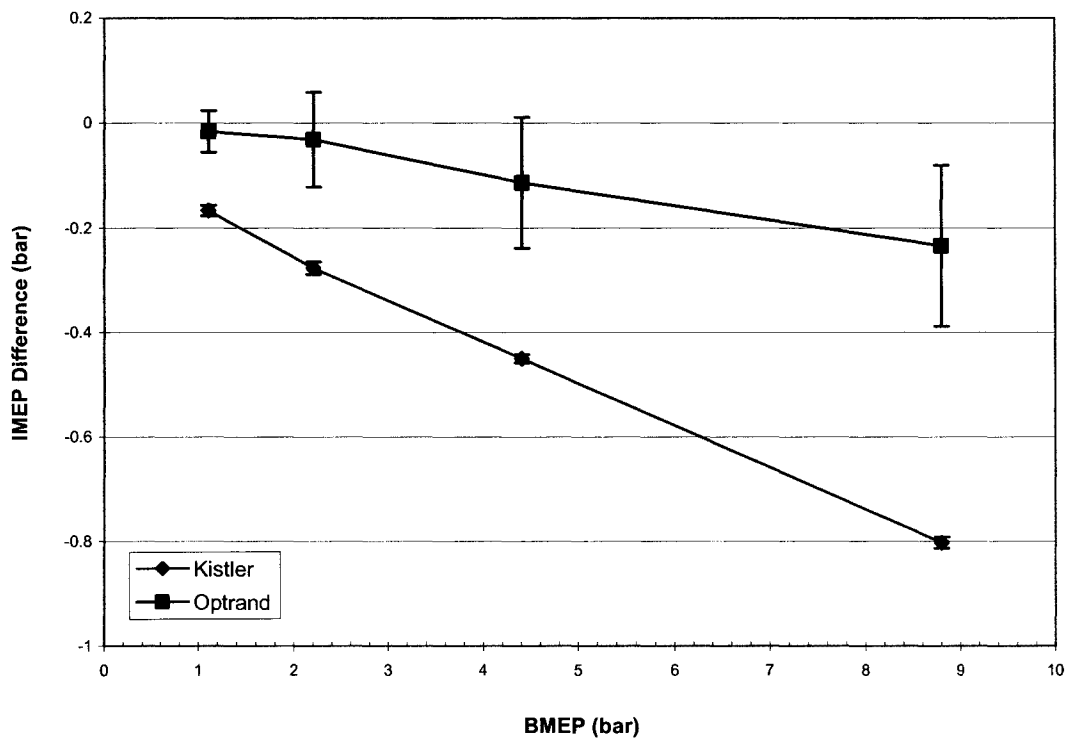


Figure 30: Effect of Engine Load on IMEP Difference (bar)

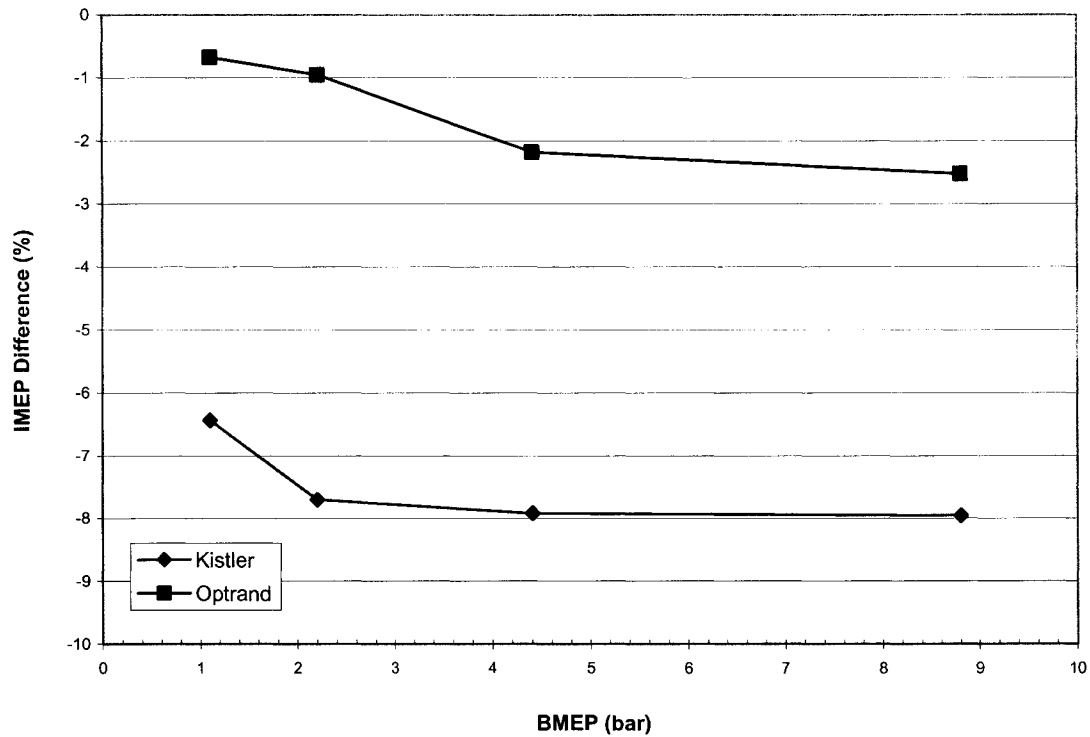


Figure 31: Effect of Engine Load on IMEP Difference (%)

The difference in Peak Pressure shown in Figure 32 follows an opposite trend for each transducer and is almost symmetrical about the 0 bar line. The Optrand Spark transducer increasingly overestimates peak cylinder pressure as engine load increases, whereas the Kistler Spark transducer increasingly underestimates it. This trend was seen previously when calculating the pressure difference in the Global Comparison. The variability of each transducer in terms of peak pressure is comparable. The same type of behaviour is seen in Figure 33 with almost symmetrical representations about the 0 bar line of percent difference in peak pressure. Maximum values are +3% and -3% for the Optrand Spark and Kistler Spark transducers respectively.

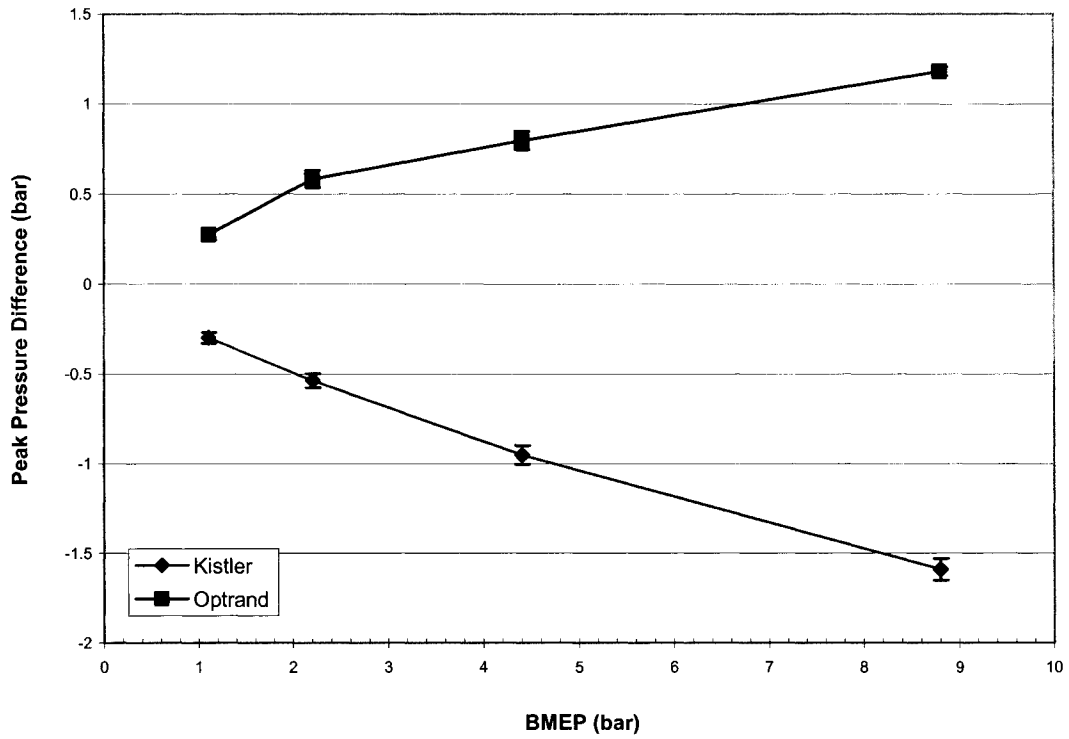


Figure 32: Effect of Engine Load on Peak Pressure Difference (bar)

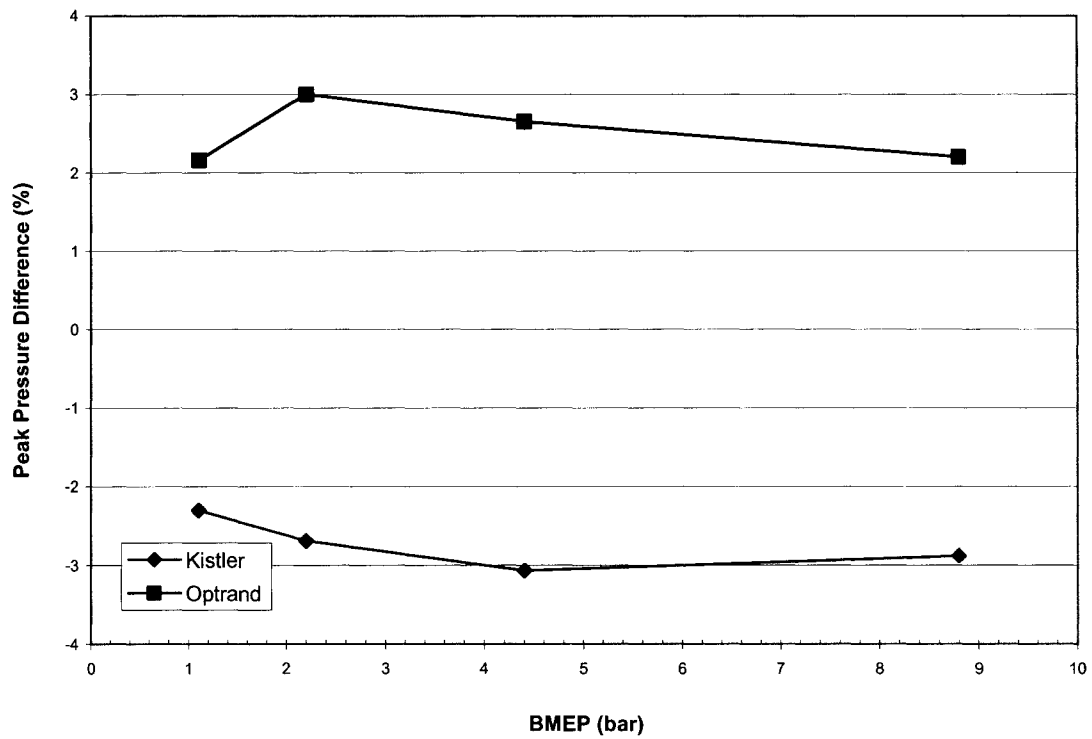


Figure 33: Effect of Engine Load on Peak Pressure Difference (%)

In Figure 34, estimates of the location of peak cylinder pressure are delayed for the Optrand Spark transducer and advanced for the Kistler Spark transducer. This is a direct effect of the overestimation of peak cylinder pressure by the Optrand Spark and the underestimation by the Kistler Spark transducers. As the output from the reference transducer starts to trail off after reaching peak pressure, the Optrand Spark transducer continues to rise for a very brief period, resulting in delayed angles of peak pressure. For the opposite reason the location of peak pressure is advanced for the Kistler Spark transducer.

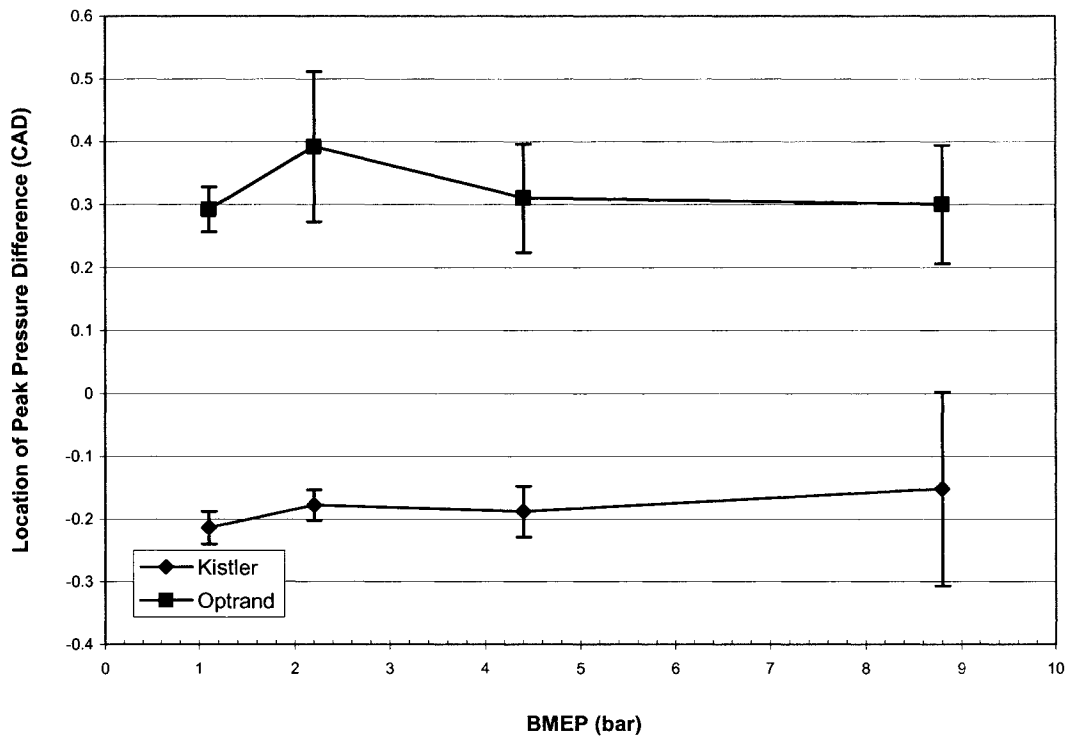


Figure 34: Effect of Engine Load on Location of PP Difference (CAD)

Figure 35 shows that angles of CA50 are again delayed for the Optrand Spark transducer and advanced for the Kistler Spark transducer. The variability of CA50 for the Kistler Spark transducer seems to be less than that of the Optrand Spark transducer.

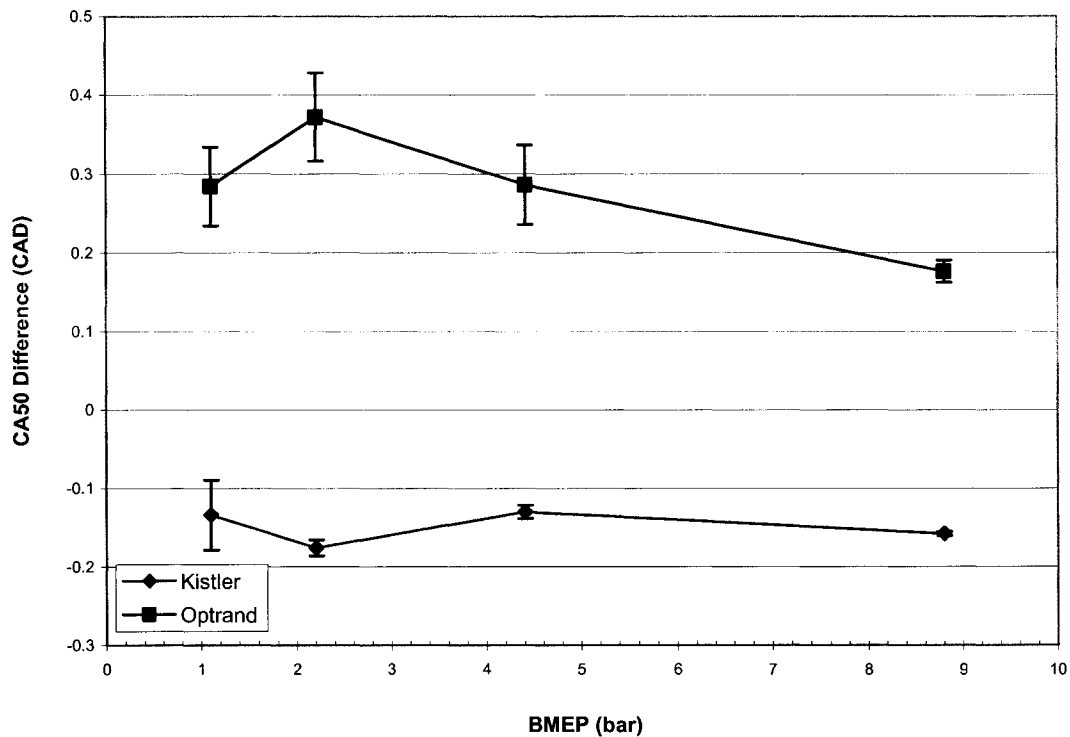


Figure 35: Effect of Engine Load on CA50 Difference (CAD)

The following six figures show the effect that engine speed has on the difference in combustion performance parameters between the test and reference transducer. In Figure 36 and Figure 37 the difference in IMEP is shown in both absolute and percentage values. The Optrand Spark transducer gives increasingly better estimates of IMEP as engine speed increases and actually overestimates it at 5000 RPM. The Kistler Spark transducer gives a nearly constant error in IMEP of approx. -7%. Again the variability in IMEP is significantly larger for the Optrand transducer than for the Kistler transducer. In terms of peak cylinder pressure, Figure 38 and Figure 39 show an overestimation by the Optrand transducer and an underestimation by the Kistler transducer as was the case with the varying engine load. However, in this case the error is generally constant at about +2% and -3% for the Optrand and Kistler transducers respectively. This behaviour is reflected in Figure 40 where

estimates of the Location of Peak Pressure for the Optrand transducer are positive and for the Kistler transducer are negative. Estimates of CA50 for both transducers are shown in Figure 41.

The following additional points can be made when comparing the differences between engine load and engine speed effects on the combustion performance parameters.

- IMEP difference increases with load for both transducers, whereas with speed the difference in IMEP decreases.
- Peak Pressure difference is almost insensitive to RPM changes, whereas there is a significant change with engine load.
- Location of Peak Pressure and CA50 difference is much more sensitive to RPM changes than to load changes for both transducers.

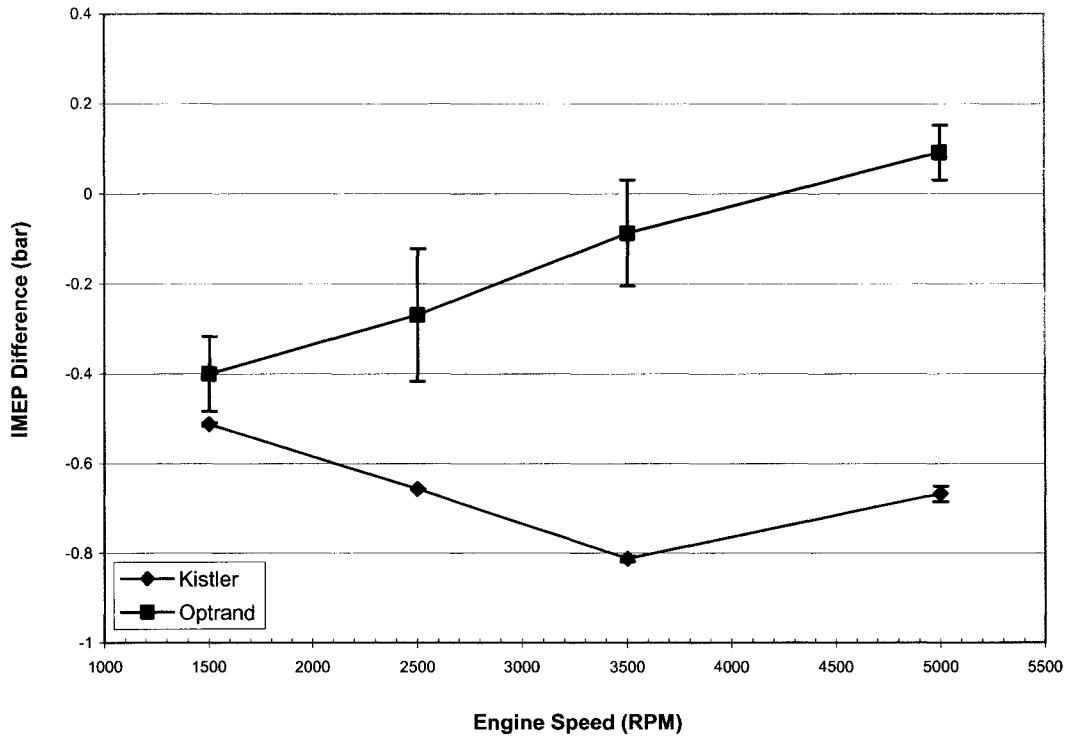


Figure 36: Effect of Engine Speed on IMEP Difference (bar)

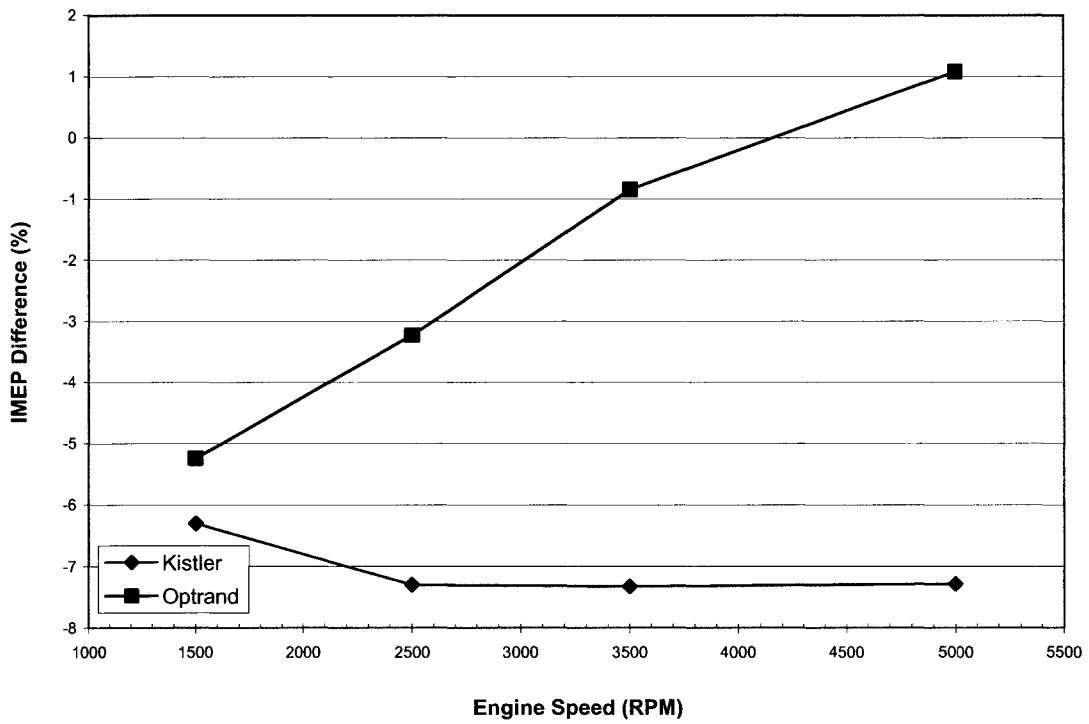


Figure 37: Effect of Engine Speed on IMEP Difference (%)

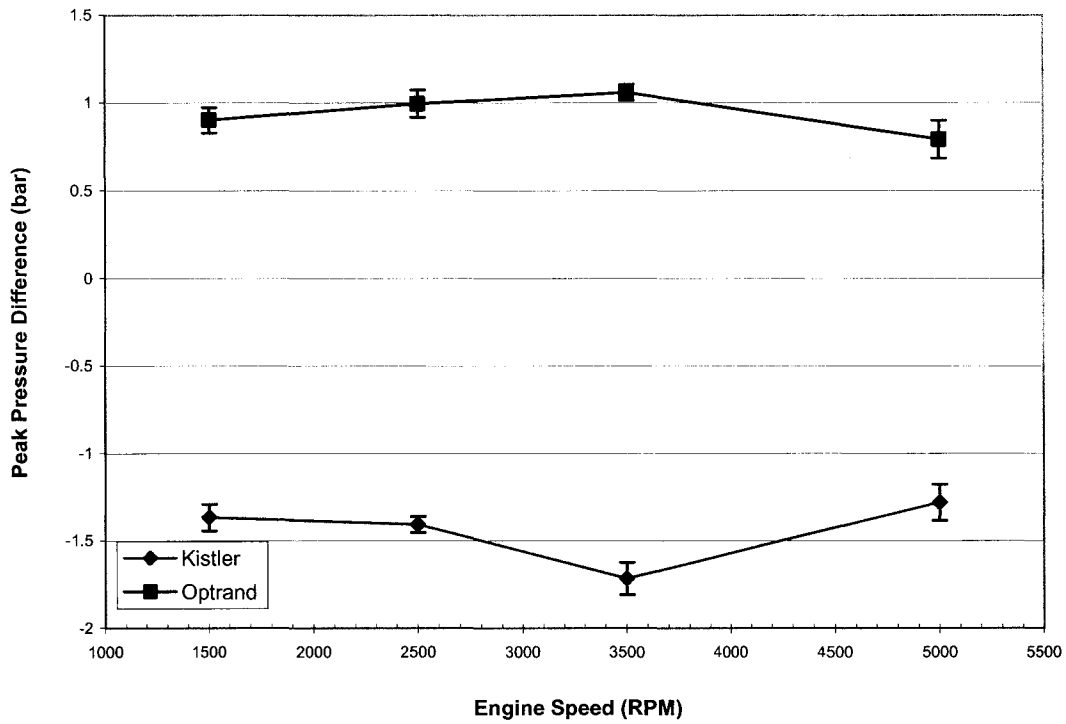


Figure 38: Effect of Engine Speed on Peak Pressure Difference (bar)

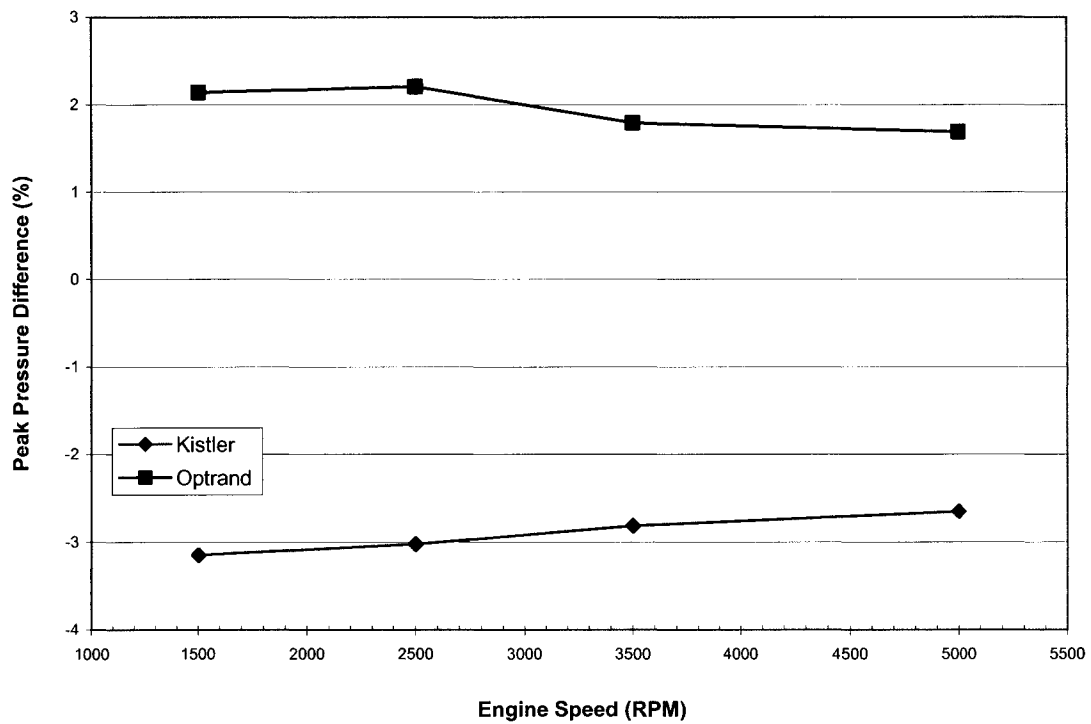


Figure 39: Effect of Engine Speed on Peak Pressure Difference (%)

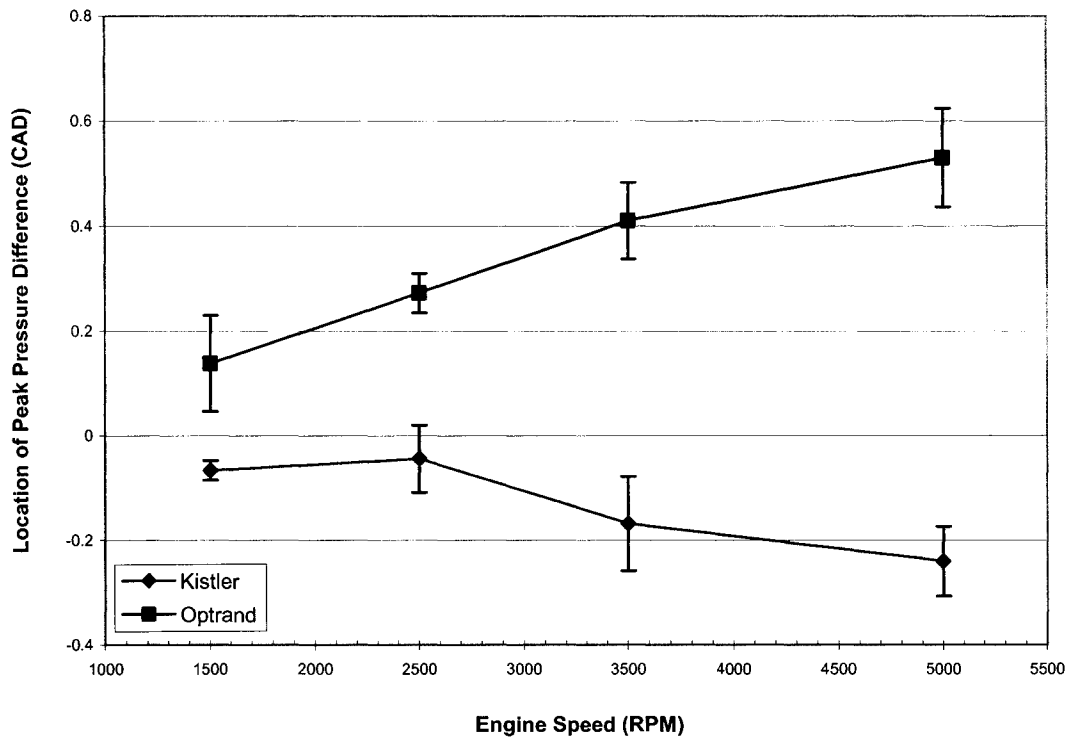


Figure 40: Effect of Engine Speed on Location of PP Difference (CAD)

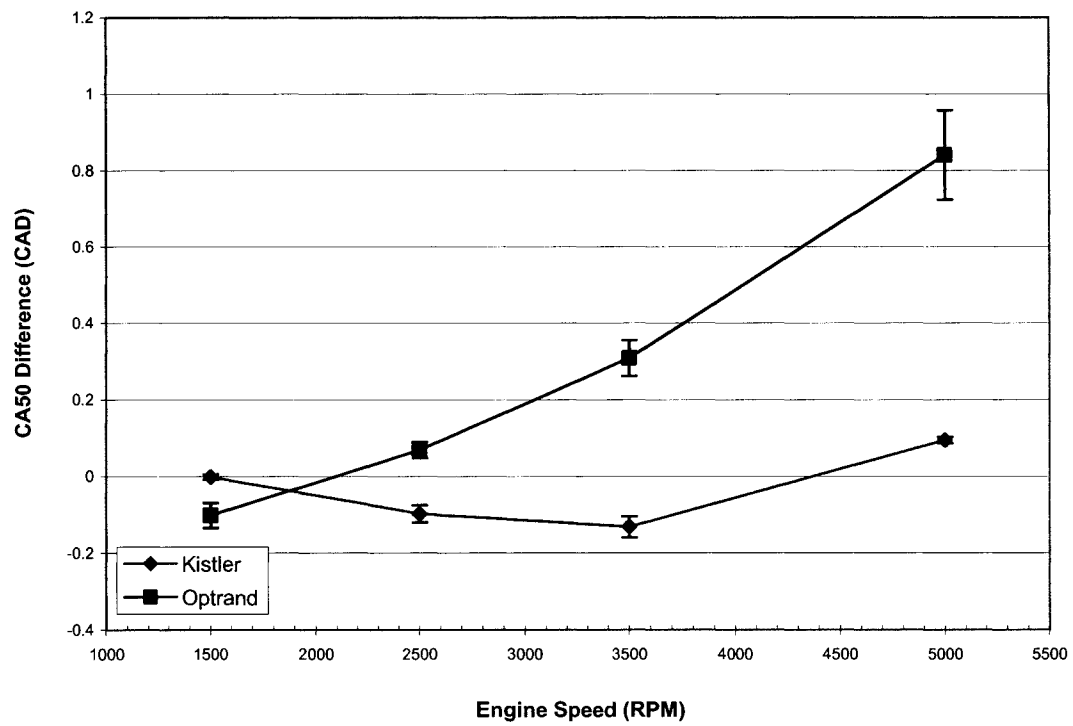


Figure 41: Effect of Engine Speed on CA50 Difference (CAD)

9.5 Cylinder-to-Cylinder Variations

Cylinder-to-Cylinder variations in an engine can cause uneven loading on the crankshaft resulting in an uncomfortable ride for the occupant. They can be caused by such things as unequal intake runner lengths with variable roughness and unequal injector pressures and hole sizes. These factors affect the amount of air and fuel entering the combustion chamber and thus the mixture strength. With unequal mixture strengths and different mixing characteristics in each cylinder, cylinder-to-cylinder variations occur. This is an especially important concern in Natural Gas fuelled engines, where the mixing characteristics of air and Natural Gas is unknown. The data for the cylinder-to-cylinder variation analysis was taken with the Kistler Wall reference transducer one cylinder at a time and is arranged in the order in which each cylinder fires (1-8-4-3-6-5-7-2).

The following four figures show the cylinder-to-cylinder variations of four important combustion performance parameters at WOT and varying engine speeds – IMEP, CA50, PP, and Location of PP averaged over 500 engine cycles. The standard deviation of these values are shown as a +/- range affixed to the value of the parameter. Missing from this data set is cylinder #3 at 1500 RPM due to a malfunction of the data acquisition system that was realized after all of the experiments had been completed.

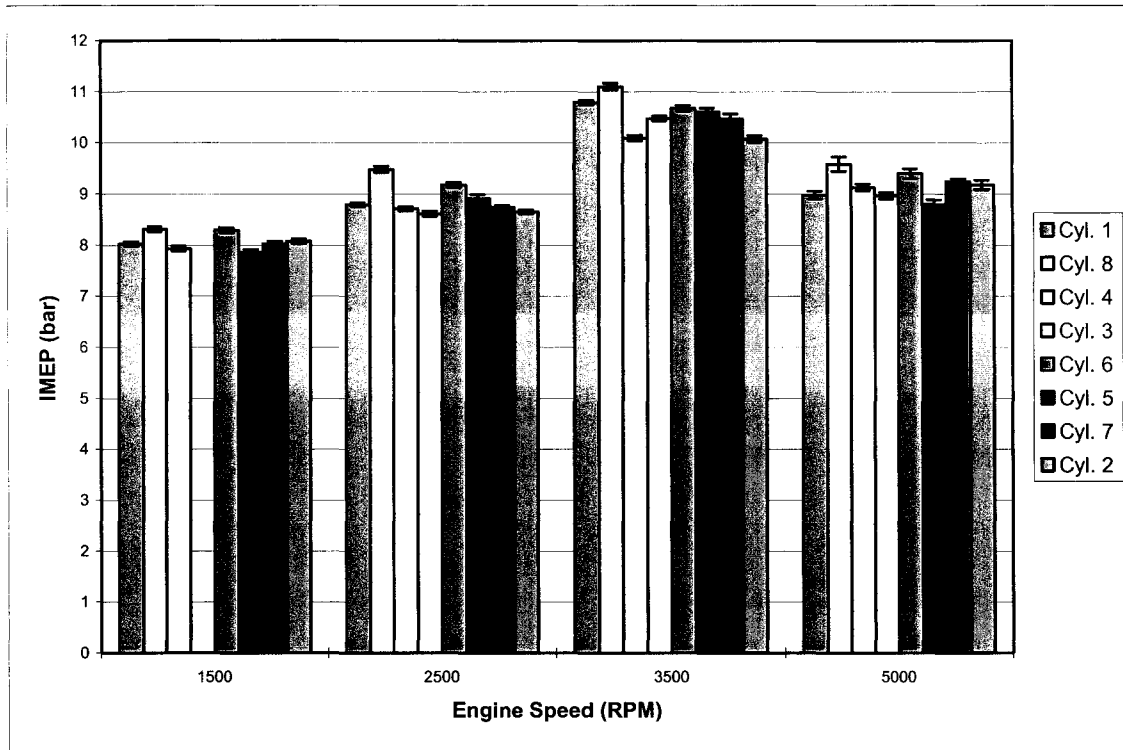


Figure 42: IMEP and its SD at WOT and Varying Engine Speeds

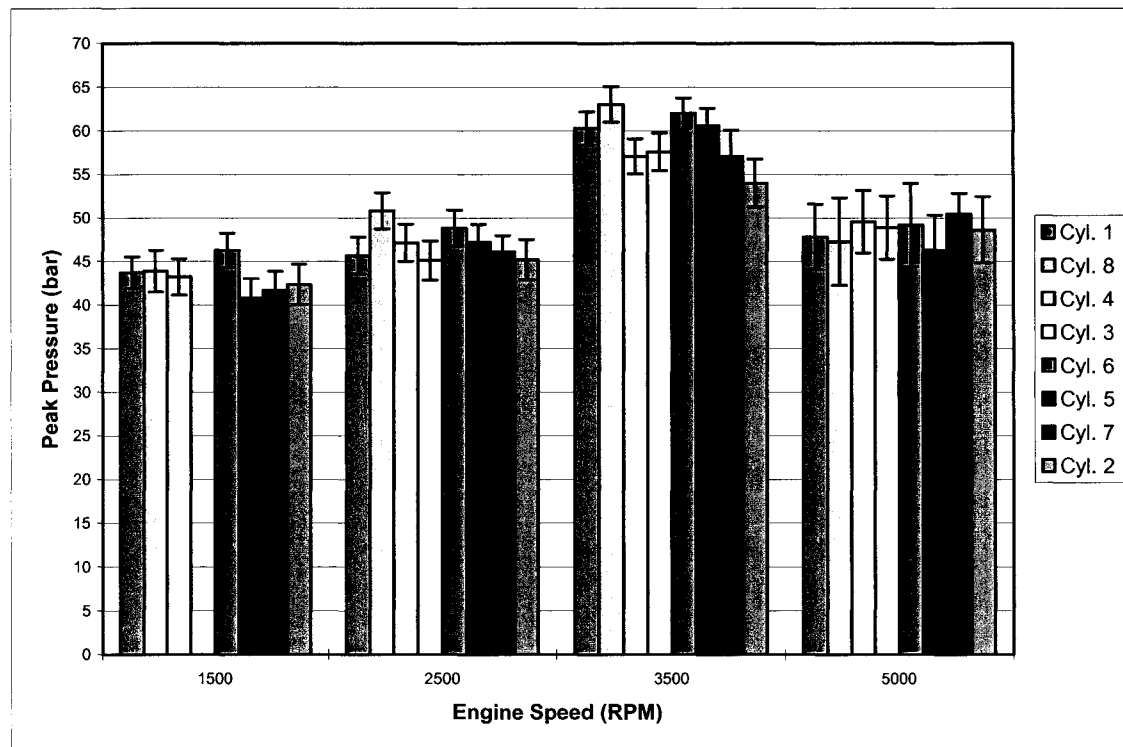


Figure 43: Peak Pressure and its SD at WOT and Varying Engine Speeds

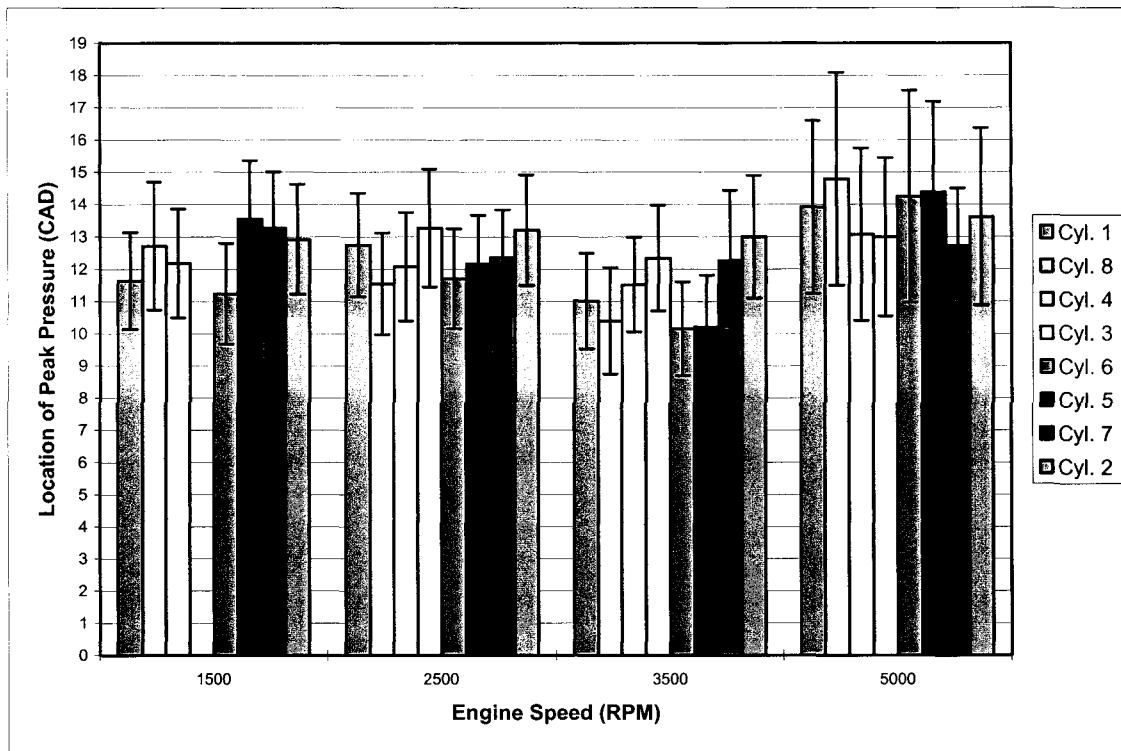


Figure 44: Location of PP and its SD at WOT and Varying Engine Speeds

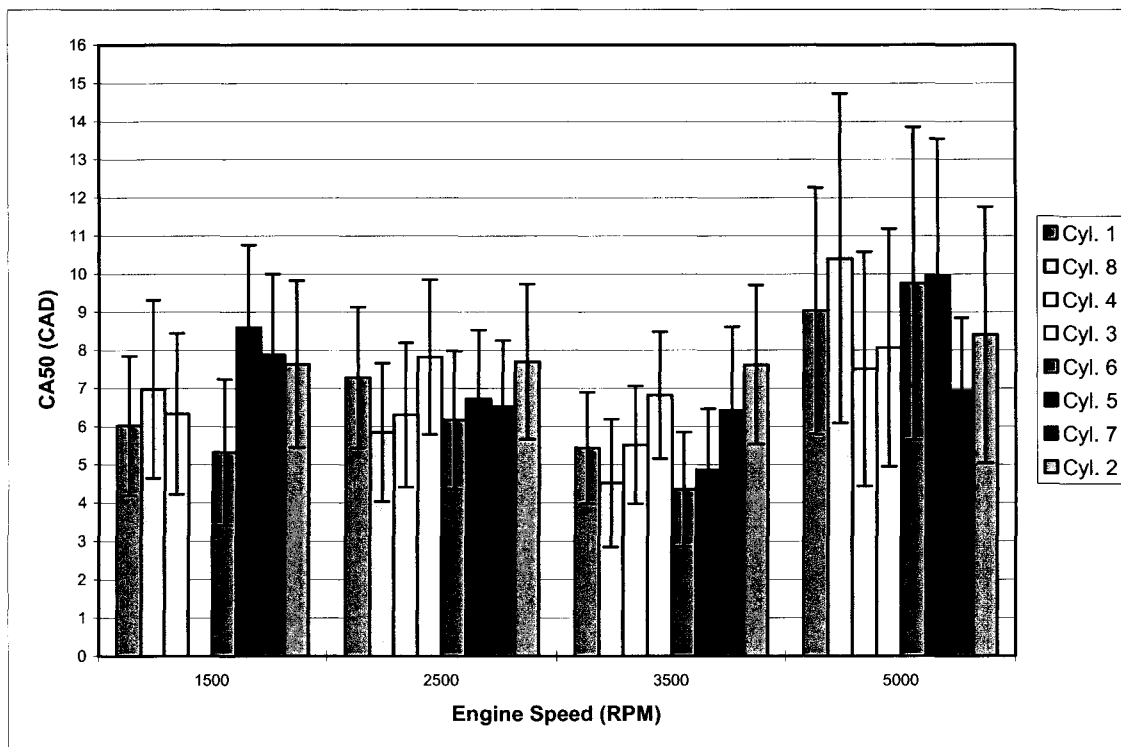


Figure 45: CA50 and its SD at WOT and Varying Engine Speeds

In Figure 42, the standard deviations of IMEP are small, suggesting that the cycle-to-cycle variability is low. In other words, over the 500 engine cycles of data taken, the calculated values of IMEP are very similar, suggesting that an equal charge is being delivered to each individual cylinder. However, in terms of cylinder-to-cylinder variations, the maximum deviation is about +/-5% from the mean at 3500 RPM suggesting that all cylinders are not receiving the same charge during each individual cycle.

In Figure 45, Figure 43, and Figure 44 the cycle-to-cycle variations are much higher. This can be expected for these parameters since they are estimated at one CAD and not over 360 CAD as is the case with IMEP. Such factors as spark plug intensity (affecting early flame development) and heat transfer to the walls can cause these variations. Cylinder-to-cylinder variations are comparable with IMEP.

These graphs follow the trends which are expected. Both IMEP and Peak Pressure increase up until maximum torque (3600 RPM & WOT), after which point they start to decrease. The explanation of the peak at 3600 RPM is that volumetric efficiency increases as engine speed increases, bringing more air into the cylinder and therefore creating more torque. Above 3600 RPM, friction effects dominate causing a decrease in torque. CA50 and Location of Peak Pressure remain approximately constant, indicating a spark timing set for MBT.

In the following four graphs, the same combustion performance parameters are shown at a constant engine speed of 3000 RPM and varying engine load. Motoring data is also shown at 3000 RPM and WOT. This was accomplished by disabling the fuel injector of the cylinder where data was to be collected. They follow in general the same trends of the

previous four graphs in terms of cycle-to-cycle and cylinder-to-cylinder variations. Also, as engine load increases IMEP and Peak Pressure increase and CA50 and Location of Peak Pressure remain relatively constant.

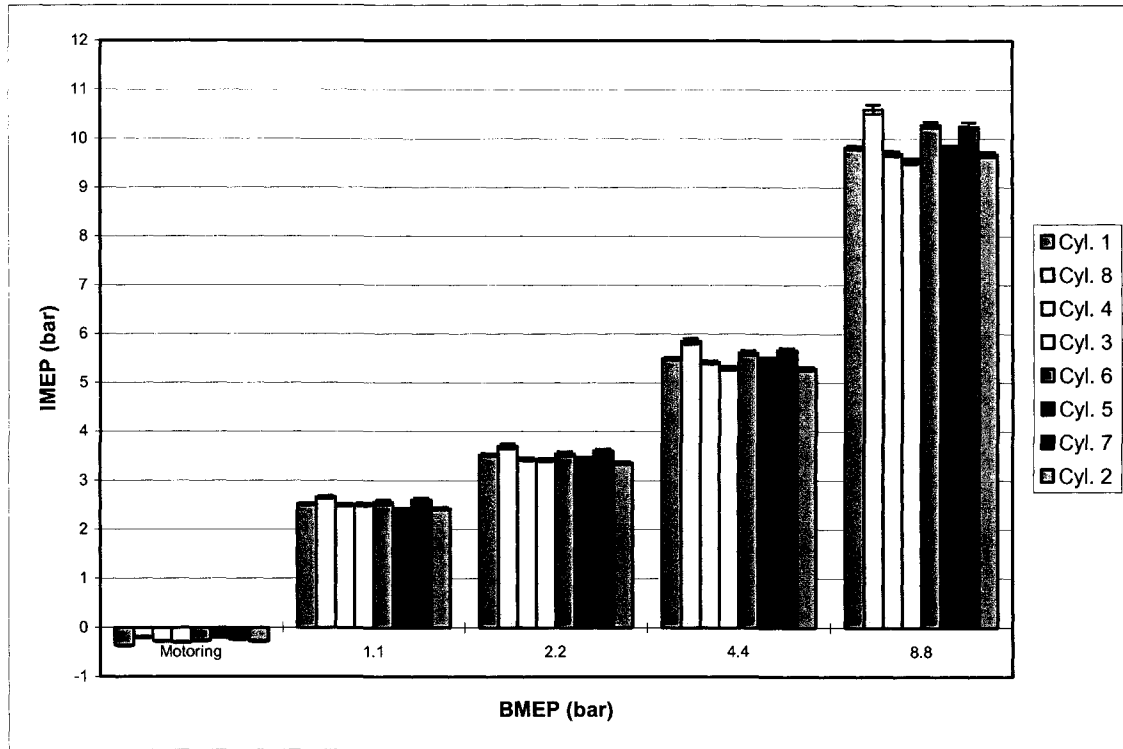


Figure 46: IMEP and its SD at 3000 RPM and Varying Engine Loads

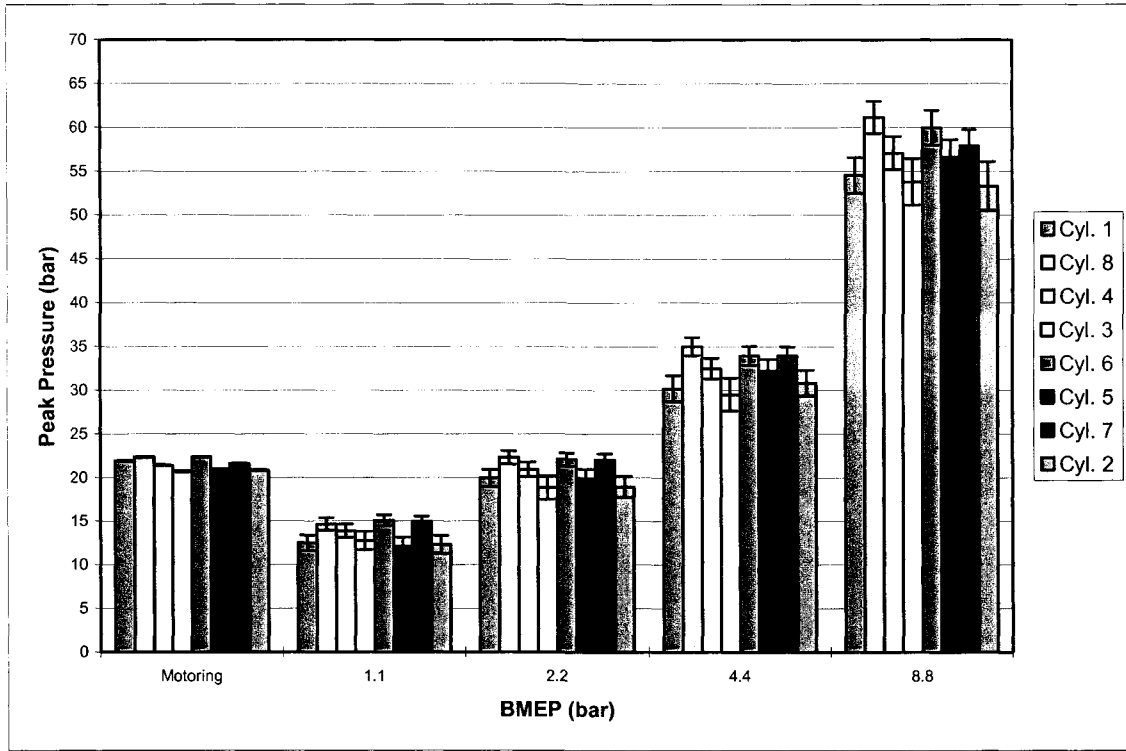


Figure 47: Peak Pressure and its SD at 3000 RPM and Varying Engine Loads

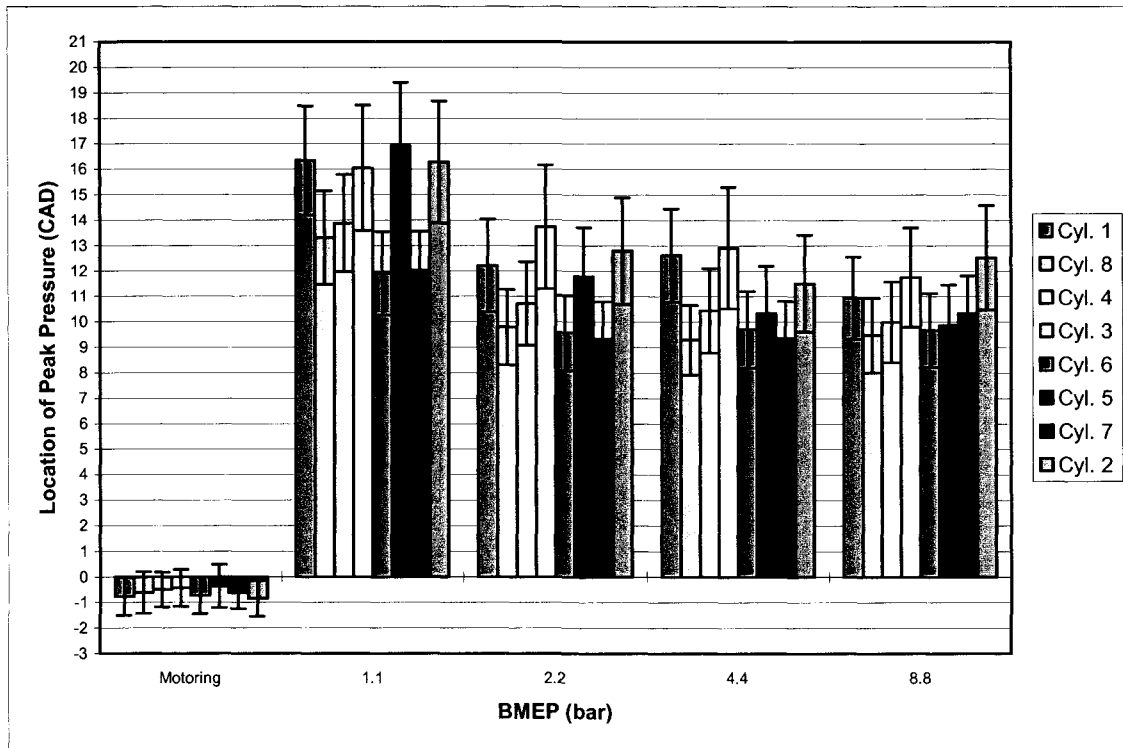


Figure 48: Location of PP and its SD at 3000 RPM and Varying Engine Loads

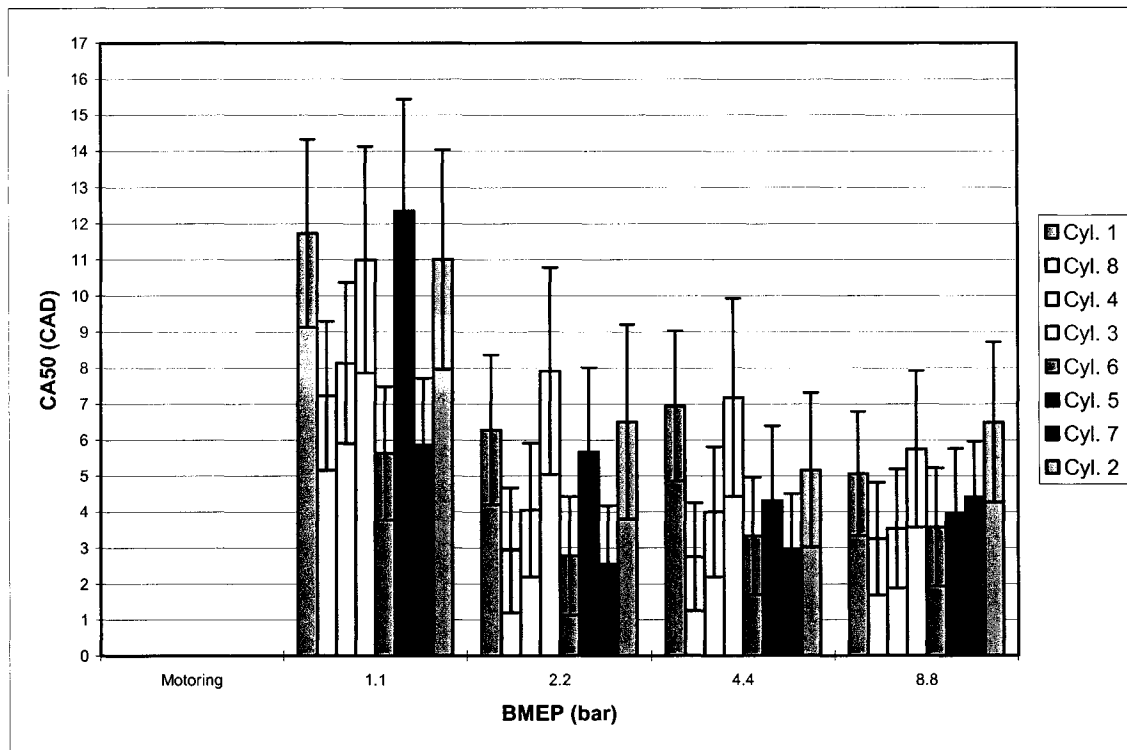


Figure 49: CA50 and its SD at 3000 RPM and Varying Engine Loads

What is interesting to note in Figure 46 and Figure 48 is the negative values for motoring conditions. This is due to the heat transfer to the walls during compression and expansion. The temperature during the expansion stroke will not be as great as the compression stroke causing a slightly decreased pressure in this region. This may also be due to a slightly incorrect estimation of where Top Dead Center is located by the 1° angle encoder.

In Figure 49, data for the motoring condition is not given since there is no fuel burning under these conditions. In Figure 47, the motoring peak pressure is noticeably large due to the large amount of air entering the cylinder under WOT conditions. Comparing this data to the data at 8.8 bar shows that an approximately 35 bar increase in pressure is due to combustion.

Having mainly focused on the mean and standard deviations of the combustion performance parameters from all eight cylinders in Figure 42 to Figure 49, the same data will be presented in a different manner in order to better understand the level of cylinder-to-cylinder variation. Figure 50 to Figure 57 show for each combustion performance parameter the percent difference in the estimated value for an individual cylinder compared to the average across the engine at each operating condition.

When looking for patterns in cylinder-to-cylinder variations, there seems to be more of a trend when varying engine load compared to engine speed. In Figure 50 to Figure 53 showing multiple engine speeds at WOT, only cylinders 8 and 6 follow a trend in the percent difference in IMEP and PP producing values that are consistently above the engine average. All other cylinders fluctuate between positive and negative values. In terms of the Location of PP and CA50, there doesn't seem to be any trend at all. However in Figure 54 to Figure 57 where engine load is varied at 3000 RPM, cylinders 8, 6, and 7 consistently produce values of IMEP and PP that are over the average, whereas cylinders 4, 3, 5, and 2 consistently produce values under the average. The only cylinder which fluctuates between positive and negative values is cylinder 1. In terms of the Location of PP and CA50, cylinders 1, 3, and 2 consistently produce values above average whereas cylinders 8, 4, 6, and 7 consistently produce values below average. Cylinder 5 shows a continually decreasing difference with increasing engine load.

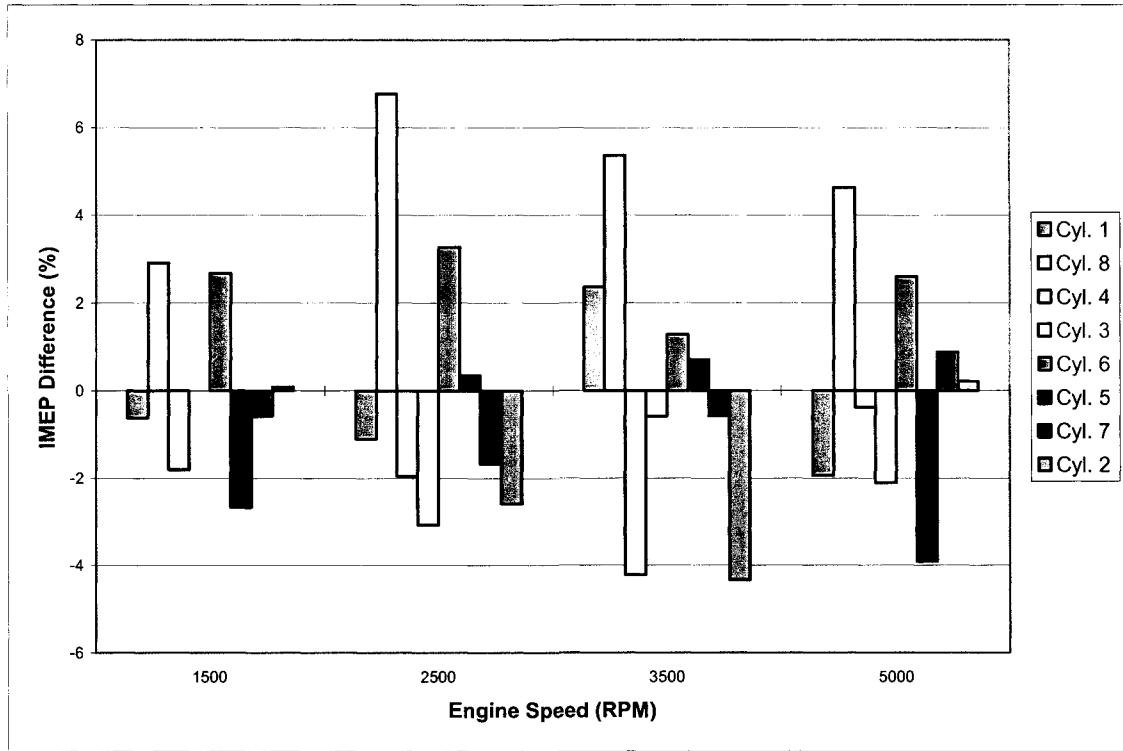


Figure 50: Effect of Engine Speed on IMEP Cylinder-to-Cylinder Variations

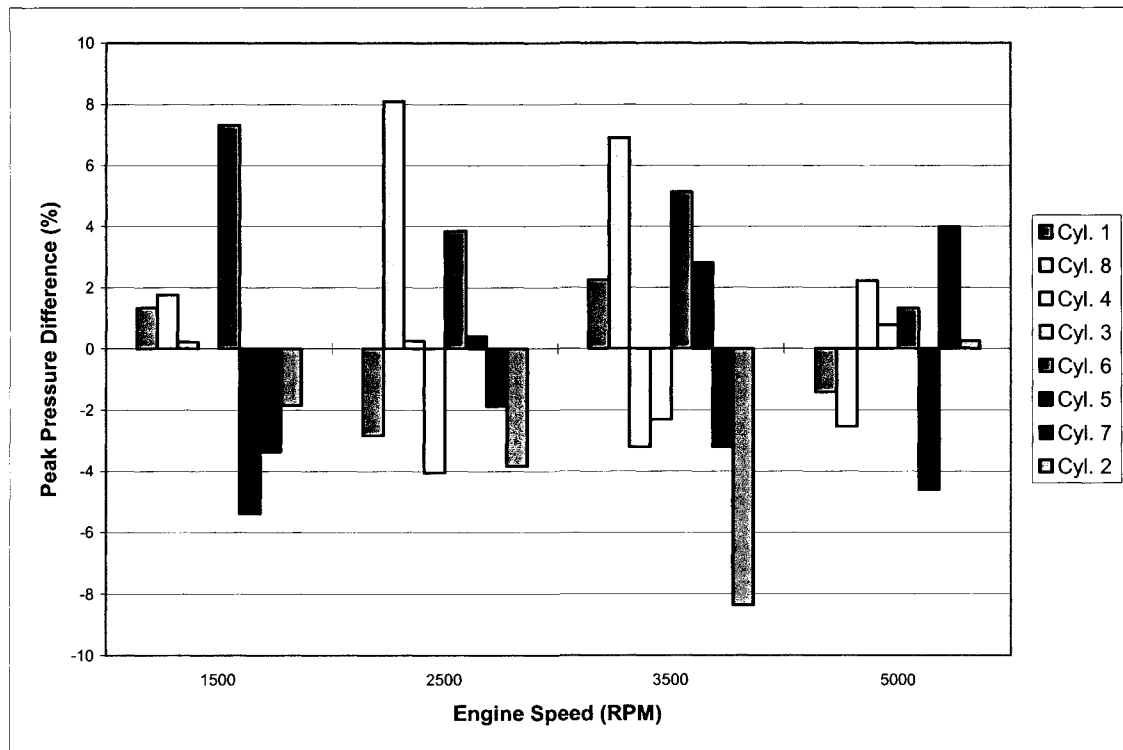


Figure 51: Effect of Engine Speed on Peak Pressure Cylinder-to-Cylinder Variations

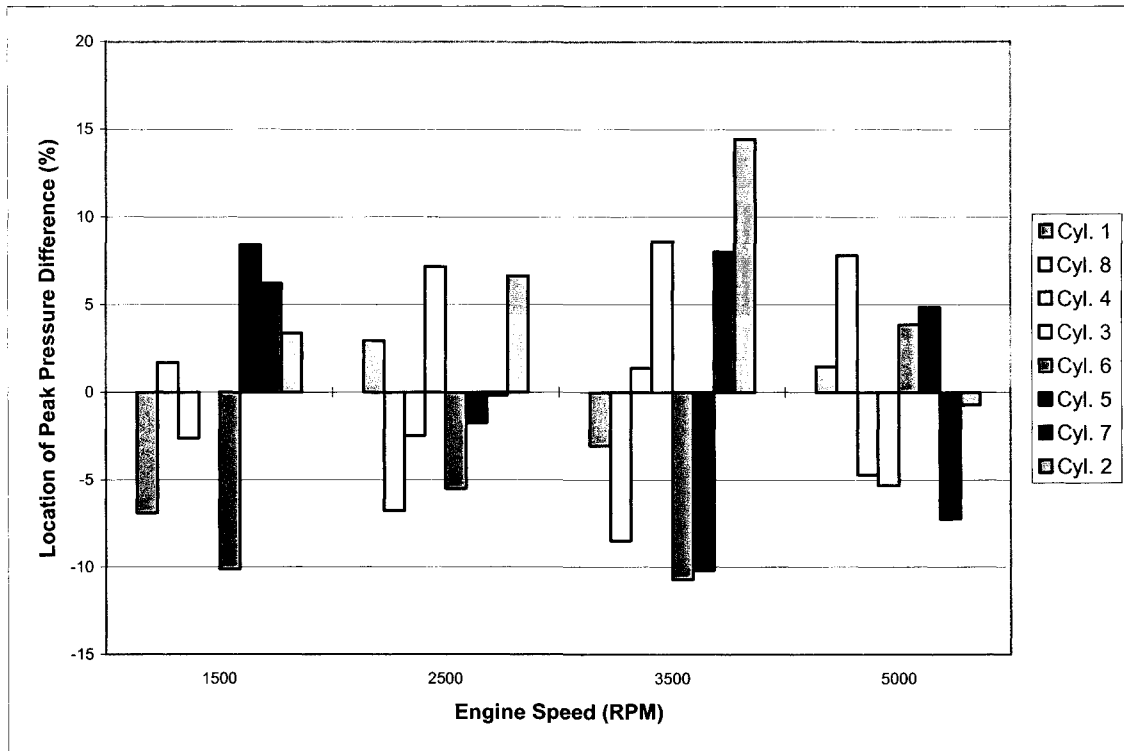


Figure 52: Effect of Engine Speed on Location of PP Cylinder-to-Cylinder Variations

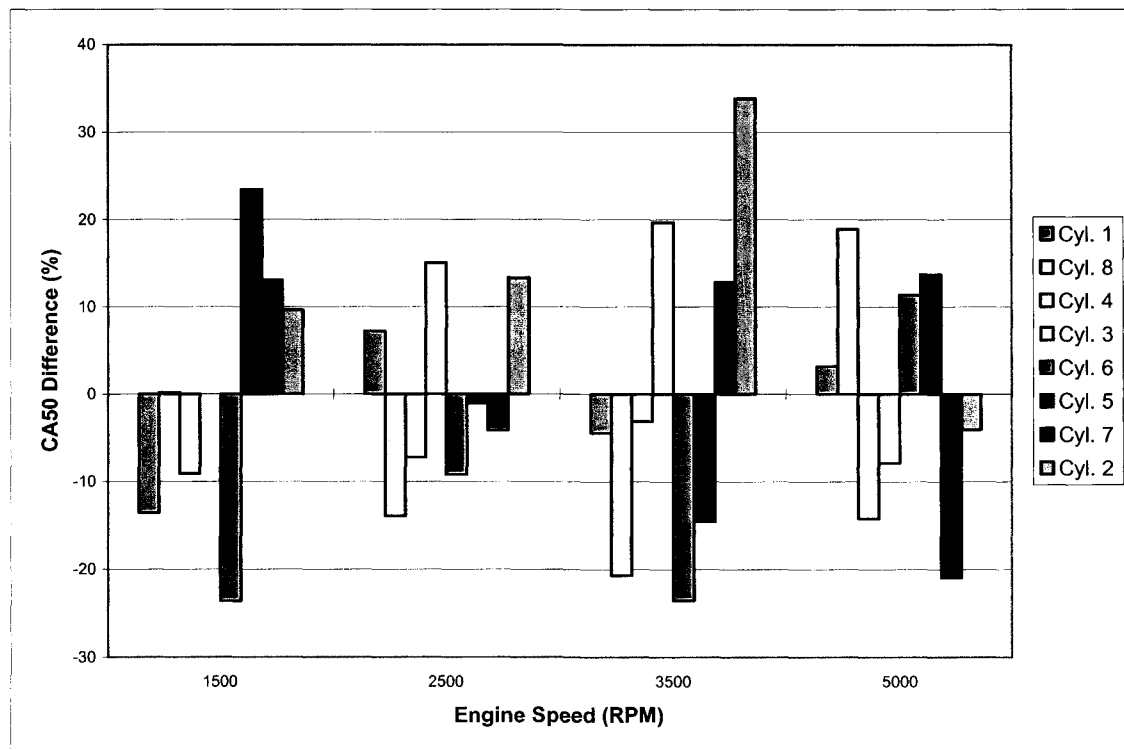


Figure 53: Effect of Engine Speed on CA50 Cylinder-to-Cylinder Variations

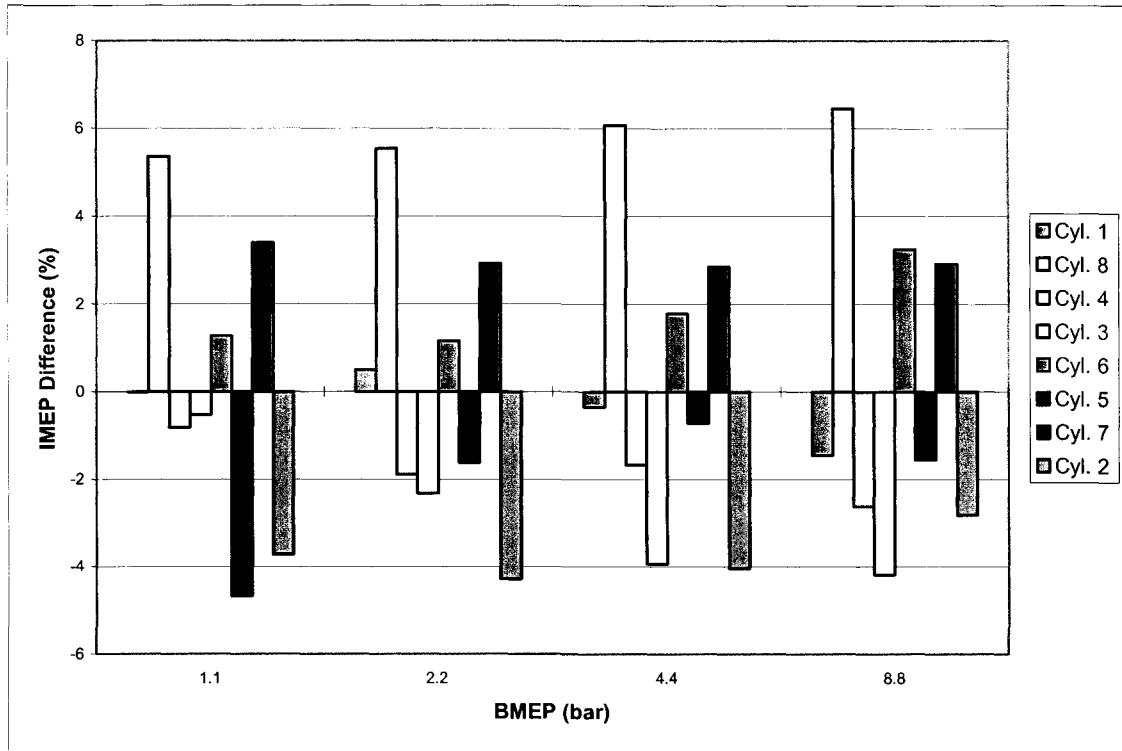


Figure 54: Effect of Engine Load on IMEP Cylinder-to-Cylinder Variations

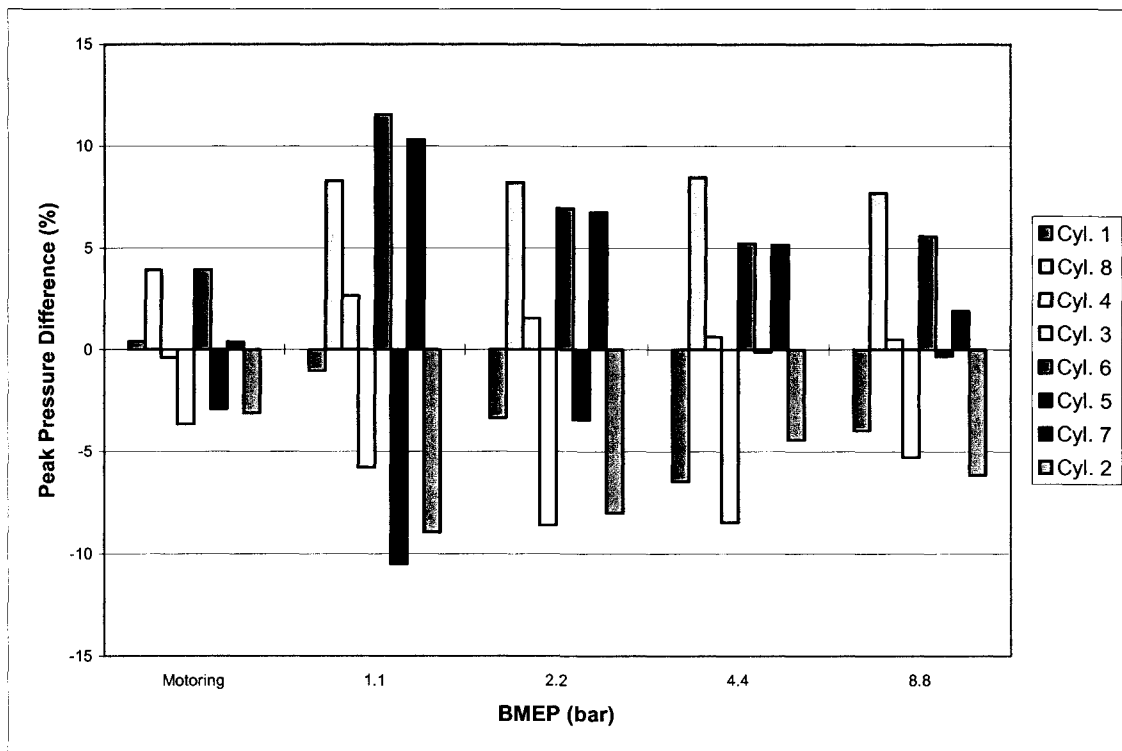


Figure 55: Effect of Engine Load on Peak Pressure Cylinder-to-Cylinder Variations

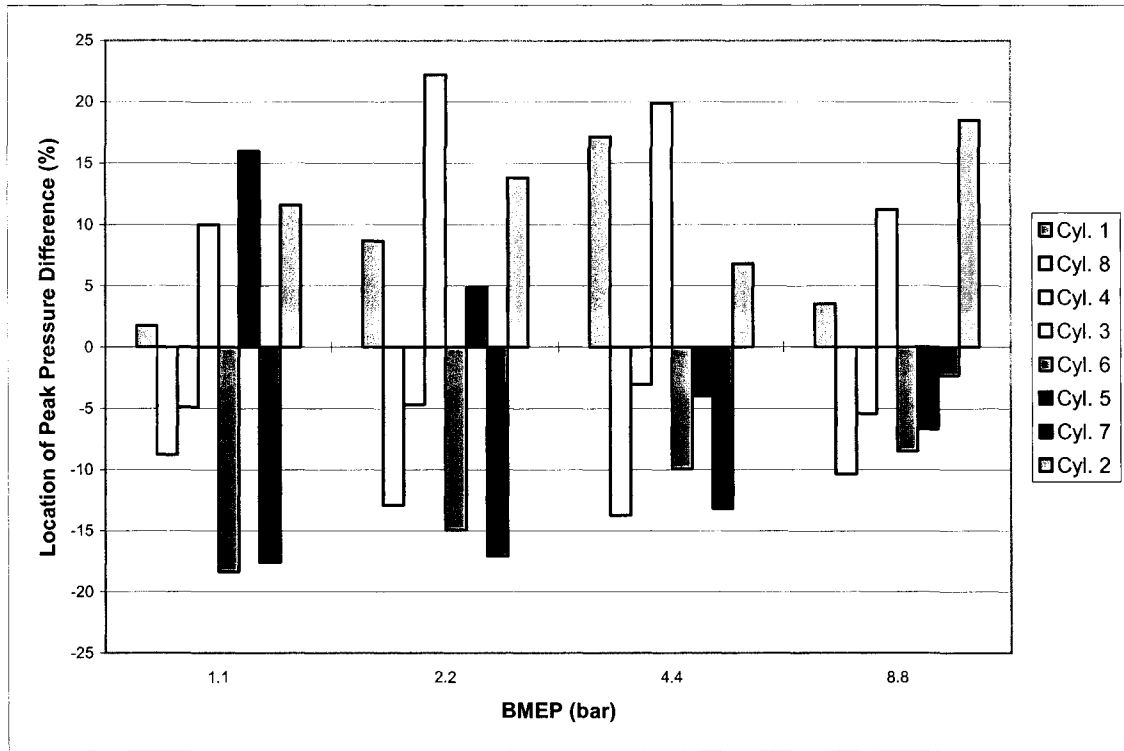


Figure 56: Effect of Engine Load on Location of PP Cylinder-to-Cylinder Variations

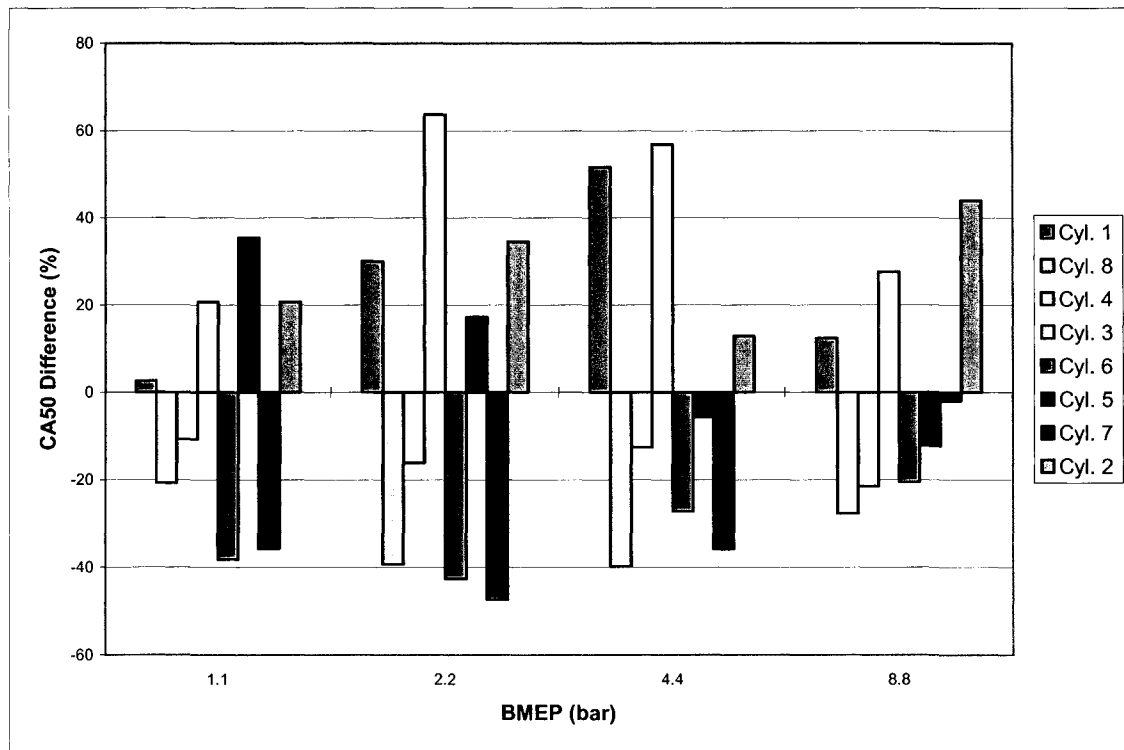


Figure 57: Effect of Engine Load on CA50 Cylinder-to-Cylinder Variations

What is glaringly obvious in these graphs which was not so clear in Figure 42 to Figure 49 is the correlation between IMEP and PP and between the Location of PP and CA50. In each case where engine load and engine RPM were varied, the shape of these plots are similar, which when thought about should be expected. When peak cylinder pressure is below the average for a single cylinder, the area surrounded by the compression and expansion strokes on a P-V diagram will also be less than the average, causing a decrease in that cylinder's IMEP compared to the engine average. When a value of CA50 is below the average, this means that the combustion process occurred at a faster rate in that particular cylinder since smaller values of CA50 translate into faster burning rates. With a faster burning rate, the location at which peak cylinder pressure occurs will be sooner in the cycle since the total combustion process occurs over fewer crank angle degrees, causing these values to be below the engine average. The opposite trends (if above average) also hold true for both cases.

What is also noticeable is the inverse relationship between the two pairs of combustion performance parameters. If values of IMEP and PP are above average then values of CA50 and the Location of PP are generally below average (and vice versa). This can be attributed to the fact that as burning rates increase (CA50 and the Location of PP decrease), PP and IMEP will increase due to a larger amount of charge already being burned at a smaller combustion chamber volume.

9.6 Bank-to-Bank Variations

The cylinder-to-cylinder variation data was also arranged bank-to-bank (1-3-5-7-2-4-6-8) and is shown in Appendix C. Having not provided any additional insight into the analysis of cylinder-to-cylinder variation, two additional tables were created with the same

data to investigate bank-to-bank variation. Shown here are the combustion performance parameters arranged in three different groups for each engine RPM (Table 5) and engine load (Table 6). The right bank data is an average of cylinders 1, 3, 5, and 7 and the left bank data is an average of cylinders 2, 4, 6, and 8. The engine average data involves all eight cylinders. In both tables, the IMEP and PP values for the left bank are consistently higher than the engine average with the exception of 3500 RPM and WOT. Differences are larger at larger throttle openings as expected. In terms of the Location of PP and CA50, the values given for the left bank are generally lower than the average, following the same trend seen in the cylinder-to-cylinder variation analysis.

		1500 (RPM)	2500 (RPM)	3500 (RPM)	5000 (RPM)
IMEP	<i>Engine Average</i>	8.07	8.88	10.54	9.16
	<i>Right Bank</i>	7.97	8.76	10.59	9.00
	<i>Left Bank</i>	8.15	9.01	10.48	9.32
PP	<i>Engine Average</i>	43.14	47.03	58.96	48.53
	<i>Right Bank</i>	42.07	46.05	58.90	48.38
	<i>Left Bank</i>	43.94	48.01	59.03	48.69
Location of PP	<i>Engine Average</i>	12.50	12.38	11.36	13.72
	<i>Right Bank</i>	12.82	12.63	11.46	13.50
	<i>Left Bank</i>	12.26	12.13	11.26	13.93
CA50	<i>Engine Average</i>	6.96	6.79	5.69	8.75
	<i>Right Bank</i>	7.50	7.08	5.88	8.49
	<i>Left Bank</i>	6.57	6.50	5.50	9.02

Table 5: Effect of Engine Speed on Combustion Performance Parameters arranged Bank-to-Bank

		1.1 (bar)	2.2 (bar)	4.4 (bar)	8.8 (bar)
IMEP	<i>Engine Average</i>	2.52	3.51	5.51	9.96
	<i>Right Bank</i>	2.51	3.50	5.48	9.85
	<i>Left Bank</i>	2.53	3.51	5.54	10.06
PP	<i>Engine Average</i>	13.53	20.62	32.27	56.79
	<i>Right Bank</i>	13.07	20.18	31.47	55.71
	<i>Left Bank</i>	13.99	21.07	33.06	57.87
Location of PP	<i>Engine Average</i>	14.59	11.24	10.77	10.56
	<i>Right Bank</i>	15.33	11.76	11.31	10.72
	<i>Left Bank</i>	13.84	10.71	10.24	10.41
CA50	<i>Engine Average</i>	9.12	4.84	4.58	4.50
	<i>Right Bank</i>	10.23	5.60	5.34	4.80
	<i>Left Bank</i>	8.00	4.07	3.81	4.21

Table 6: Effect of Engine Load on Combustion Performance Parameters arranged Bank-to-Bank

9.7 Durability

Although the transducers were not specifically investigated for durability issues, the testing was completed over a time span of approximately 100 hours during which the performance of the Optrand transducers started to degrade. This is considerably poor performance in terms of durability since a standard durability test runs for 650 hours. Appendix A (Figure 58 to Figure 73) shows the pressure difference data collected for the Kistler Spark transducer on all eight cylinders. The data is presented in the order in which it was taken in order to see if there was any signal degradation. Inspection of this data does not provide any evidence that the performance of this transducer has degraded. In fact, by looking at Figure 64 and Figure 65 one can see that this transducer provided essentially the exact same output that it had many hours before. This data can be compared to Figure 22 and Figure 25 to see that the results are repeatable up to 0.7 bar, even with numerous hours of testing completed between the two sets of data.

The results for the Optrand transducer shown in Appendix B (Figure 74 to Figure 89) show significant signal degradation and eventually transducer failure. Results from the Optrand transducer in cylinder #1 (Figure 80 and Figure 81) differ significantly with the data taken numerous hours earlier in the same cylinder (Figure 23 and Figure 26). At WOT and 1500 RPM the maximum negative thermal shock jumped from -0.5 bar to -1.4 bar and the maximum positive thermal shock jumped from 1.7 bar to 2.5 bar. This was followed by a transducer failure after testing one more cylinder (cylinder 2). The output from the diagnostic cable was 3.5 Volts, indicating a failed transducer along with erroneous pressure data. To complete the testing, transducer Optrand 7 replaced the failed transducer and produced similar results in Figure 84 to Figure 89 as is shown in Figure 21.

CHAPTER 10: SUMMARY, CONCLUSIONS, AND RECOMMENDATIONS

A comparative study of Kistler 6117 piezoelectric and Optrand C222-CP optical fiber spark plug mounted transducers was conducted on a DaimlerChrysler 4.7L V-8 CNG fuelled test engine.

Variations in performance in terms of thermal shock error among the four Optrand C222-CP transducers were much larger than those among the four Kistler 6117 transducers.

The Optrand C222-CP No. 9 optical fibre transducer demonstrated a different response to thermal shock than the Kistler 6117BF17 No. 13 transducer. The Optrand transducer reacts to thermal shock in two opposing ways (cylinder pressure was underestimated or overestimated) at different crank angles throughout the region where IMEP is calculated, whereas thermal shock always caused the Kistler transducer to underestimate cylinder pressure in the same region. This behaviour of the Optrand transducer led to more accurate estimates of IMEP, and suggests this transducer's potential to be a useful and inexpensive tool for IMEP evaluation.

The Kistler transducer provided smaller values of maximum thermal shock error compared to the Optrand transducer which suggests that the Kistler transducer gives a more accurate estimation of actual cylinder pressure during the expansion stroke. In terms of ΔP averaged over the entire engine cycle, the Optrand transducer provides smaller values than the Kistler transducer, which suggests that the Optrand transducer more adequately represents actual cylinder pressure over the entire engine cycle.

Both transducers provided inaccurate results of cylinder peak pressure. The Optrand transducer overestimated peak cylinder pressure while the Kistler transducer underestimated peak cylinder pressure.

The individual cylinder raw pressure data analysis showed that the two Kistler transducers tested, regardless of their mounting location, introduce a smaller amount of intracycle variability than the Optrand optical fiber transducer. It is the prolonged time response of the optical fiber transducer to thermal shock that limits this transducer's ability for recovery earlier in the cycle.

The prolonged recovery of the Optrand transducer from thermal shock also introduced drastic errors in PMEP. In all remaining aspects investigated, the Optrand and Kistler test transducers and the Kistler 6052A1 reference transducer measured reliably and had comparable results up until the Optrand transducer failed. After less than 100 hours of testing, the Optrand transducer started to produce erroneous pressure data and had to be replaced by another transducer from Optrand.

The individual cylinder analysis showed that there is a maximum deviation in IMEP of approximately +/-5% between all eight cylinders, suggesting that all cylinders are not burning a similar charge. Standard Deviations of IMEP for all cylinders are small, suggesting that each cylinder is receiving a similar charge from cycle to cycle.

It is recommended that a similar analysis of the Kistler and Optrand spark-plug mounted transducers be completed with a Kistler water-cooled transducer used as the reference. Significant time was spent analyzing the pressure difference curves to determine

which transducer was most affected by thermal shock. This analysis would not be necessary with a large, water-cooled transducer since it exhibits almost no thermal shock effects.

One additional step that should be added to the analysis is the response of the transducers to engine knock. Controlling knock is of paramount importance in spark-ignited engines and failing to do so could result in engine failure. Use of a cylinder pressure transducer is an ideal way to detect engine knock and should therefore be investigated with each type of transducer.

CHAPTER 11: REFERENCES

1. M. Sellnau, F. A. Matekunas, P.A. Battiston, C.-F. Chang, and D.R. Lancaster, "Cylinder-Pressure-Based Engine Control Using Pressure-Ratio-Management and Low-Cost Non-Intrusive Cylinder Pressure Sensors", SAE Paper 2000-01-0932, 2000.
2. R. Muller, M. Hart, A. Truscott, A. Noble, G. Krotz, M. Eickhoff, C. Cavalloni, and M. Gnielka, "Combustion Pressure Based Engine Management System", SAE Paper 2000-01-0928, 2000.
3. H.S. Rai, M.F.J. Burnt, and C. P. Loader, "Quantification and Reduction of IMEP Errors Resulting from Pressure Transducer Thermal Shock in an S.I. Engine", SAE Paper 1999-01-1329, 1999.
4. J. D. Powell, "Engine Control Using Cylinder Pressure: Past, Present, and Future", *Journal of Dynamic Systems, Measurements, and Control*, Vol.111/343, June 1993.
5. M. Mladek and C. H. Onder, "A Model for The Estimation of Induced Air Mass and the Residual Gas Fraction Using Cylinder Pressure Measurements", SAE Paper 2000-1-0958, 2000.
6. J. K. Ball, C. R. Stone, and R. R. Raine, "A Technique for Estimating Completeness of Combustion and its Use in Modeling Cycle-By-Cycle Variations in Combustion", SAE Paper 2000-01-0953, 2000.
7. O. Ulrich, R. Wlodarczyk, and M. Wlodarczyk, "High-Accuracy Low-Cost Cylinder Pressure Sensor for Advanced Engine Controls", SAE Paper 2001-01-0991, 2001.
8. R. Stone, "Introduction to Internal Combustion Engines", Third Edition, Society of Automotive Engineers, 1999.
9. E. F. Obert, "Internal Combustion Engine", Third Edition, International Text Book Company, 1968.
10. J. B. Heywood, "Internal Combustion Engine Fundamentals", McGraw-Hill, 1988.
11. "Redline ADAPT CAS Workshop", MTS Systems Corporation, DSP Technology Division, 2001.
12. W. L. Brown, "Methods for Evaluating Requirements and Errors in Cylinder Pressure Measurement", SAE Paper 670008, 1967.
13. D. R. Lancaster, R. B. Krieger, and J. H. Lienesch, "Measurement and Analysis of Engine Pressure Data", SAE Paper 750026, 1975.
14. A. L. Randolph, "Cylinder-Pressure-Transducer Mounting Techniques to Maximize Data Accuracy", SAE Paper 900171, 1990.

15. R. H. Kuratle and B. Märki, "Influencing Parameters and Error Sources During Indication on Internal Combustion Engines", SAE Paper 920233, 1992.
16. R. H. Kuratle, "Measuring Spark Plugs with Integrated Cylinder Pressure Sensor", Kistler Instruments AG Winterthur/Switzerland, 1993.
17. M. C. Selnau, F. A. Matekunas, P. A. Battiston, C. F. Chang, D. R. Lancaster, "Cylinder-Pressure-Based Engine Control Using Pressure-Ratio –Management and Low-Cost Non-Intrusive Cylinder Pressure Sensors", SAE Paper 2000-01-0932, 2000.
18. R. Kail and W. Mahr, "Piezoelectric Measuring Instruments and their Applications", "Messen + Prüfen", Vol. 20, No. 7/12, 1984.
19. U. Rösli and P. Wolfer, "Piezoelectric Transducers Measure Pressure", Technische Akademie Esslingen, 1986.
20. <http://www.kistler.com>, Kistler Instrument Corp., 2001.
21. T. Poorman, L. Xia, and M. T. Wlodarczyk, "Ignition System-Embedded Fiber-Optic Combustion Pressure Sensor for Automotive Engine Control and Monitoring", SAE Paper 970853, 1997.
22. "Combustion Engine Measurements", Kistler Instrument Corp., 2000.
23. K. J. Roth, A. Sobiesiak, L. Robertson, and S. Yates, "In-Cylinder Pressure Measurements with Optical Fiber and Piezoelectric Pressure Transducers", SAE Paper 2002-01-0745, 2002.

APPENDIX A: COMPLETE ENGINE DATA USING KISTLER SPARK TRANSDUCER

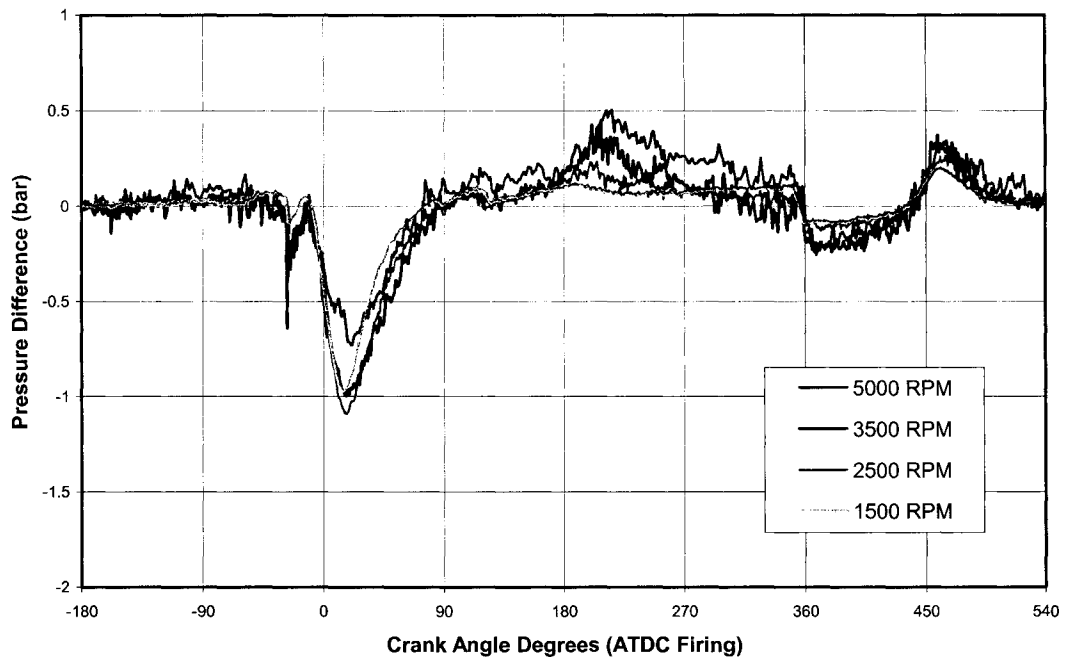


Figure 58: Effect of Engine Speed on Cylinder #3

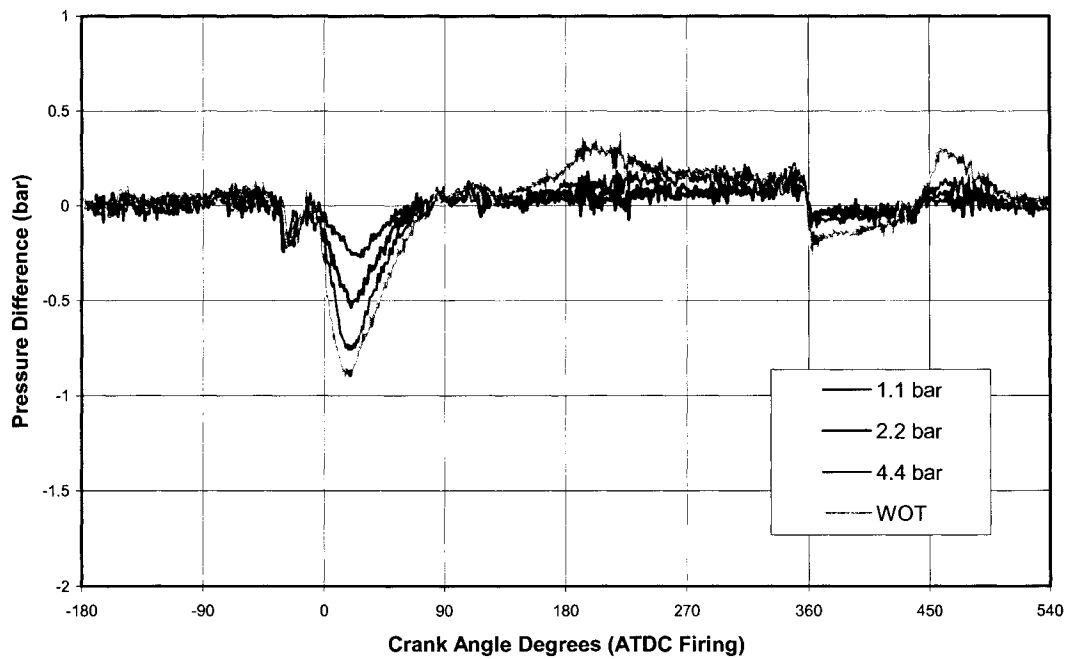


Figure 59: Effect of Engine Load on Cylinder #3

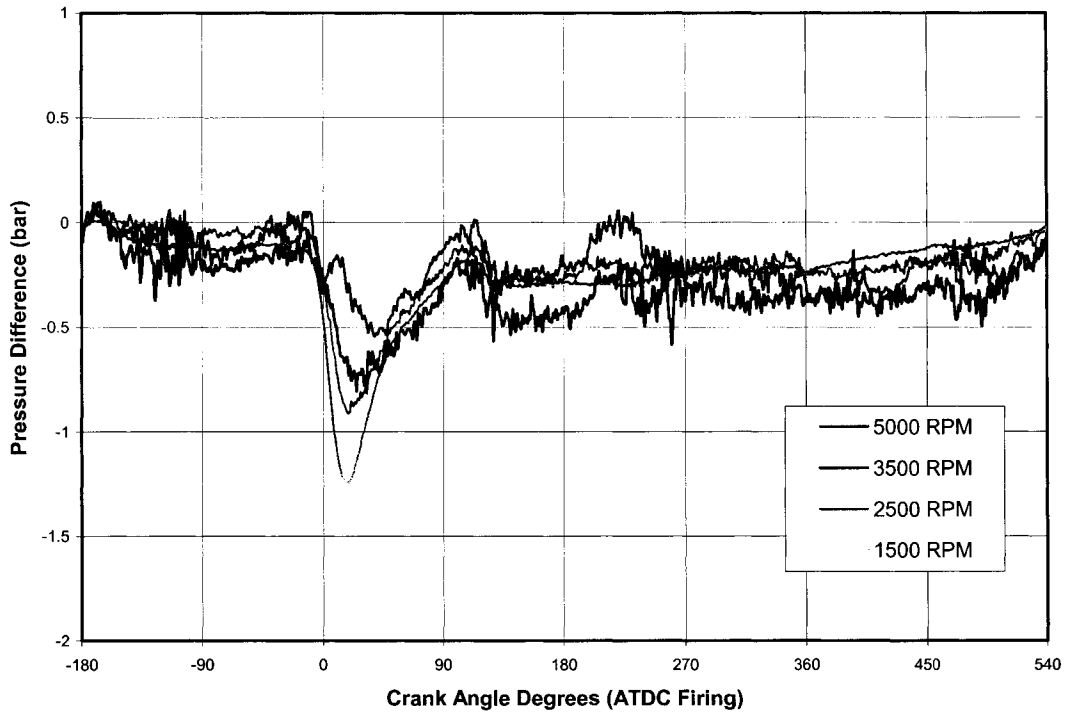


Figure 60: Effect of Engine Speed on Cylinder #5

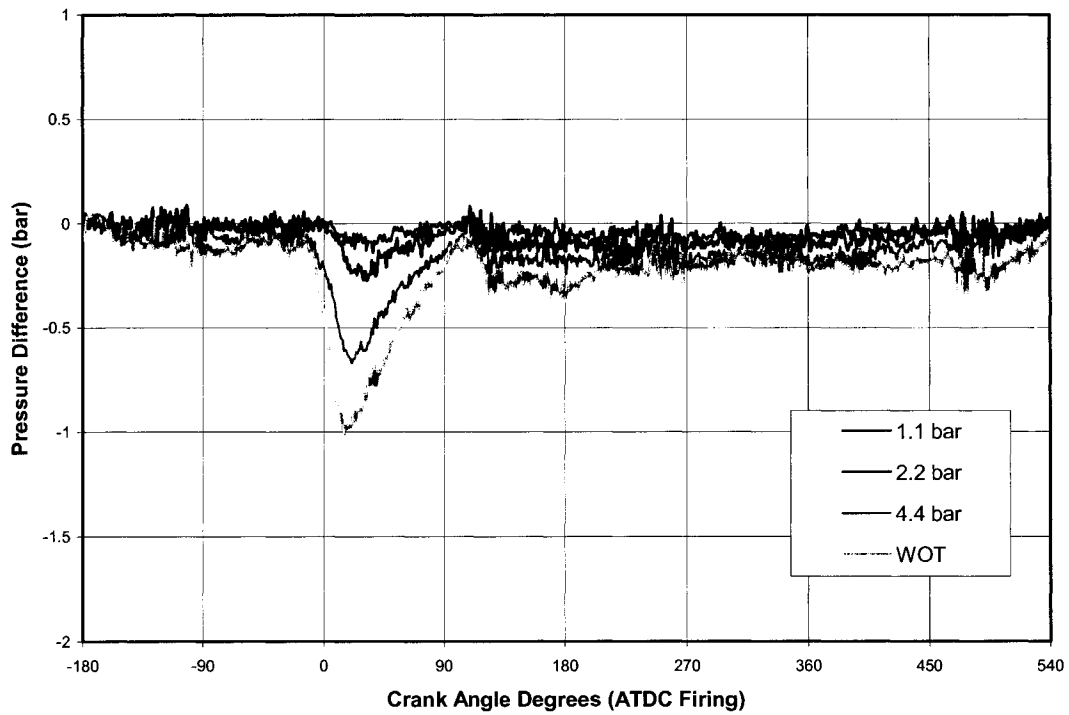


Figure 61: Effect of Engine Load on Cylinder #5

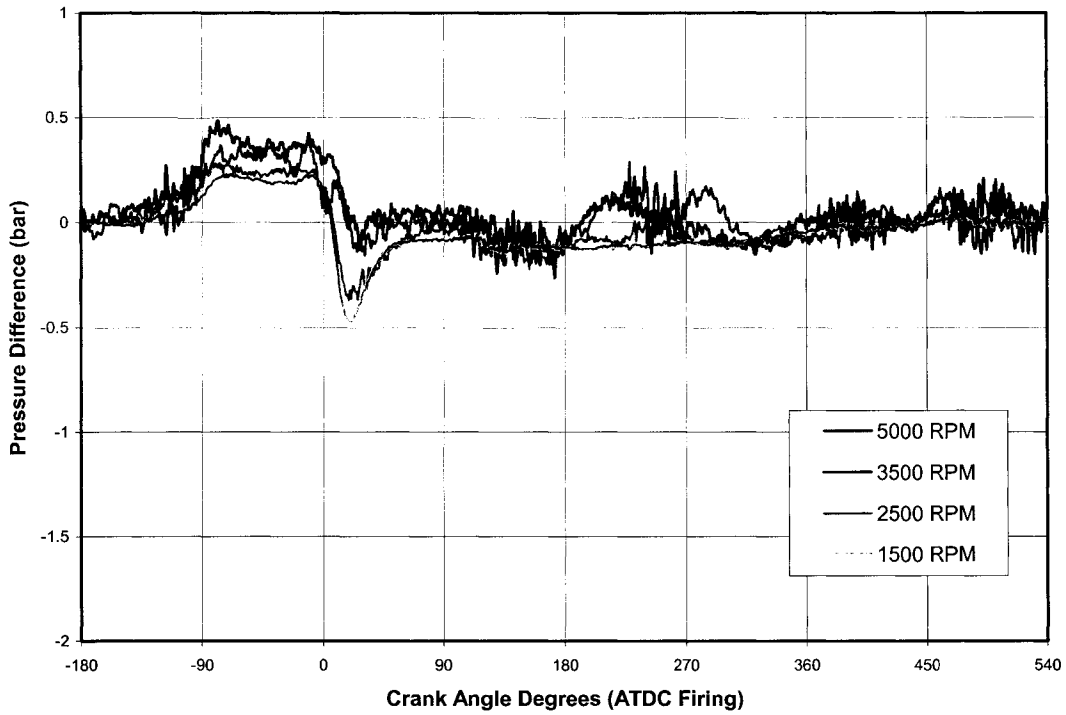


Figure 62: Effect of Engine Speed on Cylinder #7

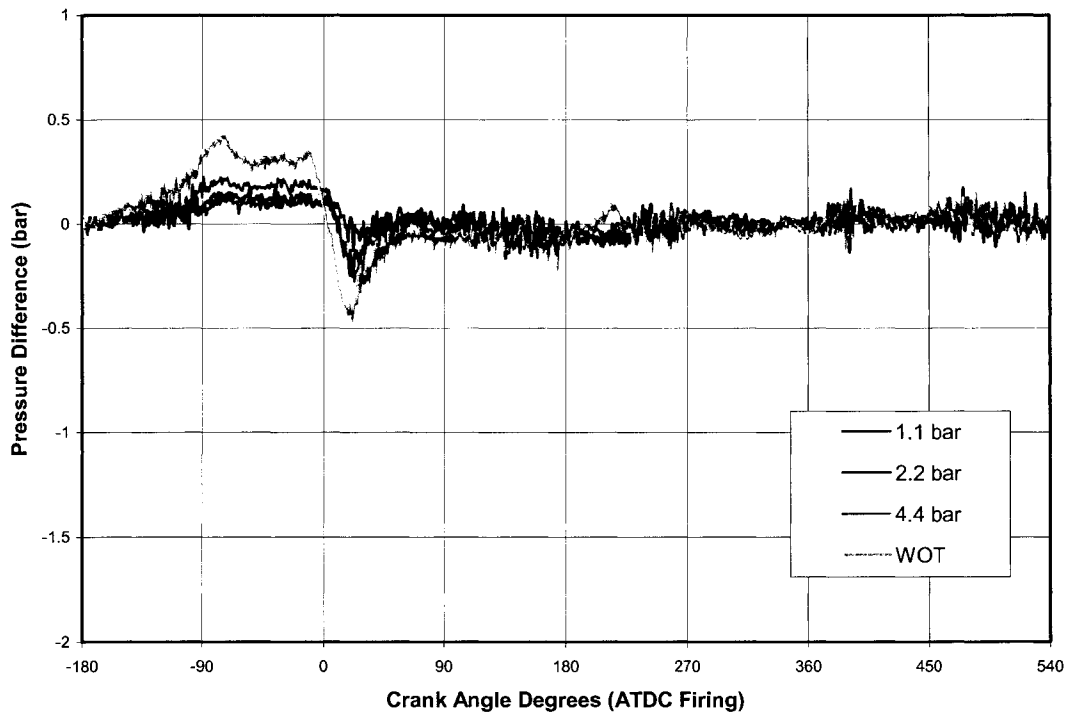


Figure 63: Effect of Engine Load on Cylinder #7

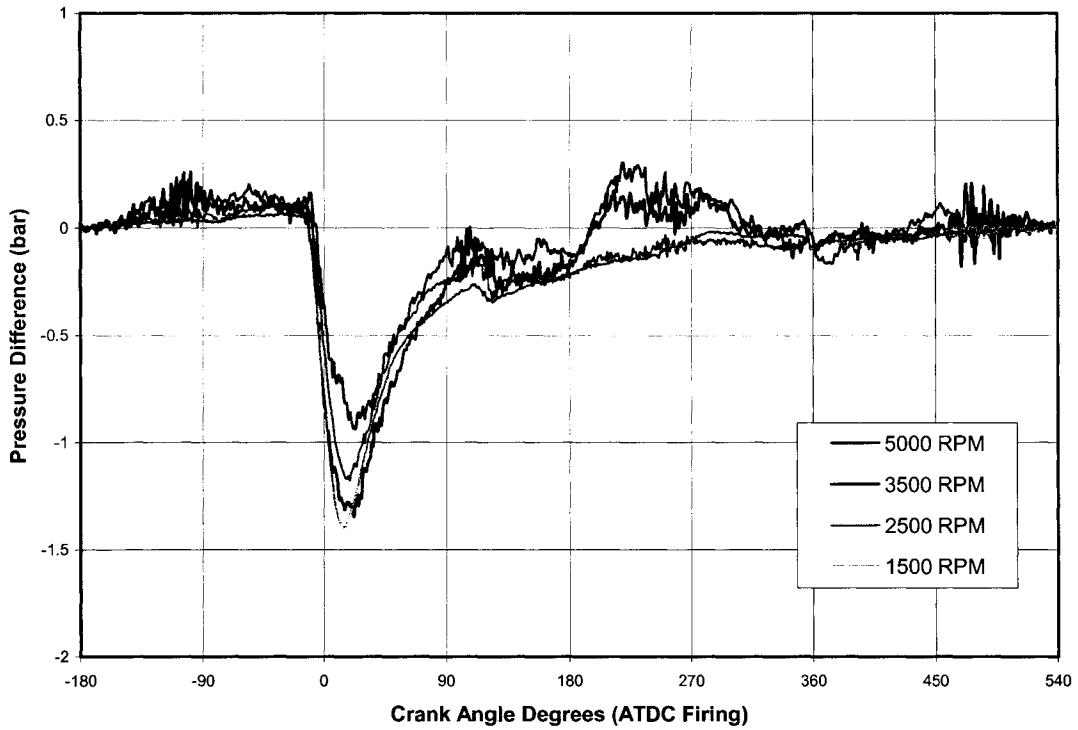


Figure 64: Effect of Engine Speed on Cylinder #1 (Repeated)

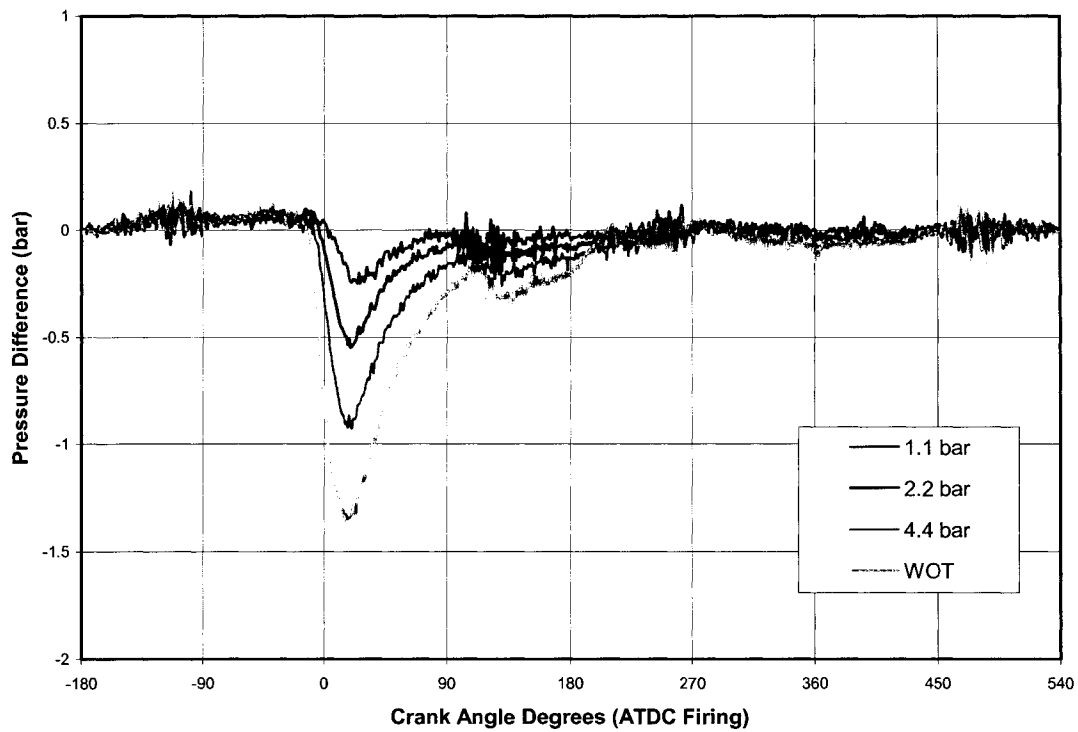


Figure 65: Effect of Engine Load on Cylinder #1 (Repeated)

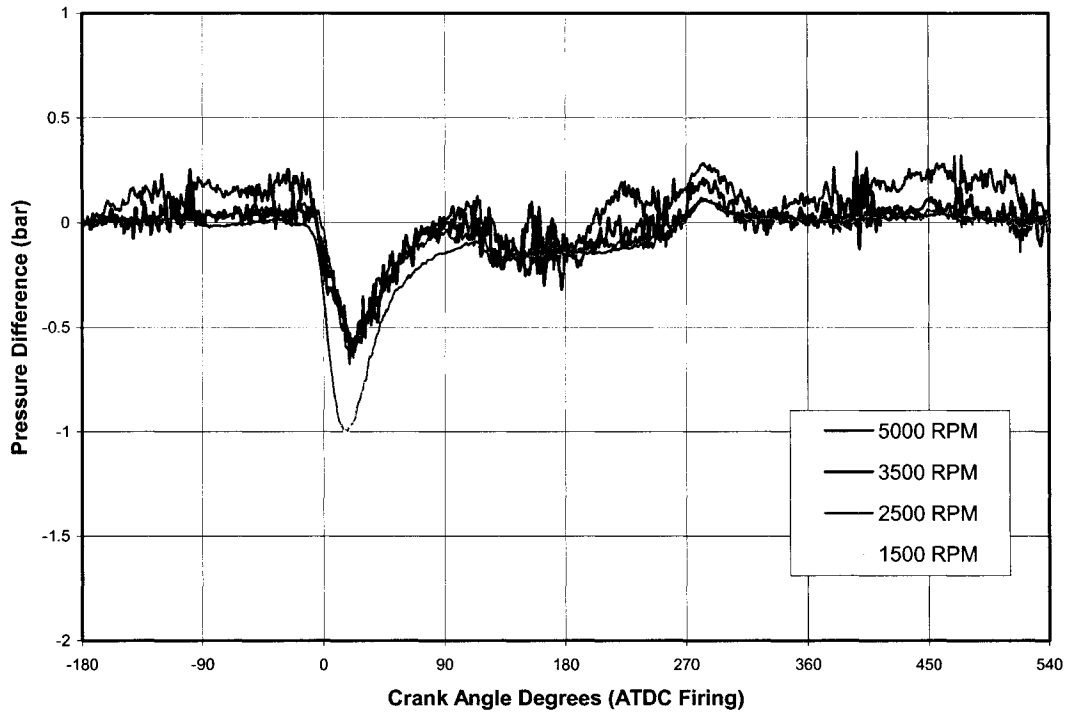


Figure 66: Effect of Engine Speed on Cylinder #2

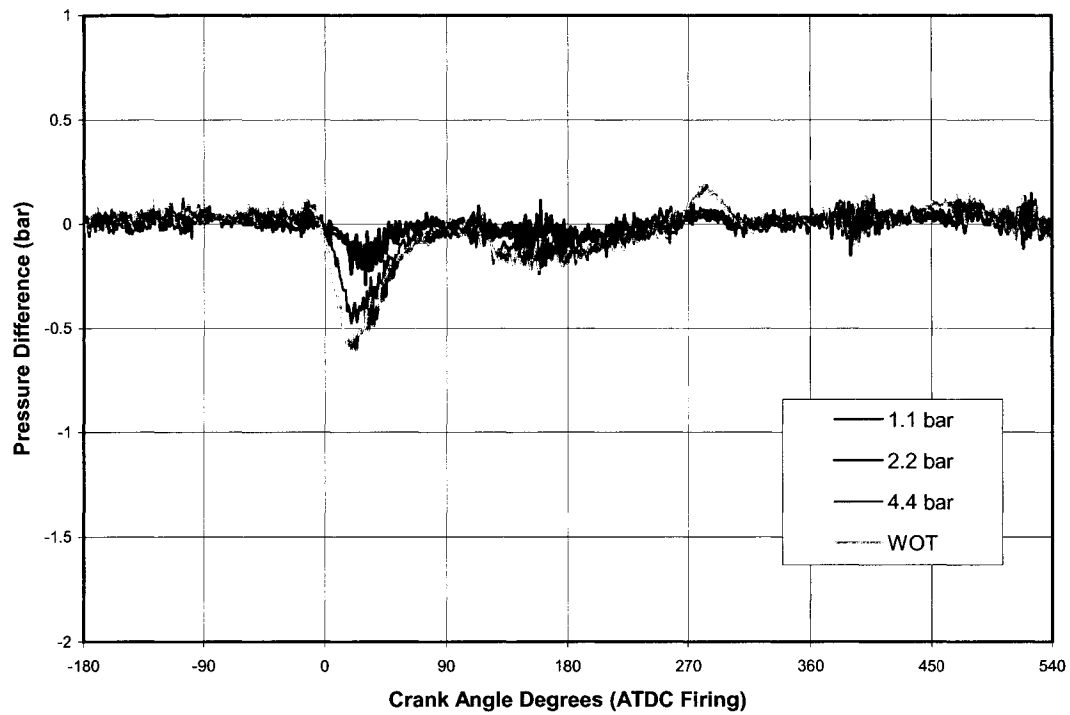


Figure 67: Effect of Engine Load on Cylinder #2

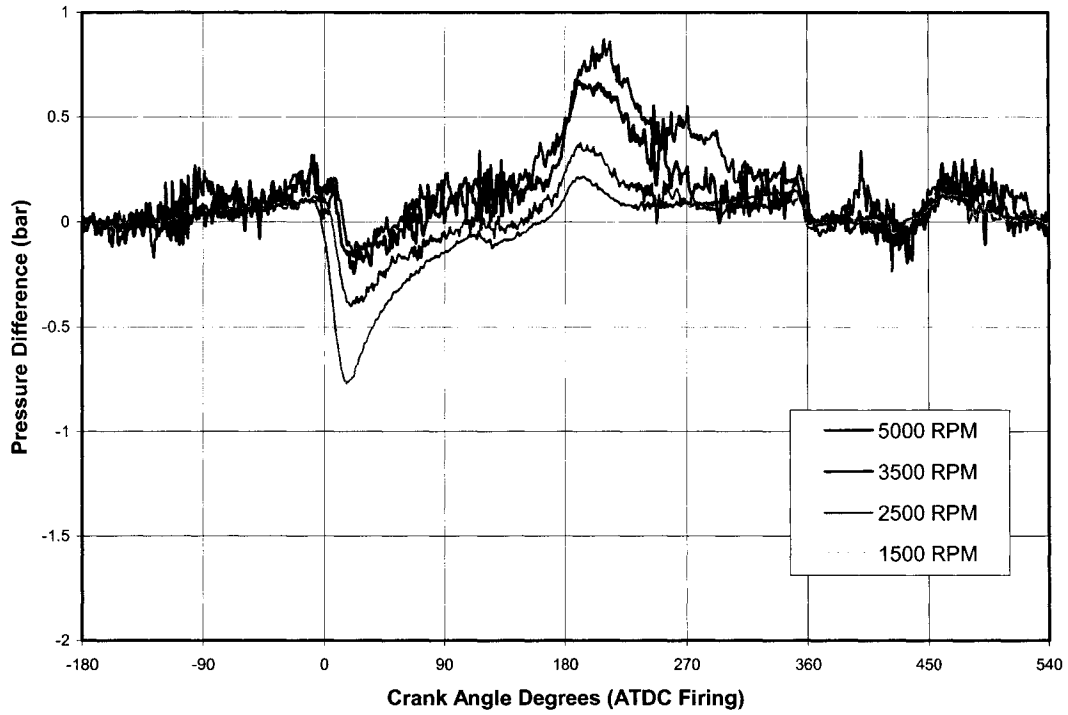


Figure 68: Effect of Engine Speed on Cylinder #4

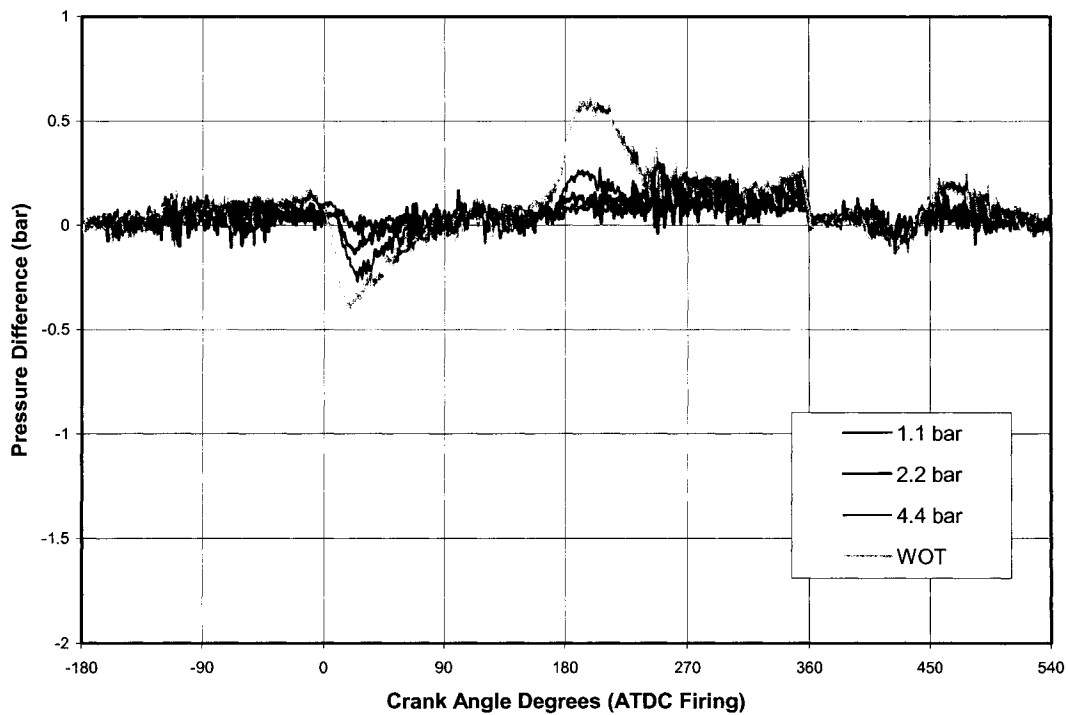


Figure 69: Effect of Engine Load on Cylinder #4

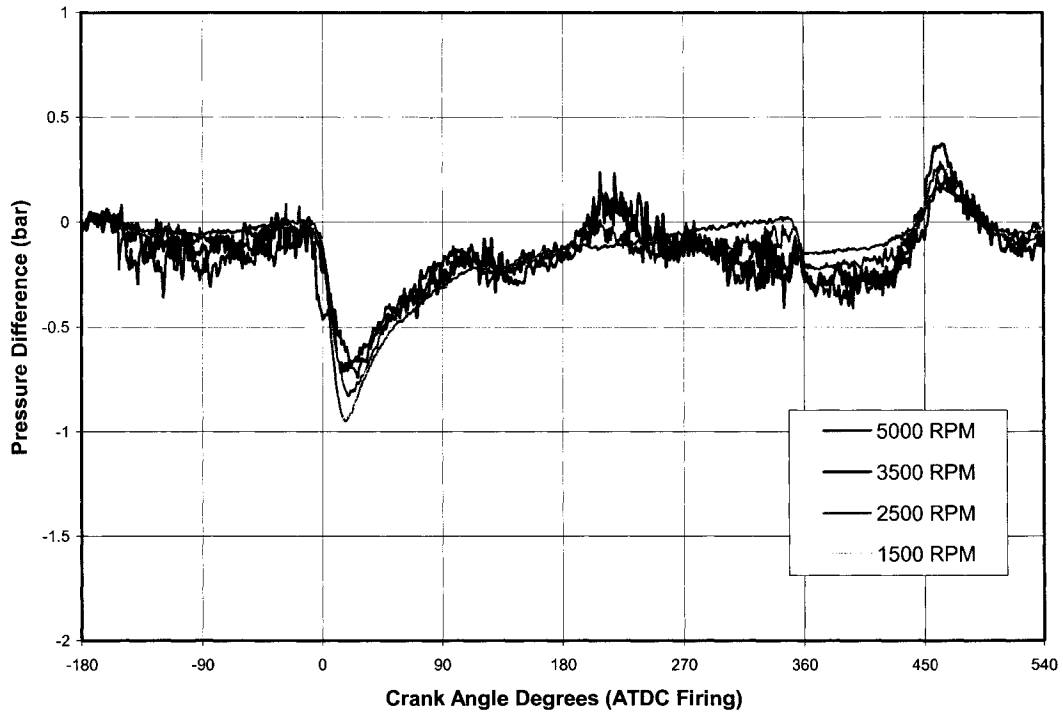


Figure 70: Effect of Engine Speed on Cylinder #6

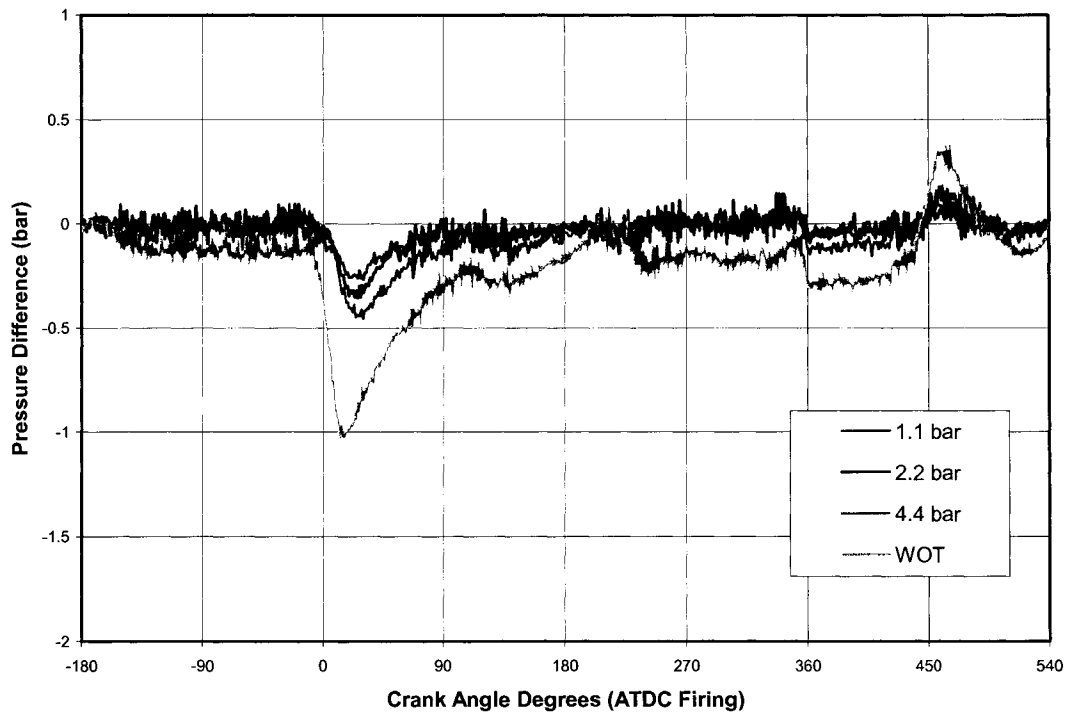


Figure 71: Effect of Engine Load on Cylinder #6

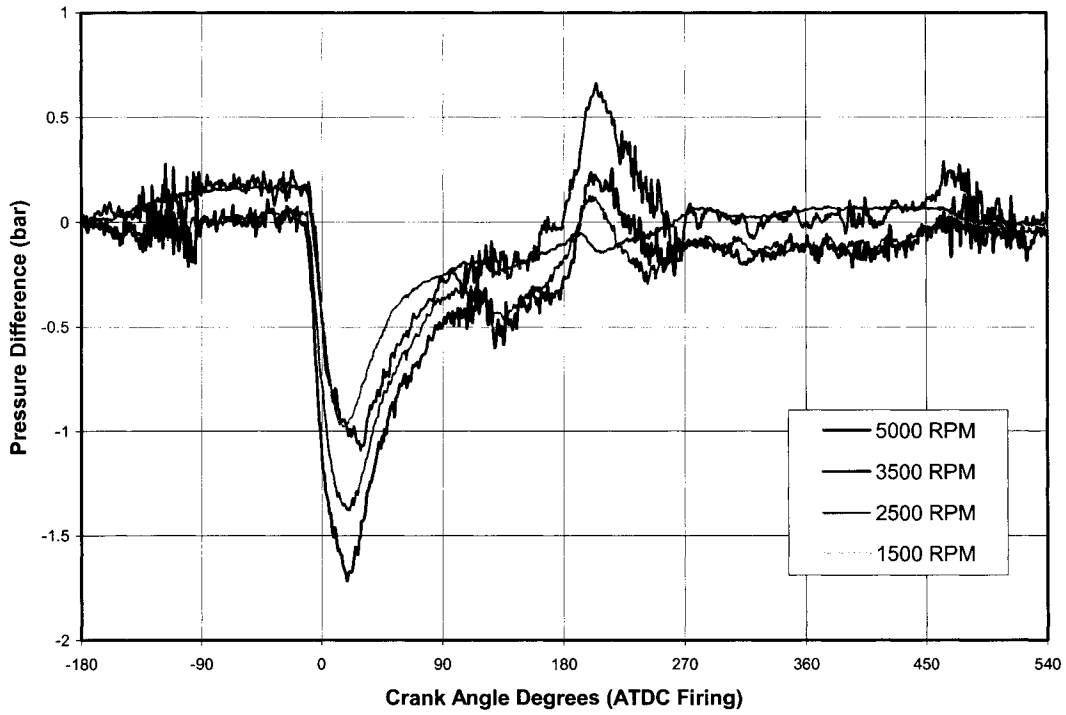


Figure 72: Effect of Engine Speed on Cylinder #8

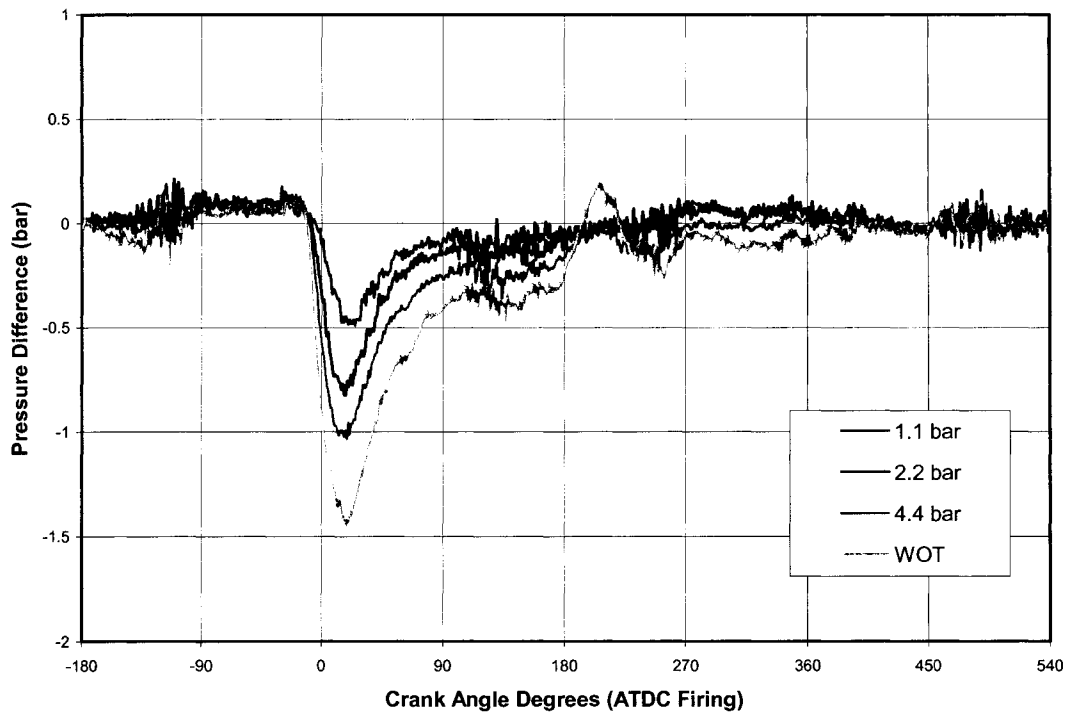


Figure 73: Effect of Engine Load on Cylinder #8

APPENDIX B: COMPLETE ENGINE DATA USING OPTRAND SPARK TRANSDUCER

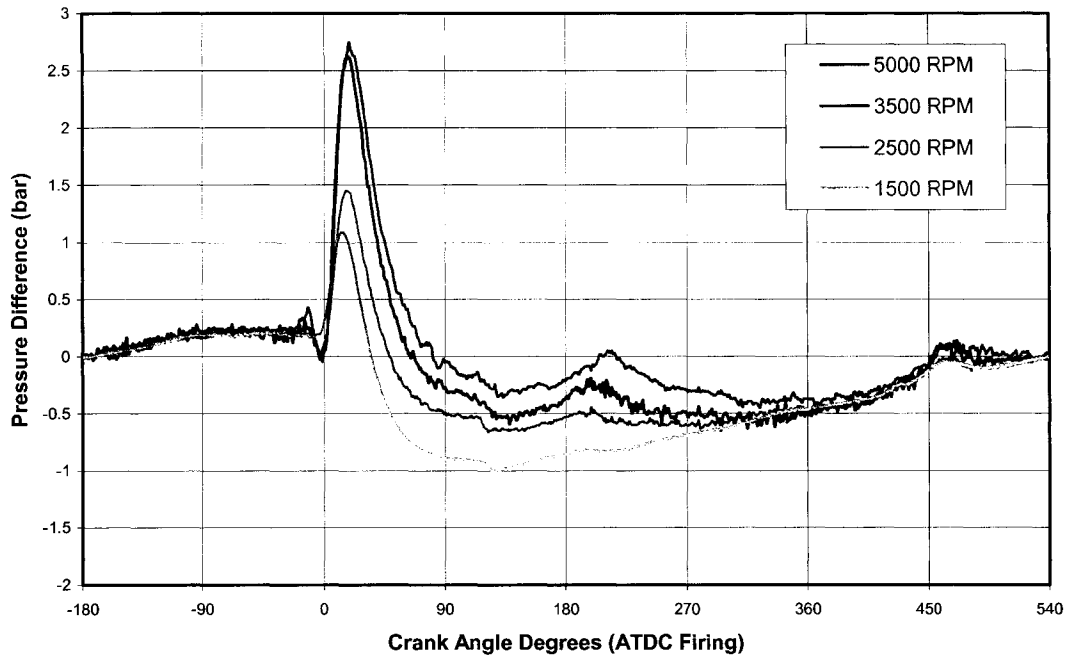


Figure 74: Effect of Engine Speed on Cylinder #3

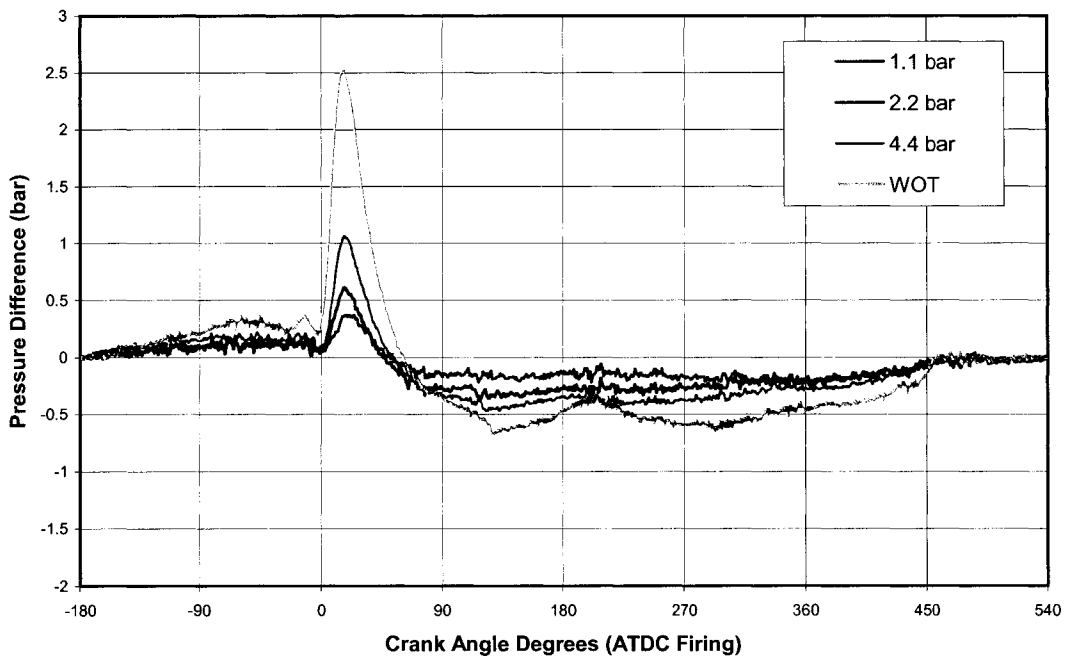


Figure 75: Effect of Engine Load on Cylinder #3

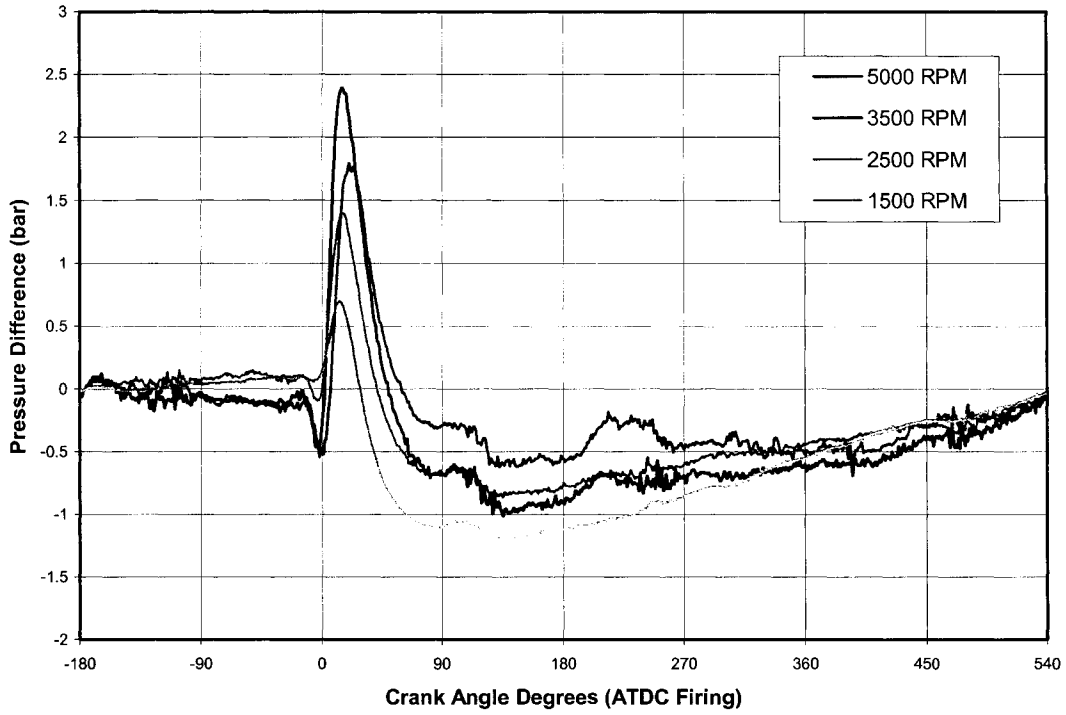


Figure 76: Effect of Engine Speed on Cylinder #5

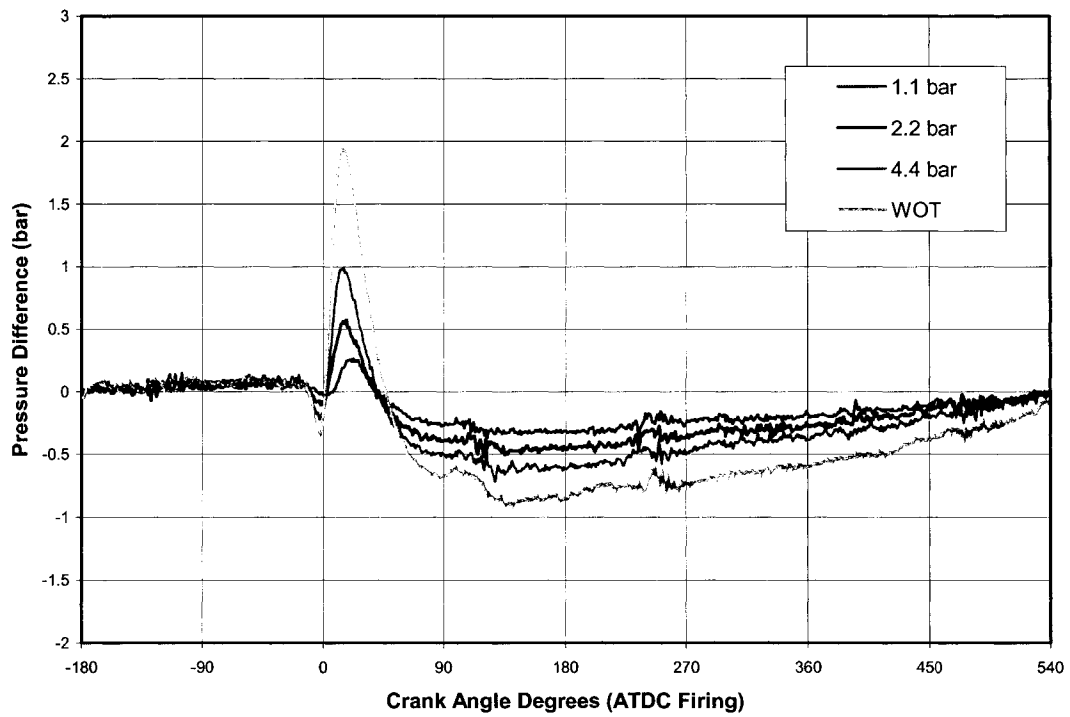


Figure 77: Effect of Engine Speed on Cylinder #5

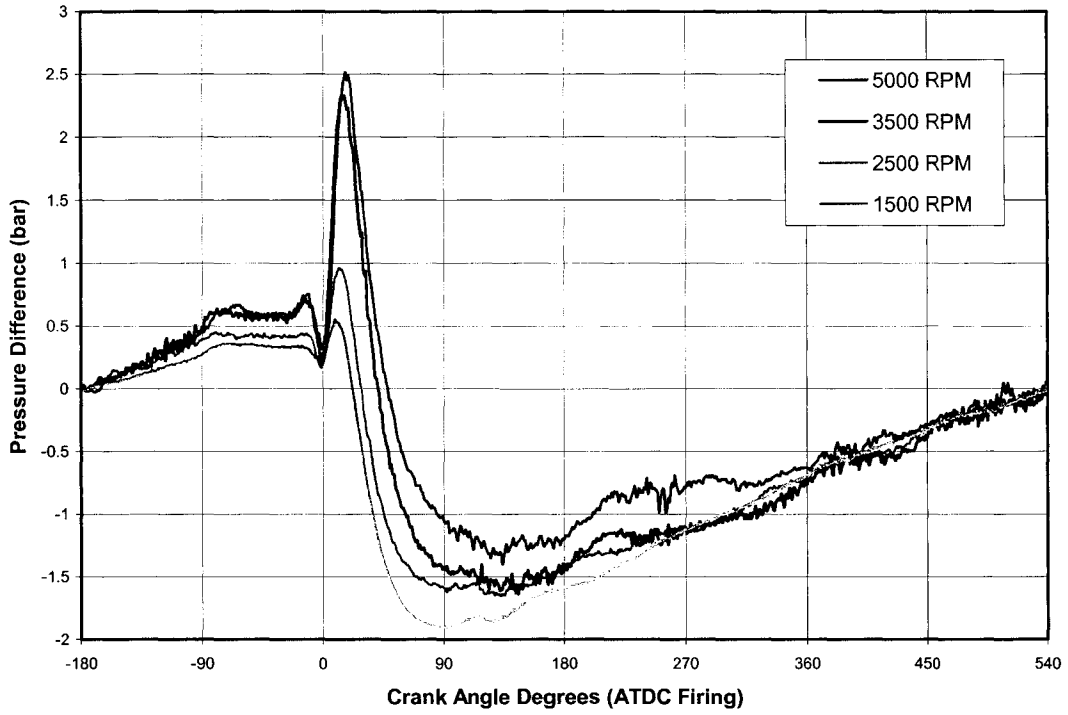


Figure 78: Effect of Engine Speed on Cylinder #7

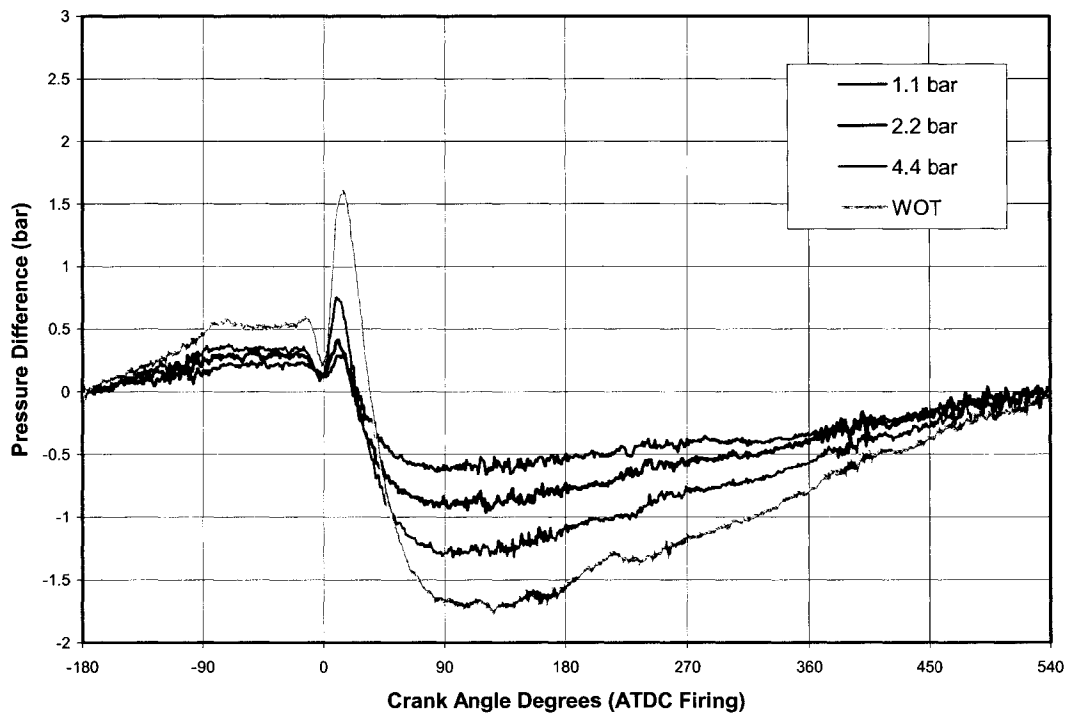


Figure 79: Effect of Engine Speed on Cylinder #7

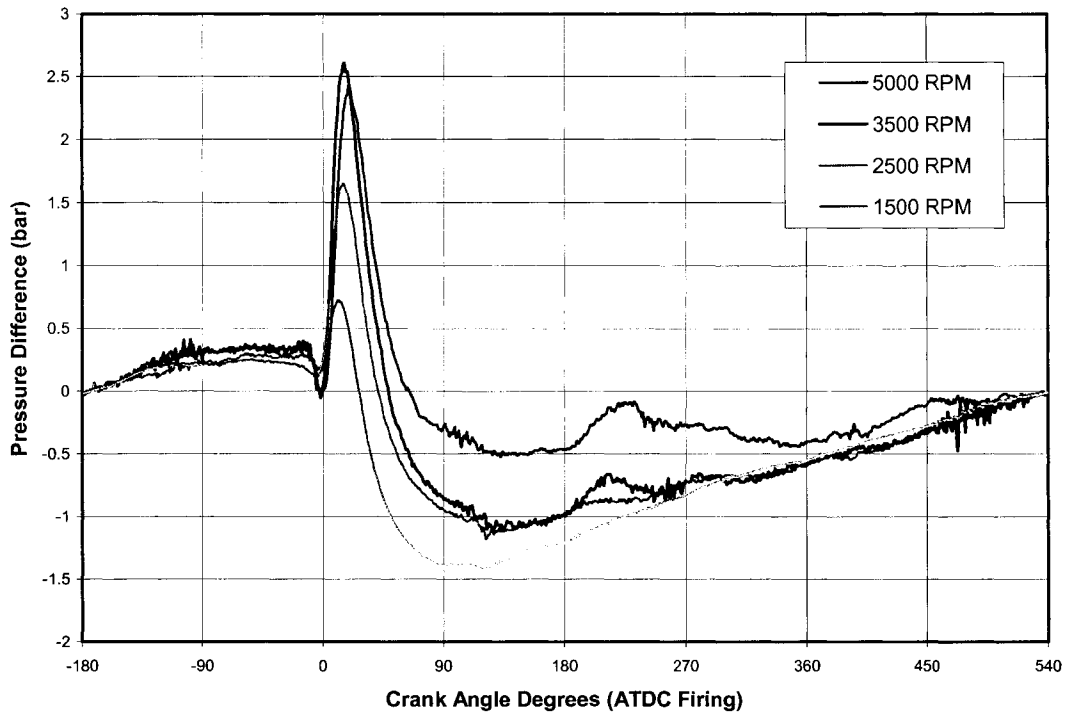


Figure 80: Effect of Engine Speed on Cylinder #1 (Repeated)

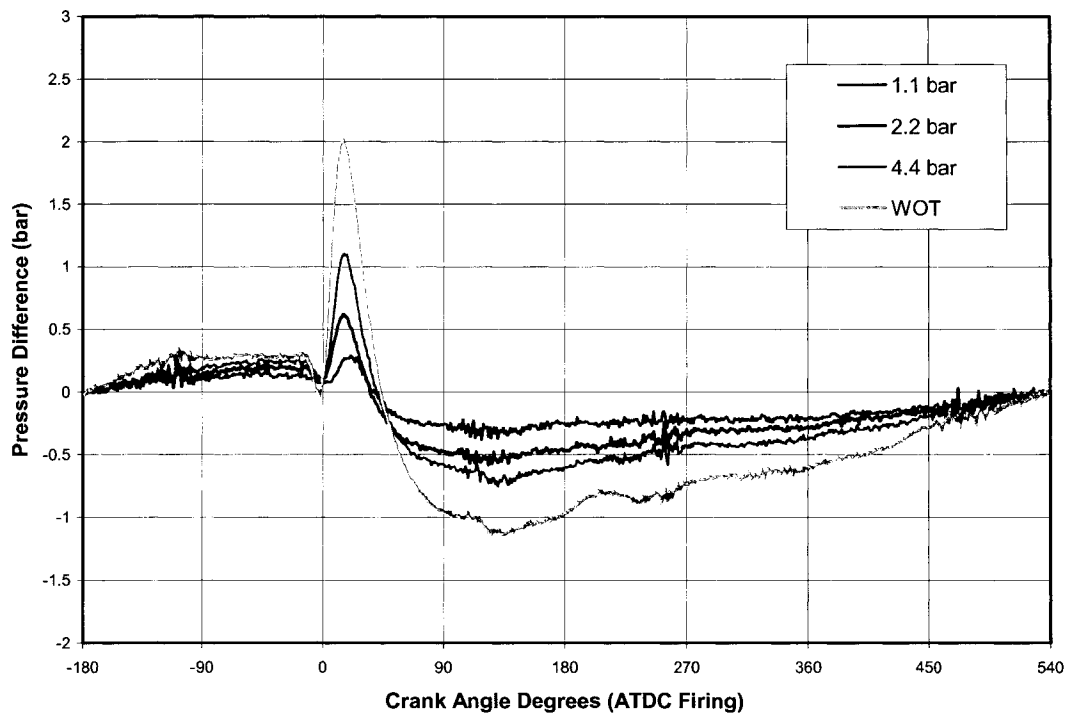


Figure 81: Effect of Engine Load on Cylinder #1 (Repeated)

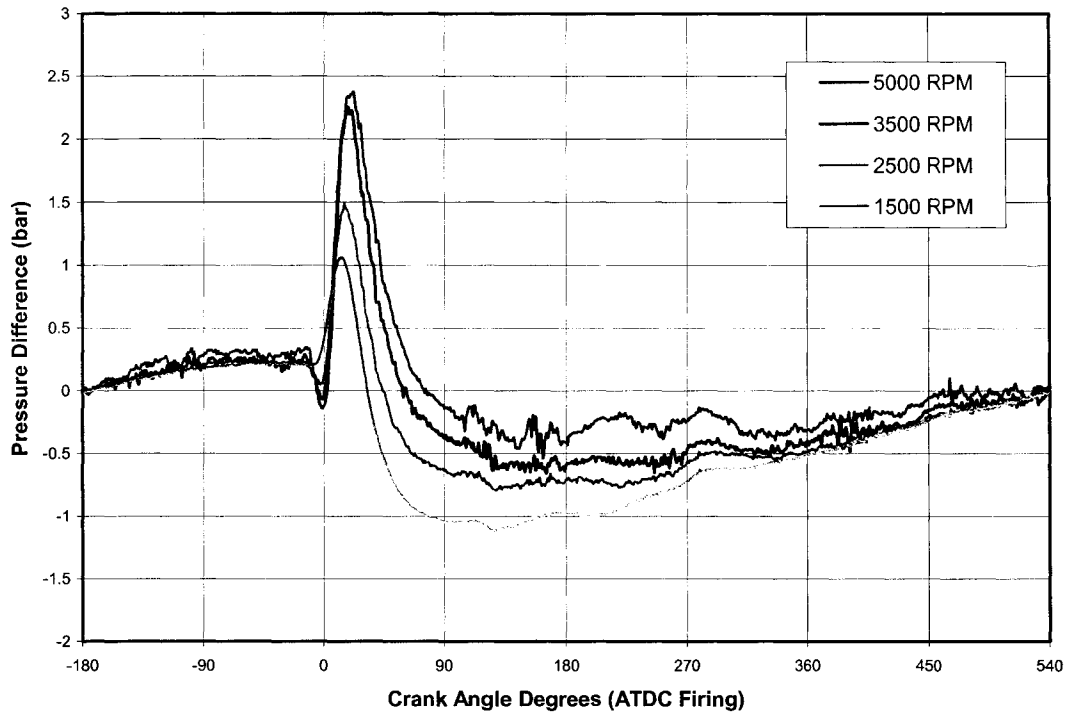


Figure 82: Effect of Engine Speed on Cylinder #2

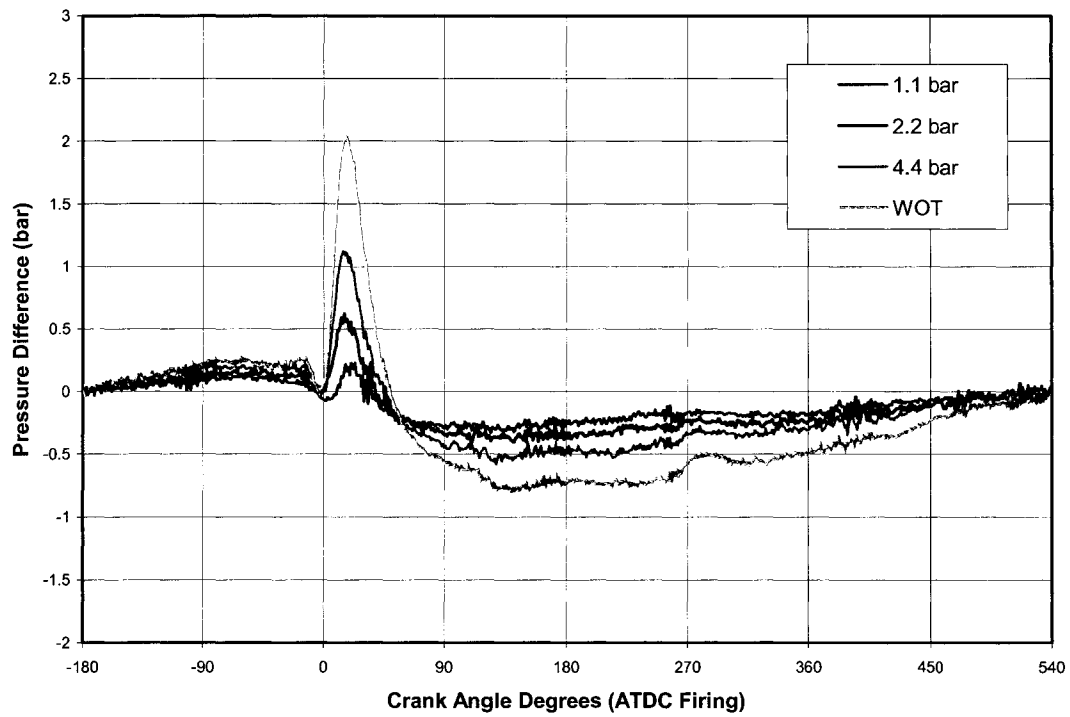


Figure 83: Effect of Engine Load on Cylinder #2

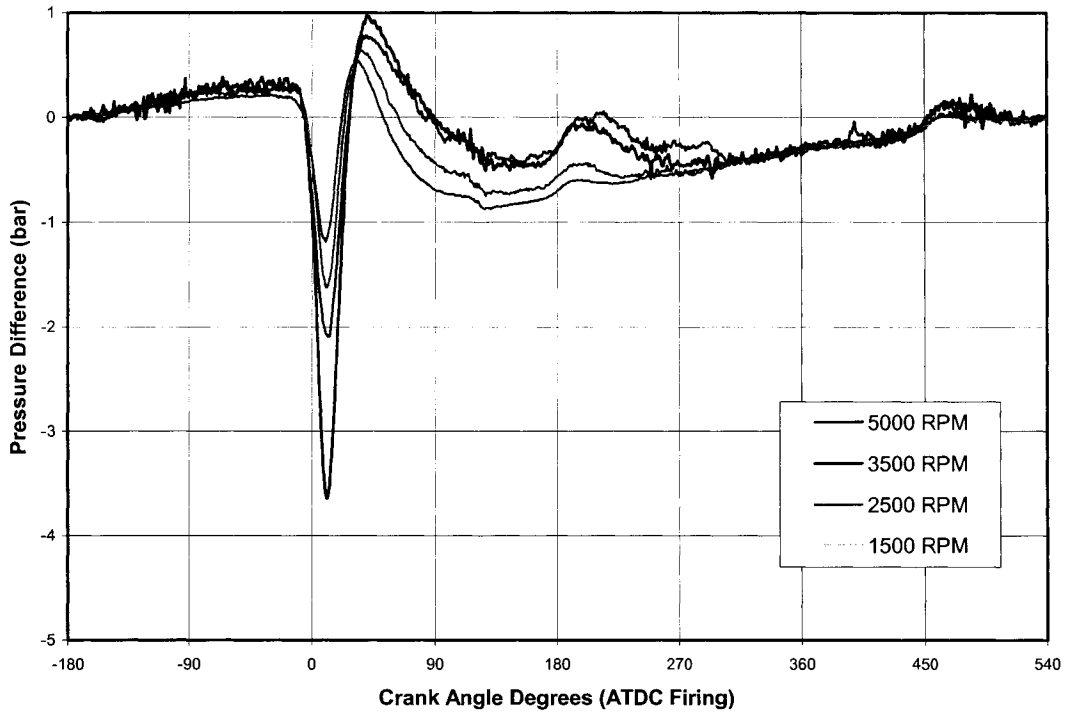


Figure 84: Effect of Engine Speed on Cylinder #4

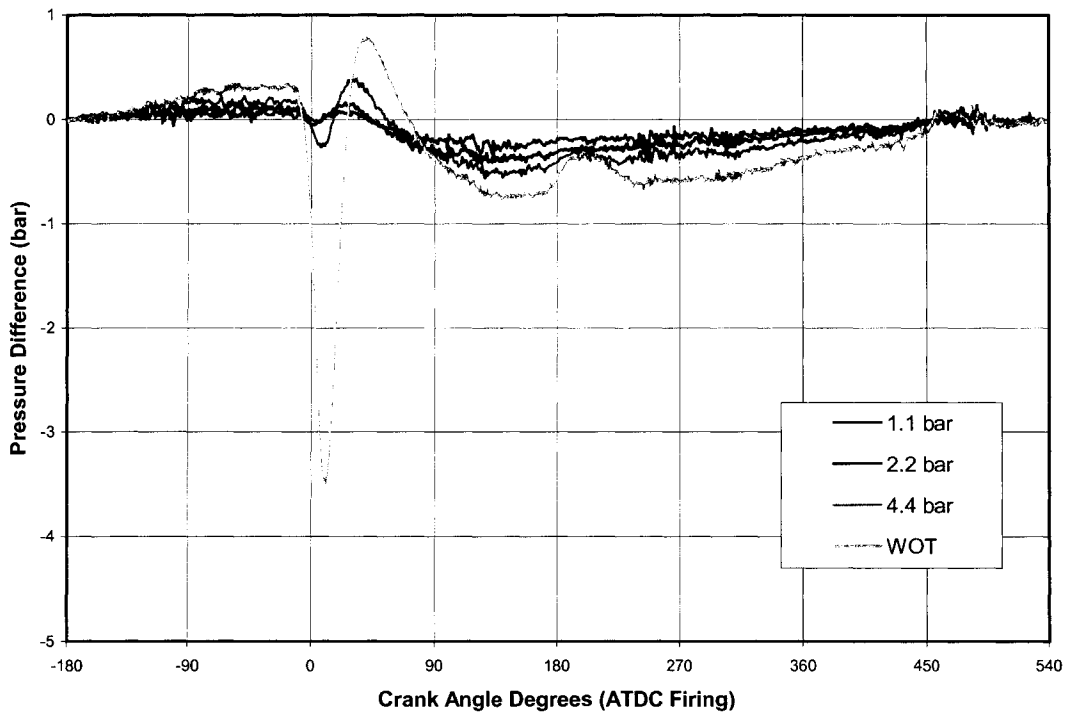


Figure 85: Effect of Engine Load on Cylinder #4

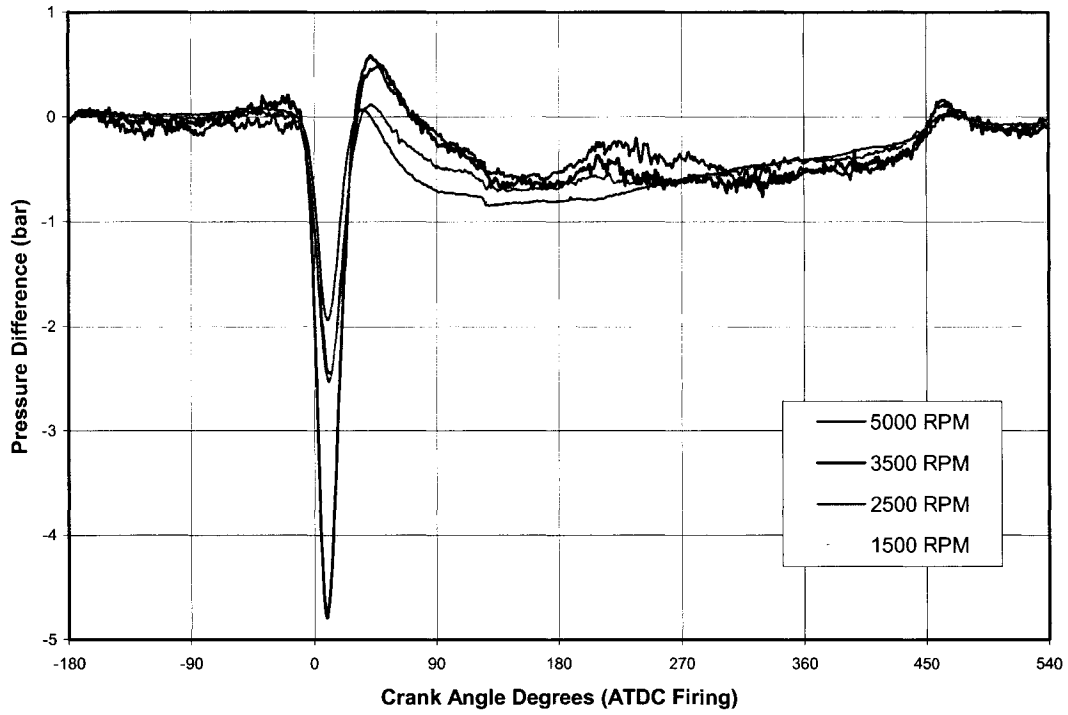


Figure 86: Effect of Engine Speed on Cylinder #6

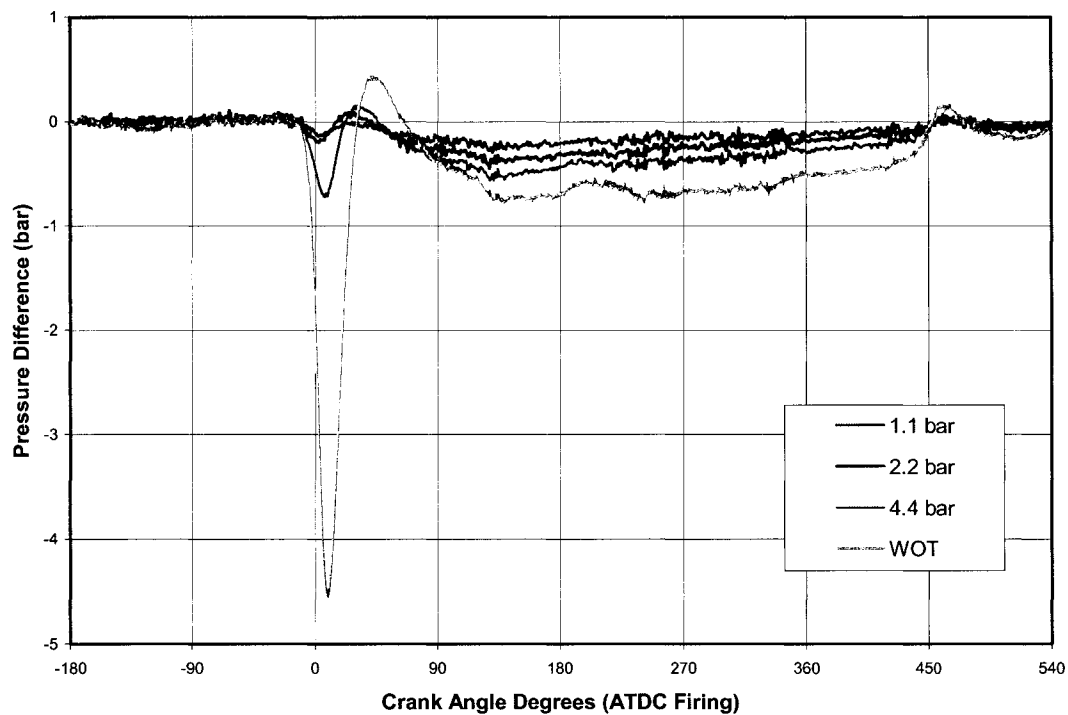


Figure 87: Effect of Engine Load on Cylinder #6

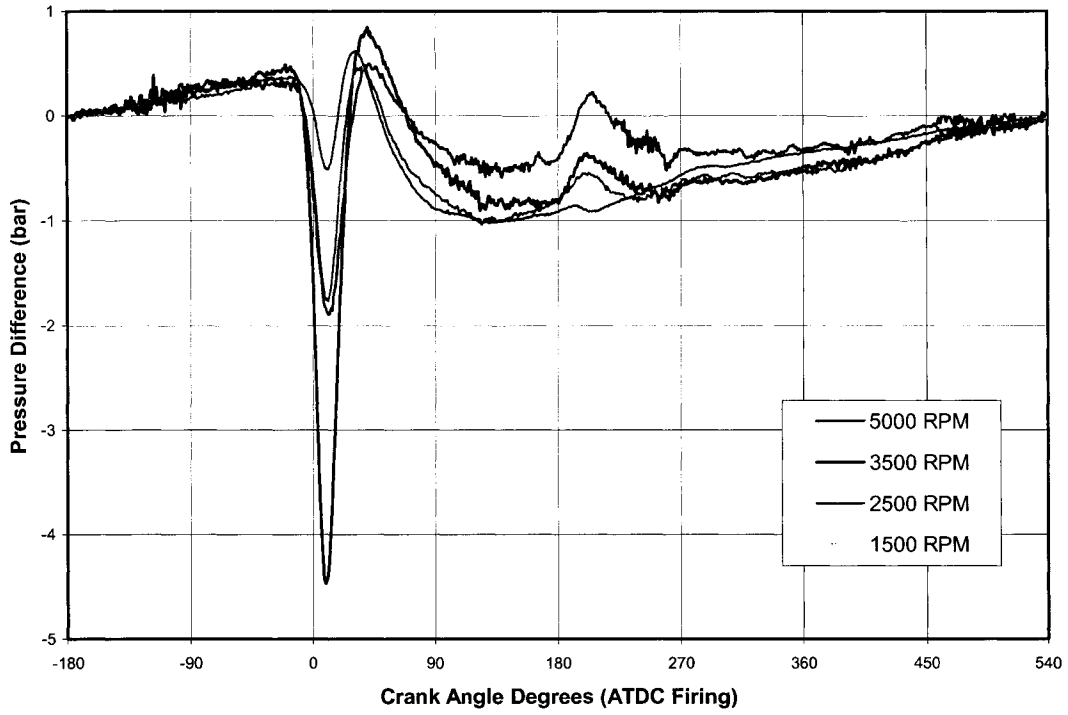


Figure 88: Effect of Engine Speed on Cylinder #8

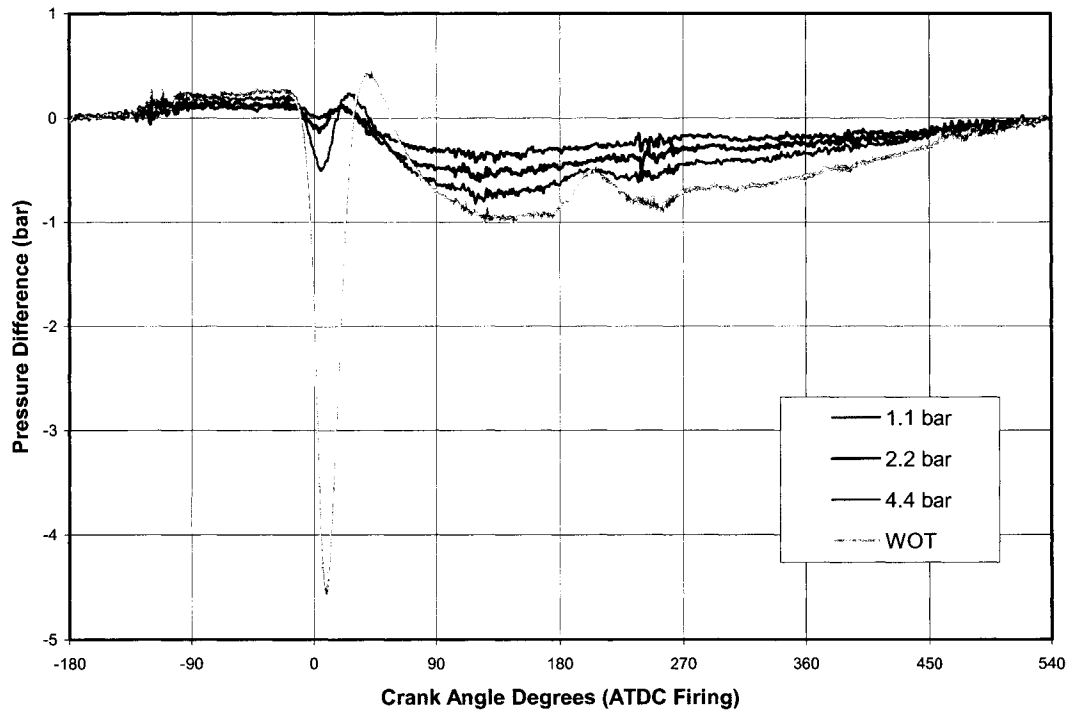


Figure 89: Effect of Engine Load on Cylinder #8

APPENDIX C: CYLINDER-TO-CYLINDER VARIATIONS ARRANGED BANK-TO-BANK

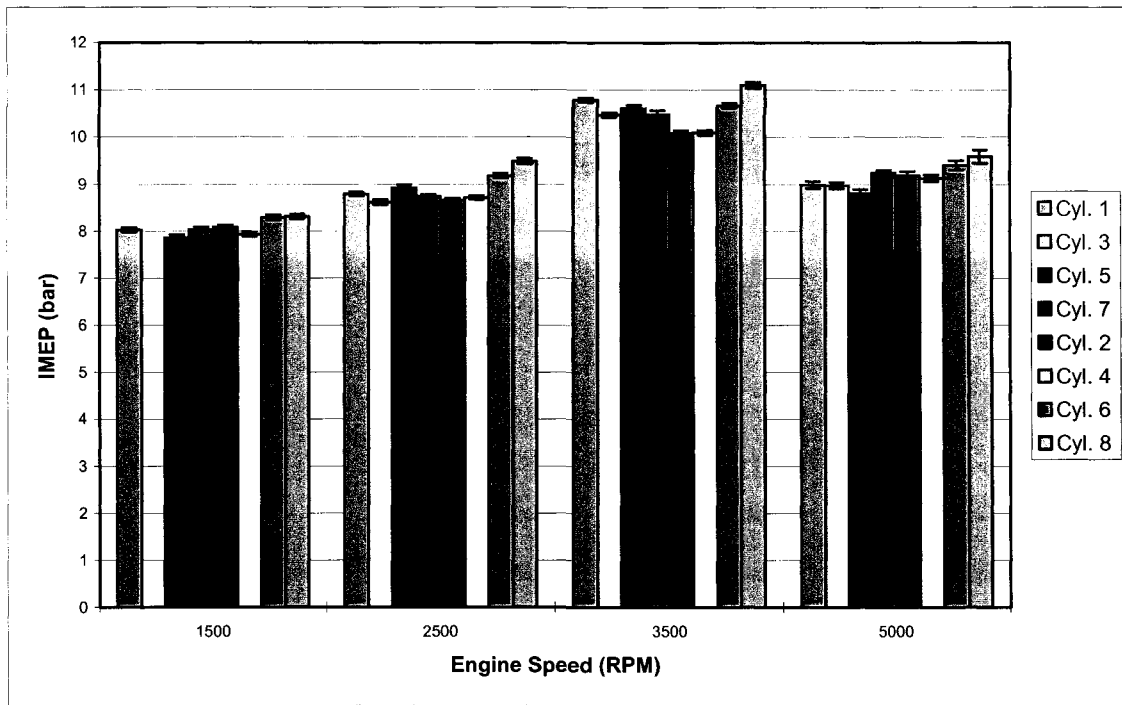


Figure 90: IMEP and its SD at WOT and Varying Engine Speeds

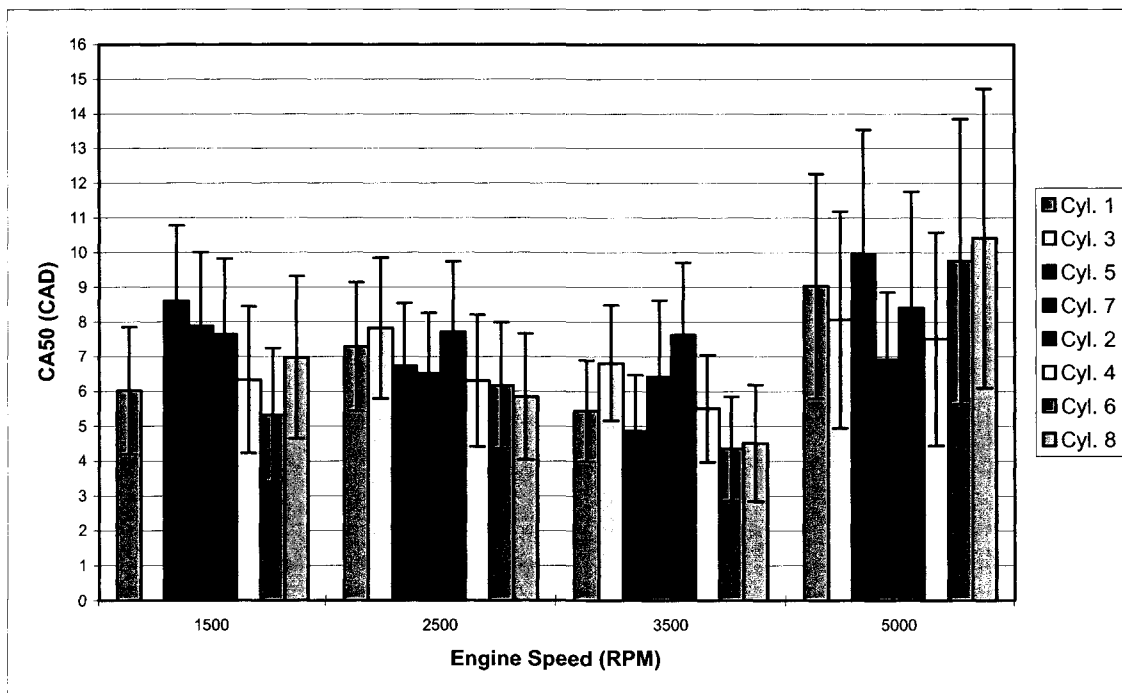


Figure 91: CA50 and its SD at WOT and Varying Engine Speeds

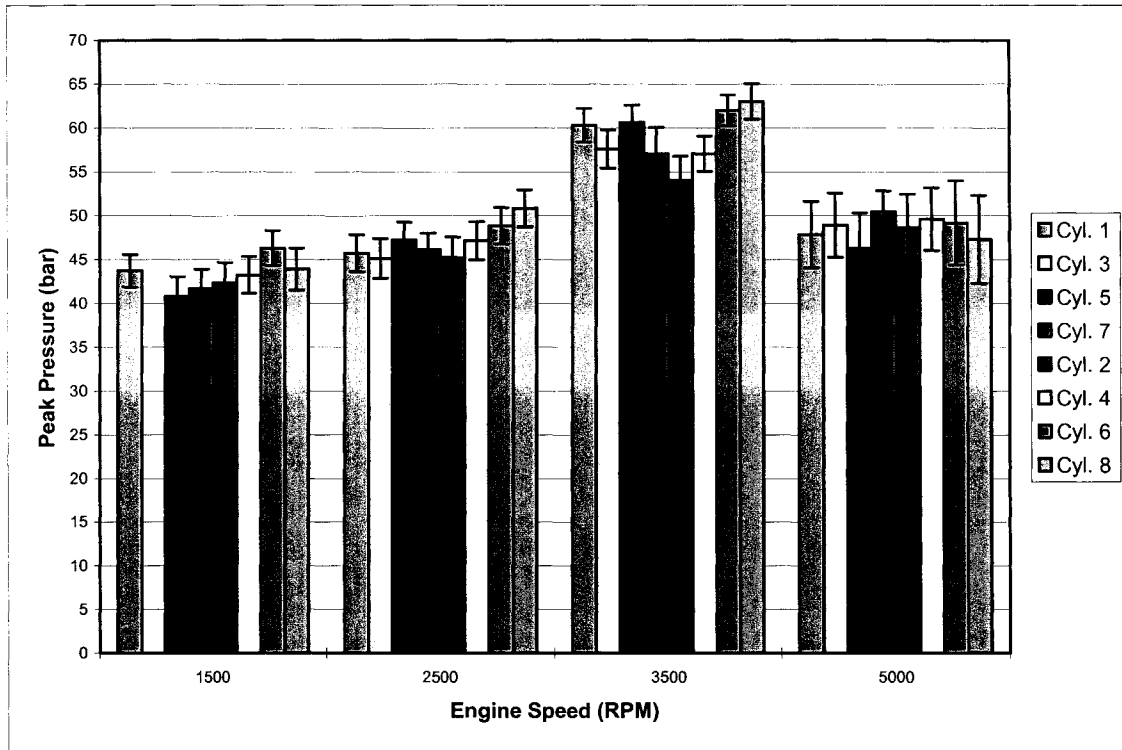


Figure 92: Peak Pressure and its SD at WOT and Varying Engine Speeds

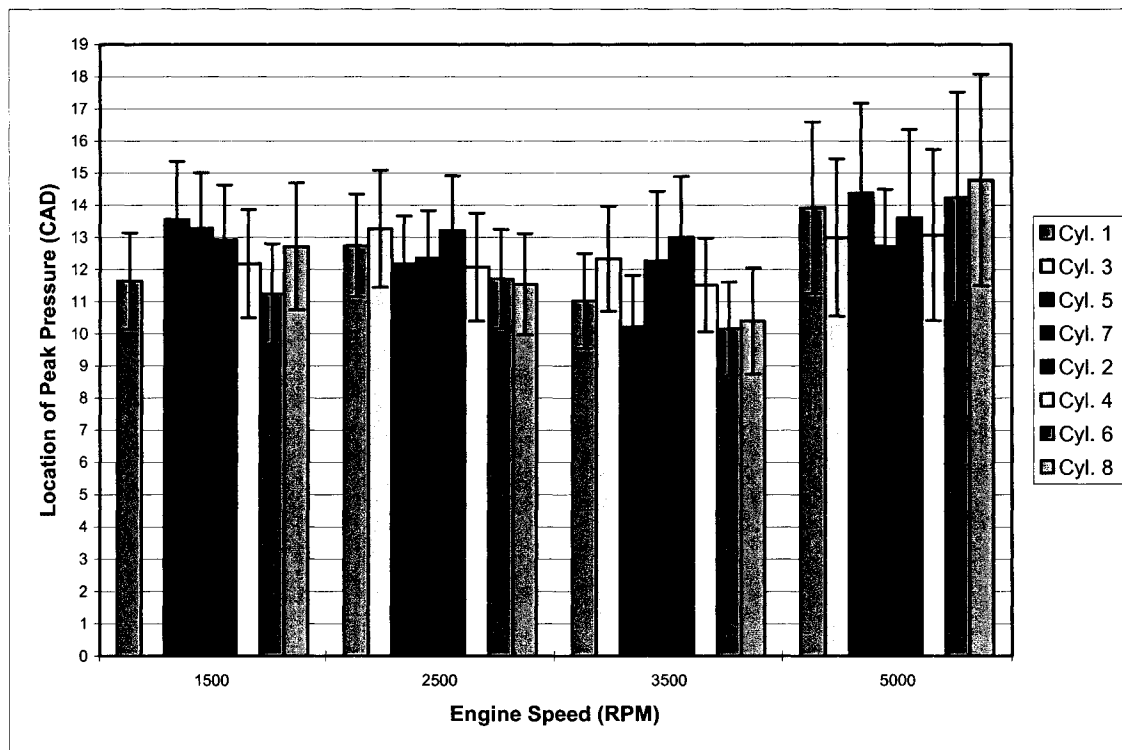


Figure 93: Location of PP and its SD at WOT and Varying Engine Speeds

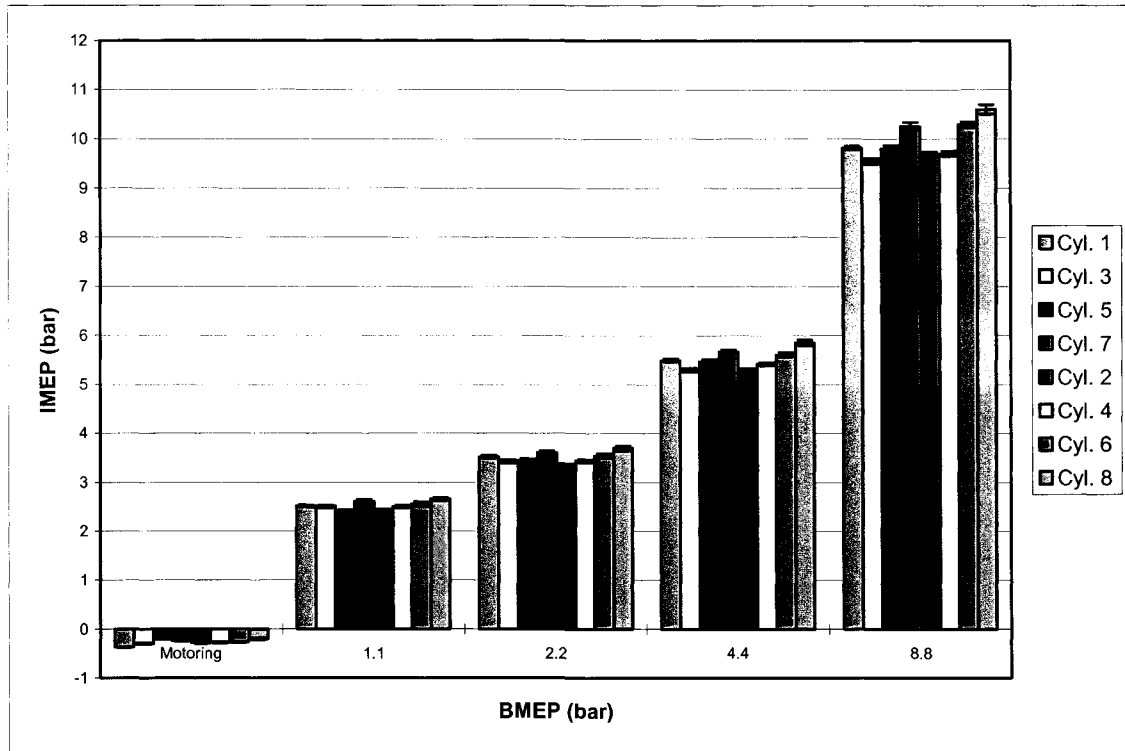


Figure 94: IMEP and its SD at 3000 RPM and Varying Engine Loads

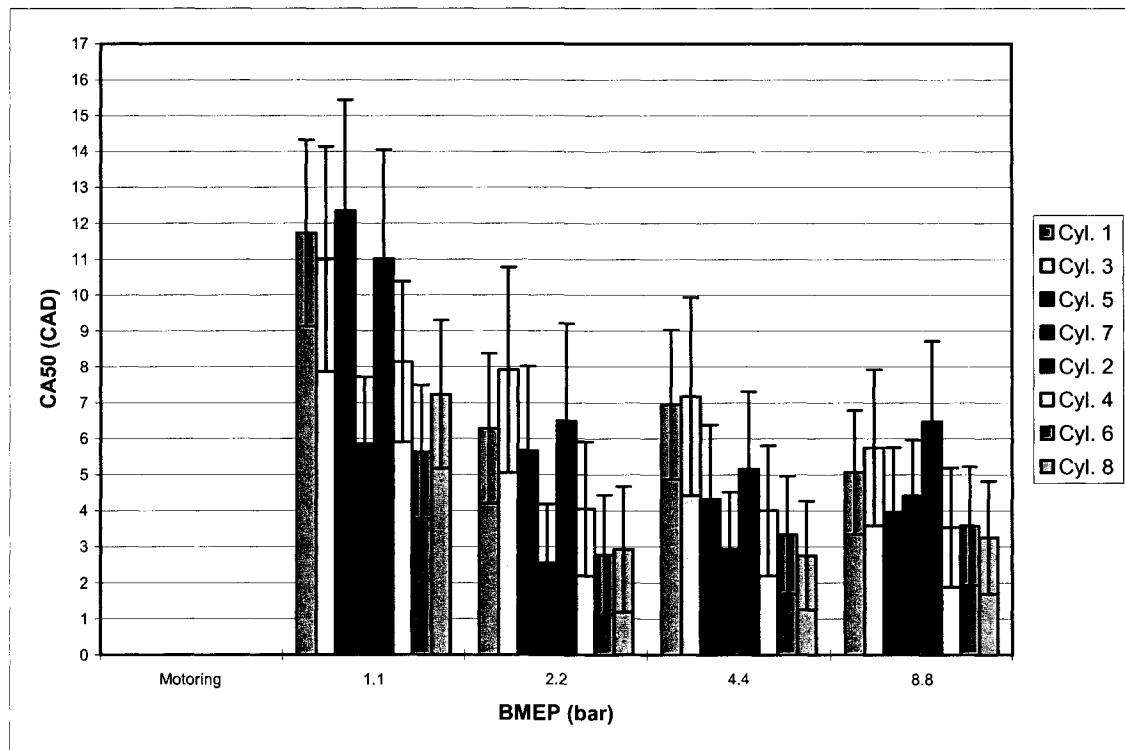


Figure 95: CA50 and its SD at 3000 RPM and Varying Engine Loads

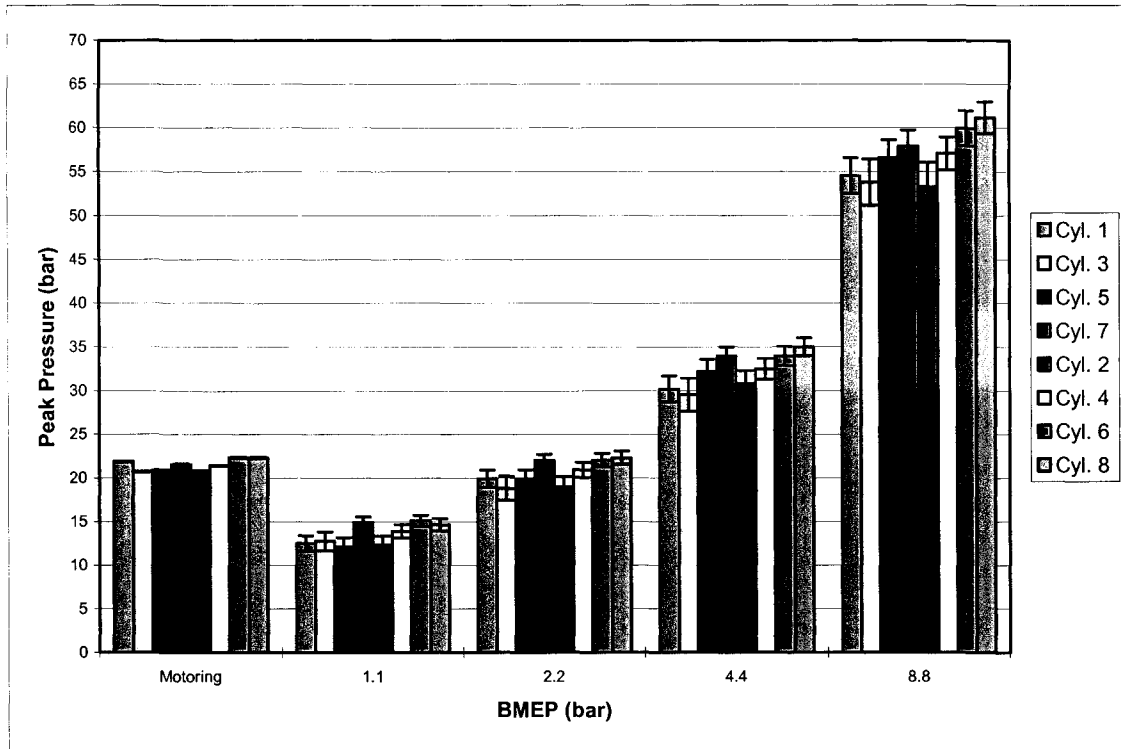


Figure 96: Peak Pressure and its SD at 3000 RPM and Varying Engine Loads

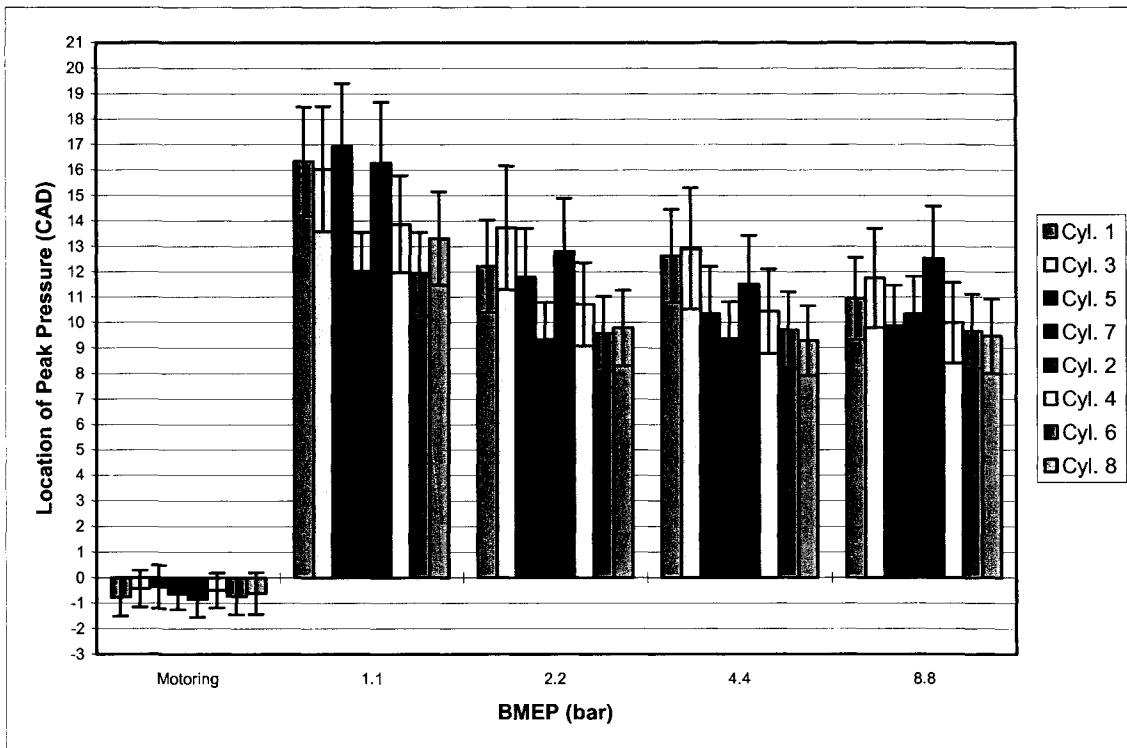


Figure 97: Location of PP and its SD at 3000 RPM and Varying Engine Loads

APPENDIX D: MANUFACTURER SPECIFICATIONS

Range	bar	0 ... 250
Calibrated partial range	bar	0 ... 50
Overload	bar	300
Sensitivity	pC / bar	≈ -19
Natural frequency (Force link)	kHz	≈ 130
Linearity, all ranges at RT	% FSO	$\leq \pm 0,4$
Acceleration sensitivity	bar / g	$\leq 0,001$
Operating temperature range	°C	-50 ... 350
Sensitivity shift 200 ... ± 50 °C	%	$\approx \pm 1$
Thermo shock error (at 1500 r/min, 9 bar IMEP)		
Δp (short-time drift)	bar	$< \pm 0,5$
Δ IMEP	%	$\leq \pm 2$
Δp_{max}	%	$\leq \pm 2$
Insulation resistance at 20 °C	T Ω	≥ 10
Shock resistance	g	2000
Tightening torque	Nm	1,5
Capacitance, without cable	pF	5
Weight, with cable	g	20
Plug, ceramic insulator		M4 x 0,35

Figure 98: Technical Data for Kistler Reference Transducer 6052A1

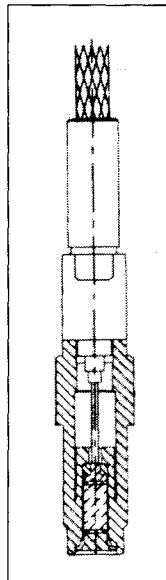


Figure 99: Schematic of Kistler Reference Transducer 6052A1

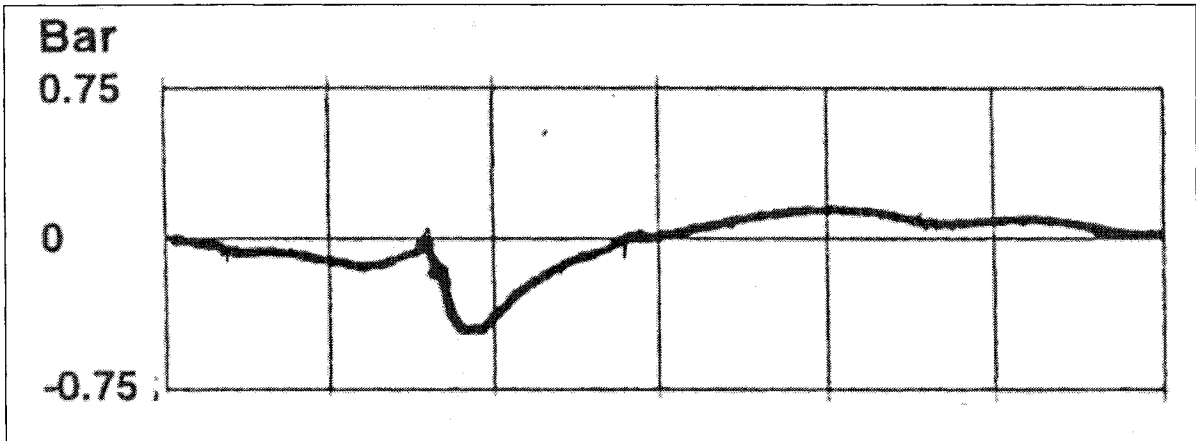


Figure 100: 6052A1 Pressure Difference Curve compared to a Water-Cooled Kistler 7061B [22]

Range	bar	0 ... 200
Calibrated partial range	bar	0 ... 50
Overload	bar	250
Sensitivity at 200 °C	pC/bar	≈ -15
Natural frequency (spark plug with integrated sensor)	kHz	≈ 130
Linearity	% FSO	≤ ±0,6
Acceleration sensitivity		
axial	bar/g	< 0,005
radial	bar/g	< 0,005
Operating temperature range	°C	≤ 350
Sensitivity shift 200 ± 50 °C	%	< ± 1,5
Thermo shock at 1500 min ⁻¹ , 9 bar IMEP		
Δp (short-time drift)	bar	< ± 0,8
ΔIMEP	%	< ± 4
Δ _{max}	%	< ± 2
Insulation resistance of sensor		
at 20 °C	Ω	> 10 ¹³
at 200 °C	Ω	> 10 ¹¹
Insulation resistance of spark plug at ambient temperature (between central electrode and spark plug body at 1000 V)	MΩ	> 100
Electrical final test of spark plug Spark discharge for	7 bar / 20 kV	
Tightening torque of sensor	Nm	1,2 ... 1,3
Tightening torque of spark plug	Nm	25
Capacitance of sensor with 1 m cable	pF	110
Weight (with protection cartridge)	g	130

Figure 101: Technical Data and Schematic for Kistler Test Transducer 6117

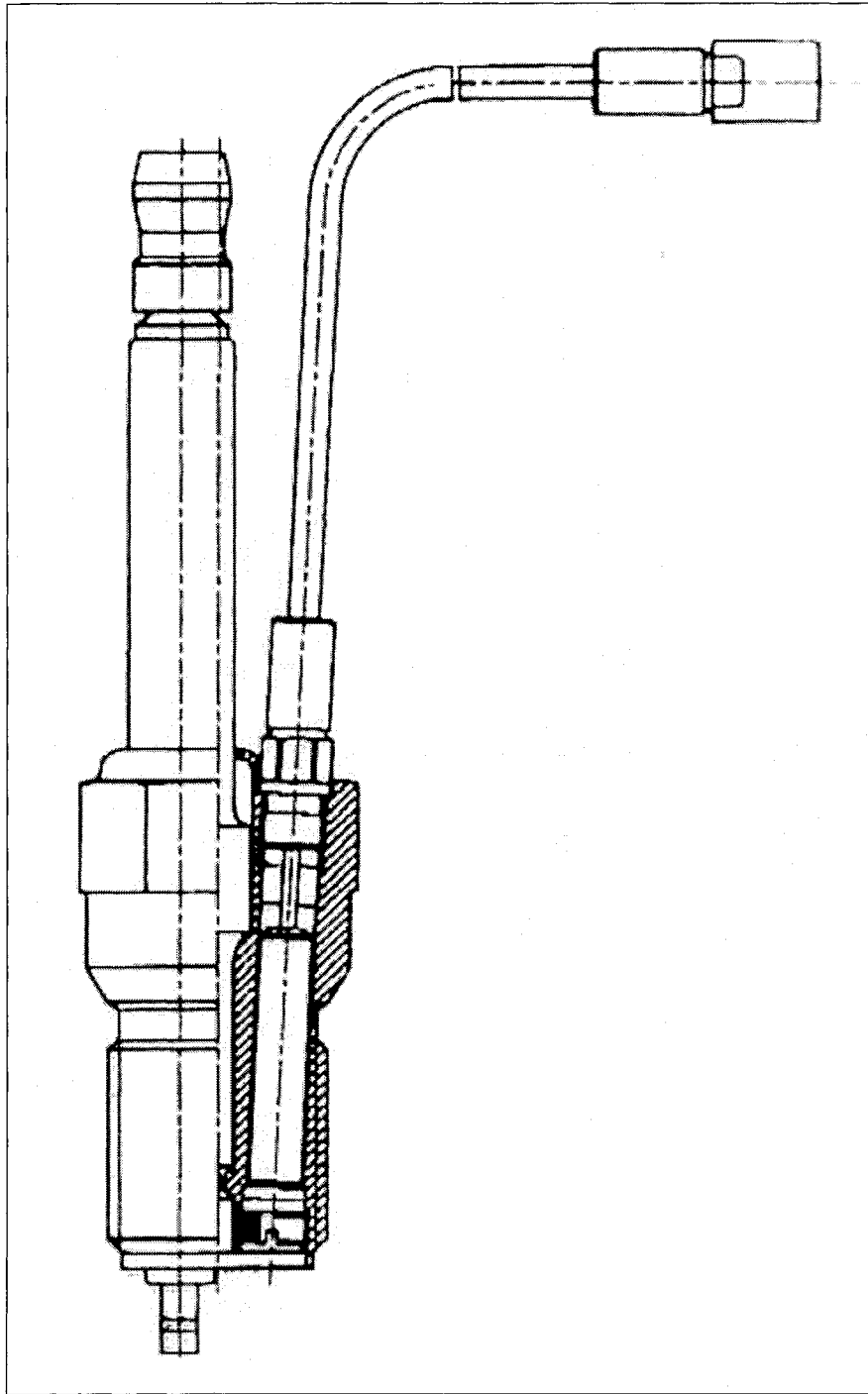


Figure 102: Schematic of Kistler Test Transducer 6117

<i>Over Pressure:</i>	2 x Pressure Range (typical)
<i>Non-Linearity & Hysteresis:</i>	±0.5% FS under non-combustion conditions, under constant temperature ±1% FS under combustion conditions, i.e., varying temperature within one combustion cycle
<i>Diaphragm Resonant Frequency:</i>	Approx. 120 kHz
<i>Frequency Range:</i>	0.1 Hz to 15 kHz
<i>Sensor Housing Temperature Range:</i>	-40°C to 350°C
<i>Cable Operating Temperature:</i>	-40°C to 200°C
<i>Fiber optic Cable Length:</i>	2m (6.5')
<i>Fiber optic Cable Min. Bending Radius:</i>	5mm (3/16")
<i>Sensor Operational Mode:</i>	Sealed Gauge
<i>Interface Unit:</i>	Integrated with Sensor
<i>Pressure Output Signal:</i>	Analog, 0.5 - 5 V
<i>Diagnostic Output Signal:</i>	Analog, 0 - 3.6V
<i>Power Supply:</i>	9 - 18V DC (85mA)
<i>Interface Temperature Range:</i>	-20°C to 65°C
<i>Pressure Media:</i>	Gaseous or Liquid
<i>Vibration:</i>	100G
<i>Guaranteed Lifetime:</i>	200 Million Pressure Cycles or 2 Years

Figure 103: Technical Data for Optrand Transducer

KISTLER

Kistler Instrumente AG Winterthur,
Switzerland

Eulachstrasse 22, PO Box 304, CH-8408 Winterthur
Telephone + 41 - 52 224 11 11
Telefax + 41 - 52 224 14 14
E-mail sales@kistler.ch
Internet www.kistler.com

KALIBRIERSCHEIN DRUCK

CALIBRATION CERTIFICATE PRESSURE

Typ	Type	6052A
Serien-Nr	Serial No	1073693
Betriebstemperaturbereich	Operating Temperature Range	°C -50 ... 350
Messbereich	Measuring Range	bar 0 ... 250
Hochtemperatur-Kalibrierung bei	High Temperature Calibration at	°C 200,250,300,350

Messungen		Measurements	
Kalibrierter Bereich / Calibrated Range	Empfindlichkeit / Sensitivity	Linearität / Linearity	
bar	$\mu\text{C}/\text{bar}$	$\leq \pm\% \text{FSO}$	
0 ... 250 (23°C)	-18,8	0,1	
0 ... 50 (23°C)	-18,8	0,1	
0 ... 250 (200°C)	-19,2	0,1	
0 ... 50 (200°C)	-19,1	0,1	
0 ... 250 (250°C)	-19,3	0,2	
0 ... 50 (250°C)	-19,2	0,2	
0 ... 250 (300°C)	-19,5	0,2	
0 ... 50 (300°C)	-19,4	0,1	
0 ... 250 (350°C)	-19,7	0,2	
0 ... 50 (350°C)	-20,0	0,5	

Umgebungstemperatur	Ambient Temperature	°C	23	±1
Relative Feuchte	Relative Humidity	%	46	±5

Kalibriert durch	Calibrated by	E. Weniger
Datum	Date	14.11.00

Wir bestätigen, dass das oben identifizierte Gerät nach den vorgeschriebenen Verfahren geprüft wurde. Alle Messmittel sind auf nationale Normale rückverfolgbar, die Bezugsnormale über die von Kistler betriebene SCS (Swiss Calibration Service) Kalibrierstelle Nr. 049, akkreditiert nach EN 45001.

We confirm that the device identified above was tested by the prescribed procedures. All measuring devices are traceable to national standards, the reference standards through the SCS (Swiss Calibration Service) Calibration Laboratory No. 049, operated by Kistler and accredited per EN 45001.

Referenz Geräte	Reference Equipment	Typ / Type	Serial-Nr / Serial No
Sensor (Gebrauchsnormale)	Sensor (Working Standard)	Kistler 7005	492592
Ladungsverstärker	Charge Amplifier	Kistler 5011A	333916
Ladungskalibrator	Charge Calibrator	Kistler 5395A1	530623

ISO 9001 certified

Figure 104: Calibration Certificate for Reference Transducer

KISTLER

Kistler Instrumente AG Winterthur,
Switzerland

Eulachstrasse 22, PO Box 304, CH-8400 Winterthur
Telephone + 41 - 52 224 11 11
Telefax + 41 - 52 224 14 14
E-mail sales@kistler.ch
internet www.kistler.com

KALIBRIERSCHEIN DRUCK

CALIBRATION CERTIFICATE PRESSURE

Typ	Type	6117BF17
Serien-Nr	Serial No	1006647
Betriebstemperaturbereich	Operating Temperature Range	°C <350
Messbereich	Measuring Range	bar 0 ... 200
Hochtemperatur-Kalibrierung bei	High Temperature Calibration at	°C 23,200

Messungen

Measurements

Kalibrierter Bereich / Calibrated Range	Empfindlichkeit / Sensitivity	Linearität / Linearity
bar	µC/bar	≤±%FSO
0 ... 200 (23°C)	-16,1	0,1
0 ... 50 (23°C)	-16,1	0,1
0 ... 150 (200°C)	-16,5	0,1
0 ... 50 (200°C)	-16,4	0,2

Umgebungstemperatur	Ambient Temperature	°C 22 ±1
Relative Feuchte	Relative Humidity	% 50 ±5
Kalibriert durch	Calibrated by	K.Schmid
Datum	Date	01.10.1999

Wir bestätigen, dass das oben identifizierte Gerät nach den vorgeschriebenen Verfahren geprüft wurde. Alle Messmittel sind auf nationale Normale rückverfolgbar, die Bezugswerte über die von Kistler betriebene SCS (Swiss Calibration Service) Kalibrierstelle Nr. 049, akkreditiert nach EN 45001.

We confirm that the device identified above was tested by the prescribed procedures. All measuring devices are traceable to national standards, the reference standards through the SCS (Swiss Calibration Service) Calibration Laboratory No. 049, operated by Kistler and accredited per EN 45001.

Referenz Geräte	Reference Equipment	Typ / Type	Serien-Nr. / Serial No
Sensor (Gebrauchsnormale)	Sensor (Working Standard)	Kistler 6961A250	992713
Ladungsverstärker	Charge Amplifier	Kistler 5011B	602394
Ladungskalibrator	Charge Calibrator	Kistler 5395A1	605251

ISO 9001 certified

Figure 105: Calibration Certificate for Kistler Test Transducer #13

VITA AUCTORIS

Kevin Roth was born on October 21, 1977 in Windsor, Ontario, Canada. He graduated from Kennedy Collegiate Institute in 1996. From there he went on to the University of Windsor where he obtained the degree of Bachelor of Applied Science in Mechanical Engineering (Automotive Option) in 2000. He is currently a candidate for the Master's degree of Applied Science in Mechanical Engineering at the University of Windsor and is scheduled to graduate in the fall of 2002.